

**SYNTHESIS OF ZEOLITE BETA AS A SUPPORT OF
METAL SUPPORTED CATALYSTS FOR TOLUENE
HYDROGEANTION AND APPLICATION OF IN SITU
XAS ON CATALYSTS CHARACTERIZATION**

Sirinuch Loiha

**A Thesis Submitted in Partial Fulfillment of the Requirements for the
Degree of Doctor of Philosophy in Chemistry
Suranaree University of Technology
Academic Year 2008**

การสังเคราะห์ซีโอไลต์แบบตาเป็นตัวรองรับสำหรับตัวเร่งปฏิกิริยาของโลหะบน
ปฏิกิริยาการเติมไฮโดรเจนของโทลูอีน และการประยุกต์ใช้เทคนิคการดูดกลืน
รังสีเอกซ์แบบ in situ สำหรับวิเคราะห์คุณลักษณะของตัวเร่งปฏิกิริยา

นางสาวศิรินุช ลอยหา

วิทยานิพนธ์นี้เป็นส่วนหนึ่งของการศึกษาตามหลักสูตรปริญญาวิทยาศาสตรดุษฎีบัณฑิต
สาขาวิชาเคมี
มหาวิทยาลัยเทคโนโลยีสุรนารี
ปีการศึกษา 2551

**SYNTHESIS OF ZEOLITE BETA AS A SUPPORT OF METAL
SUPPORTED CATALYSTS FOR TOLUENE HYDROGEANTION
AND APPLICATION OF IN SITU XAS ON CATALYSTS
CHARACTERIZATION**

Suranaree University of Technology has approved this thesis submitted in partial fulfillment of the requirements for the Degree of Doctor of Philosophy.

Thesis Examining Committee

(Assoc. Prof. Dr. Malee Tangsathitkulchai)

Chairperson

(Assoc. Prof. Dr. Jatuporn Wittayakun)

Member (Thesis Advisor)

(Dr. Wantana Klysubun)

Member

(Dr. Karin Föttinger)

Member

(Assoc. Prof. Dr. Nurak Grisdanurak)

Member

(Dr. Sanchai Prayoonpokarach)

Member

(Prof. Dr. Pairote Sattayatham)

Vice Rector for Academic Affairs

(Assoc. Prof. Dr. Prapan Manyum)

Dean of Institute of Science

สิรินุช ลอยหา : การสังเคราะห์ซีโอไลต์เบตาเป็นตัวรองรับสำหรับตัวเร่งปฏิกิริยาของโลหะบนปฏิกิริยาการเติมไฮโดรเจนของโทลูอีน และการประยุกต์ใช้เทคนิคการดูดกลืนรังสีเอกซ์แบบ in situ สำหรับวิเคราะห์คุณลักษณะของตัวเร่งปฏิกิริยา. อาจารย์ที่ปรึกษา : รศ. ดร. จตุพร วิทยาคณ, 126 หน้า

งานวิจัยนี้ได้สังเคราะห์ซีโอไลต์เบตาด้วยวิธีไฮโดรเทอร์มัลโดยใช้สารตั้งต้นเป็นซิลิกาจากแกลบข้าว ซีโอไลต์เบตา (เบตา) ที่ได้สังเคราะห์ประกอบด้วยเจลที่มีอัตราส่วน Si/Al ตั้งแต่ 8 ถึง 20 จากนั้นวิเคราะห์โครงสร้างเบื้องต้นด้วยเทคนิคการเลี้ยวเบนของรังสีเอกซ์ พบว่าเบตาจากเจลที่มีอัตราส่วน Si/Al ตั้งแต่ 8 ถึง 20 เท่านั้น ที่แสดงเฟสบริสุทธิ์ของเบตา และพบว่าเบตาจากเจลที่มีอัตราส่วน Si/Al เท่ากับ 13 มีความเป็นผลึกสูงที่สุด จึงนำตัวอย่างดังกล่าวมาวิเคราะห์ลักษณะต่อด้วยกล้องจุลทรรศน์อิเล็กตรอนแบบส่องกราด เครื่องวัดการกระจายตัวของขนาดอนุภาคด้วยเลเซอร์ และเครื่องวัดการดูดซับไนโตรเจน พบว่าขนาดอนุภาคของเบตาเท่ากับ 1.5 ไมโครเมตร มีพื้นที่ผิวเท่ากับ 670 ตารางเมตรต่อกรัม สำหรับข้อมูลทางโครงสร้างของตัวอย่างที่มีอัตราส่วน Si/Al ตั้งแต่ 50 ถึง 200 แสดงโครงสร้างผสมของเบตาและซีโอไลต์ ZSM-12 (MTW) และองค์ประกอบตัวหลังนี้ จะเพิ่มมากขึ้นเมื่อเพิ่มอัตราส่วน Si/Al

จากนั้นนำซีโอไลต์เบตาที่สังเคราะห์จากเจลที่มีอัตราส่วน Si/Al เท่ากับ 13 ในรูปโปรตอน (HBEA) ไปเป็นตัวรองรับของตัวเร่งปฏิกิริยาโลหะเดี่ยว และโลหะคู่ของแพลทินัมและแพลลาเดียมเพื่อทดสอบปฏิกิริยาการเติมไฮโดรเจนของโทลูอีน ตัวเร่งปฏิกิริยาประกอบด้วยแพลทินัมและแพลลาเดียม ที่มีอัตราส่วนร้อยละของโลหะโดยน้ำหนักเท่ากับ 3 โดยใช้วิธีการเตรียมแบบทำให้เอิบชุ่มได้ตัวเร่งปฏิกิริยา คือ 3Pt/HBEA 3Pd/HBEA และ 3Pt3Pd/HBEA จากนั้นนำไปวิเคราะห์โครงสร้างด้วยเทคนิคการเลี้ยวเบนของรังสีเอกซ์ พบว่าโครงสร้างของเบตาไม่มีการเปลี่ยนแปลงหลังจากบรรจุโลหะ นอกจากนี้ ผลการทดลองของ NH_3 -TPD แสดงให้เห็นว่าโลหะเข้าไปบรรจุแทนที่ตำแหน่งกรดของซีโอไลต์ เมื่อทำการเปรียบเทียบขนาดโลหะของแพลทินัมบน 3Pt/HBEA พบว่ามีขนาดเล็กกว่าแพลทินัมบน 3Pt3Pd/HBEA แสดงให้เห็นว่า แพลทินัมบน 3Pt3Pd/HBEA มีการกระจายตัวบนตัวรองรับได้ดีกว่า ผลการทดสอบประสิทธิภาพการเร่งปฏิกิริยาการเติมไฮโดรเจนของโทลูอีน พบว่าในสภาวะที่ใช้อุณหภูมิสำหรับปฏิกิริยาสูง ประสิทธิภาพการเร่งปฏิกิริยาของแพลทินัมในตัวเร่งปฏิกิริยาแบบโลหะคู่จะเพิ่มขึ้น เมื่อมีแพลลาเดียมร่วมด้วย และอุณหภูมิที่เหมาะสมที่สุดสำหรับการทำปฏิกิริยาของตัวเร่งปฏิกิริยาแบบโลหะคู่ คือ 150 องศาเซลเซียส โดยสารผลิตภัณฑ์ที่ได้จากการทดลองมีเพียงเมทิลไซโคลเฮกเซนเท่านั้น นอกจากนี้ยังพบว่า ประสิทธิภาพการเร่งปฏิกิริยาไม่มีการเปลี่ยนแปลงในระหว่างทำการทดลอง 5 ชั่วโมง

จากนั้นทำการสังเคราะห์ตัวเร่งปฏิกิริยาโลหะเดี่ยว และโลหะคู่ ของแพลทินัมและนิกเกิล โดยใช้เบตาที่มีอัตราส่วน Si/Al เท่ากับ 13 ที่อยู่ในรูปของโปรตอนเป็นตัวรองรับ เพื่อใช้ศึกษาคุณลักษณะของการเกิดอันตรกิริยาระหว่างโลหะกับตัวรองรับที่เป็นซีโอไลต์ โดยใช้เทคนิคการดูดกลืนแสงเอกซเรย์แบบ in situ ซึ่งการทดลองประกอบด้วยสภาวะของการรีดักชัน การคายของโทลูอีน (toluene desorption) และปฏิกิริยาการเติมไฮโดรเจนของโทลูอีน สำหรับตัวอย่างประกอบด้วยนิกเกิลในปริมาณร้อยละ โดยน้ำหนักเท่ากับ 1 3 และ 5 ส่วนแพลทินัมใช้ปริมาณคงที่ที่ร้อยละ 0.5 การวัดการดูดกลืนแสงเอกซเรย์แบบ in situ ใช้สเปกโทรสโกปีของการดูดกลืนที่ใกล้ค่าเอจ (X-ray absorption near edge spectroscopy, XANES) เพื่อศึกษาการเปลี่ยนแปลงของนิกเกิลอะตอม พบว่า ณ สภาวะการวัดแบบปกติ โครงสร้างของนิกเกิลบนตัวเร่งปฏิกิริยาที่มีปริมาณโลหะมาก (5Ni/HBEA) เป็นแบบทรงแปดหน้า ในขณะที่ตัวเร่งปฏิกิริยาที่มีปริมาณโลหะน้อย จะเป็นแบบทรงสี่หน้า หรือ ทรงสี่เหลี่ยมแบนราบ และเมื่อทำการศึกษาโครงสร้างของโลหะนิกเกิลบนตัวเร่งปฏิกิริยาหลังจากการรีดักชัน พบว่า ตัวเร่งปฏิกิริยาที่มีปริมาณโลหะร้อยละ 1 ไม่สามารถรีดิวซ์ได้ ดังนั้นสรุปได้ว่า ความสามารถในการเกิดรีดักชันของตัวเร่งปฏิกิริยา ขึ้นอยู่กับปริมาณโลหะที่บรรจุ อุณหภูมิ และเวลาของการรีดักชัน

การศึกษาดูตัวเร่งปฏิกิริยาของ 5Ni/HBEA ในสภาวะการคายโทลูอีน พบว่านิกเกิลอะตอมบนตัวเร่งปฏิกิริยา ไม่เกิดอันตรกิริยากับคาร์บอนในโมเลกุลของโทลูอีน เนื่องจากไม่พบการเปลี่ยนแปลงในตำแหน่งก่อนเอจ (pre-edge) ของ XANES แสดงว่าโทลูอีนเกิดอันตรกิริยากับตำแหน่งกรดของเบตา นอกจากนี้ยังพบว่ามีความเป็นไปได้ที่อะตอมของออกซิเจนจะเกิดการออกซิเดชันกับโทลูอีน เนื่องจากพบว่าหลังการเกิดการคายของโทลูอีนทำให้เลขโคออดิเนชันของนิกเกิลลดลง และจากผลการทดสอบปฏิกิริยาการเติมไฮโดรเจนของโทลูอีนบนตัวเร่งปฏิกิริยาของ 5Ni/HBEA พบว่าตัวเร่งปฏิกิริยาเกิดการรีดักชันอย่างช้า ๆ ด้วยไฮโดรเจน เนื่องจากปรากฏฟิสิกส์ที่เห็นตำแหน่งเอจของ Ni(0) แต่อย่างไรก็ตาม เนื่องจากข้อจำกัดของปริมาณผลิตภัณฑ์ที่น้อยมาก จึงไม่สามารถวิเคราะห์โครงสร้างของผลิตภัณฑ์ได้อย่างสมบูรณ์

สาขาวิชาเคมี

ปีการศึกษา 2551

ลายมือชื่อนักศึกษา _____

ลายมือชื่ออาจารย์ที่ปรึกษา _____

ลายมือชื่ออาจารย์ที่ปรึกษาร่วม _____

SIRINUCH LOIHA : SYNTHESIS OF ZEOLITE BETA AS A SUPPORT
OF METAL SUPPORTED CATALYSTS FOR TOLUENE
HYDROGENATION AND APPLICATION OF IN SITU XAS ON
CATALYSTS CHARACTERIZATION. THESIS ADVISOR : ASSOC.
PROF. JATUPORN WITTAYAKUN, Ph.D. 126 PP.

ZEOLITE BETA/PALLADIUM/PLATINUM/NICKEL/TOLUENE
HYDROGENATION/X-RAY ABSORPTION

Silica with 98% purity was prepared from rice husk by acid leaching and used as a silica source for the syntheses of zeolite beta (BEA) under hydrothermal conditions with gel Si/Al ratios from 8 to 200. Based on powder X-ray diffraction patterns, samples with gel Si/Al ratios of 8 - 20 contained only the pure phase of BEA and the highest relative crystallinity was observed in the BEA with a gel Si/Al ratio of 13. This sample was further characterized by scanning electron microscopy, particle size analyzer and N₂ adsorption analysis. The BEA particles were sphere shaped with the average particle size of 1.5 μm and a surface area of 670 m²/g. The samples with gel Si/Al ratios ranging from 50 to 200 showed mixed phases of BEA and ZSM-12 (MTW), and the latter phase was more dominant as the Si/Al ratio increased.

The BEA with the highest crystallinity from the synthesis gel Si/Al of 13 in proton form (HBEA) was used as a support for Pt and Pd catalysts which were tested for toluene hydrogenation in a fixed-bed flow reactor. The catalyst with 3 wt% loading of each metal was prepared by co-impregnation on HBEA and denoted as 3Pt3Pd/HBEA. The XRD patterns of HBEA did not change after catalyst preparation

and ammonia temperature-programmed desorption indicated that the metal occupied strong acidic sites of the zeolite. By comparing to monometallic 3Pt/HBEA, the 3Pt3Pd/HBEA had smaller Pt particle size, calculated from Scherrer formula indicating a better dispersion on the support. The catalytic performance of the bimetallic catalyst at various temperatures indicated that the presence of Pd enhanced toluene hydrogenation of Pt catalyst at high temperature. The most suitable temperature for toluene hydrogenation on 3Pt3Pd/HBEA was 150°C where a complete toluene conversion was obtained with methylcyclohexane as the only product. The performance of the bimetallic catalyst was stable during the 5-hour test.

Furthermore, monometallic nickel (Ni) or bimetallic nickel-platinum (NiPt) supported on zeolite beta in proton form (HBEA), referred to as Ni/HBEA or NiPt/HBEA catalysts were characterized by the in situ XAS to monitor metal-support interaction and changes of the Ni during a reduction by hydrogen. The loadings of Ni in monometallic catalysts were 1, 3, and 5 wt%. The Ni loadings in the bimetallic catalysts were 1 and 5 whereas the Pt loading was fixed to 0.5 wt%. Data from X-ray absorption near edge spectroscopy (XANES) at Ni K-edge provided structural and electronic information of the metal. Measurements in ambient conditions indicated that the calcined catalysts contained Ni with 5 wt% loading had octahedral geometry but Ni in the catalyst with low loading had tetrahedral or square planar. After reduction the catalysts with 1 wt% Ni loading was not reducible and the reducibility increased with metal loading, temperature and time. With high metal loading, Ni possibly located outside the zeolite pores because large crystal sizes were detected from X-ray diffraction. With low metal loading, Ni could reside in both zeolite channels and on the surface.

The Ni/HBEA with 5 wt% metal loading was further studied with the in situ XAS cell during toluene desorption and toluene hydrogenation. In toluene adsorption on calcined 5Ni/HBEA, there was no Ni-C interaction because there was no change in Ni pre-edge. Thus, toluene adsorbed on HBEA acid sites. Moreover, toluene might be oxidized by oxygen from NiO because the coordination number of Ni decreased during the in situ XANES measurement. In toluene hydrogenation on calcined 5Ni/HBEA, the NiO was slowly reduced by hydrogen as indicated by an appearance of Ni(0) edge. Although some products were detected, the catalyst performance was not fully studied.

School of Chemistry

Academic Year 2008

Student's Signature_____

Advisor's Signature_____

Co-advisor's Signature_____

ACKNOWLEDGEMENT

This work was supported by a Ph.D. Scholarship from The Synchrotron Light Research Institute (Public Organization), (SLRI), Scholarship number GS-48-D04. The equipments for the research were available at Center for Scientific and Technological Equipment (CSTE) in SUT, Institute of Material Chemistry at Vienna University of Technology and SLRI.

My thesis advisor, Assoc. Prof. Dr. Jatuporn Wittayakun, for give me the chance to study at SUT, his kind support, guidance and editing this thesis and instruction are invaluable treasures for me forever.

Dr. Wantana Klysubun, my thesis co-advisor for gives me the kind supported and the suggestion about X-ray absorption (XAS) technique and gives me the chance to test an in-situ XAS cell at BL8, SLRI.

Prof. Dr. Günther Rupprechter, Dr. Karin Föttinger, Katrin Zorn and all people in Institute of Material Chemistry, Vienna University and Technology, Austria, for supporting the a reactor for catalytic activity study and a very special appreciation is given to them for their kindness, instruction, advices and assistance during my studies in Vienna.

Assoc. Prof. Dr. Malee Tangsathitkulchai, Assoc. Prof. Dr. Nurak Grisdanurak, Asst. Prof. Dr. Prayoon Songsiriritthigul and Dr. Sanchai Prayoonpokarach for their valuable comments and suggestions during my thesis defense.

My friends: Pongtanawat Khemthong, Jitlada Chumee, Surachai Artkra, Supattra Khabuanchalad, Sittichi Kunlawong, Kamonwan Rintramee, Sudarat Sombatsri, Chen Xiaojun and all of my friends in SUT, special thanks for their kind assistance in some business related to my studies and work in this university.

Finally, I would like to thank my parent and my older brother for their inspiration, infinite love, patience and understanding during stay for this research and study.

Sirinuch Loiha

CONTENTS

	Page
ABSTRACT IN THAI.....	I
ABSTRACT IN ENGLISH	III
ACKNOWLEDGEMENT	VI
CONTENTS.....	VIII
LIST OF TABLES.....	<u>XIII</u>
LIST OF FIGURES	XIV
CHAPTER	
I INTRODUCTION.....	1
1.1 Introduction.....	1
1.1.1 Extraction of rice husk silica.....	2
1.1.2 Synthesis of zeolite beta (BEA).....	2
1.1.3 Bifunctional catalysts: Metal/zeolite support.....	3
1.1.4 Catalytic activity on toluene hydrogenation	4
1.1.5 Catalyst characterization by (XAS) X-ray absorption.....	4
1.2 Research objectives.....	6
1.3 Scope and limitations of the study	6
1.4 References.....	7
II LITERATURE REVIEW	9
2.1 Zeolite beta (BEA).....	9

CONTENTS (Continued)

	Page
2.1.1 Zeolite beta from rice husk silica.....	9
2.1.2 Transformation of BEA with Si/Al ratio	10
2.1.3 Supported BEA catalysts on hydrogenation of aromatics	12
2.2 Catalytic hydrogenation of aromatics on bimetallic catalysts	13
2.3 X-ray absorption spectroscopy (XAS).....	16
2.3.1 In situ XAS cell design	16
2.3.2 Electronic and geometric structures of supported metal studied using XAS	18
2.4 References.....	21
 III SYNTHESIS OF ZEOLITE BETA WITH PRETEATED RICE	
HUSK SILICA AND ITS TRANSFORMATION TO ZSM-12.....	
27	
Abstract.....	28
3.1 Introduction.....	28
3.2 Experimental	29
3.2.1 Materials and chemicals.....	29
3.2.2 Preparation of rice husk silica (RHS)	30
3.2.3 Synthesis of zeolite beta.....	30
3.2.4 Characterization of zeolite beta	31
3.3 Results and discussion	32
3.3.1 XRD Characterization.....	32
3.3.2 Acid amount of H-BEA zeolite with pure phase	36

CONTENTS (Continued)

	Page	
3.3.3 Characterization of H-BEA with gel Si/Al ratio of 13	37	
3.4 Conclusions.....	42	
3.5 References.....	43	
IV CATALYTIC ENHANCEMENT OF PLATINUM SUPPORTED		
ON ZEOLITE BETA FOR TOLUENE HYDROGENATION BY		
ADDITION OF PALLADIUM.....		45
Abstract.....	45	
4.1 Introduction.....	45	
4.2 Experimental.....	48	
4.3.1 Catalyst preparation	48	
4.3.2 Characterization techniques	49	
4.3.3 Toluene hydrogenation testing.....	50	
4.3 Results and discussion	51	
4.3.1 XRD patterns of HBEA and HBEA-supported catalysts.....	51	
4.3.2 BET surface area of HBEA and HBEA-supported catalysts	53	
4.3.3 Acidity of HBEA and HBEA-supported catalysts from NH ₃ -TPD	54	
4.3.4 Characterization of Pd/HBEA by XANES	55	
4.3.4 Effect of temperature on catalytic conversion	62	
4.4 Conclusions.....	60	
4.5 References.....	61	

CONTENTS (Continued)

	Page
V THE APPLICATION OF IN SITU XAS CELL ON REDUCTION, TOLUENE DESORPTION, TOLUENE HYDROGENATION OF NICKEL SUPPORTED ON ZEOLITE BETA.....	72
Abstract.....	72
5.1 Introduction.....	73
5.2 Experimental.....	76
5.2.1 Catalyst preparation.....	76
5.2.2 Reduction of Ni/HBEA and NiPt/HBEA.....	77
5.2.3 Toluene desorption on 5Ni/HBEA by in situ XAS.....	80
5.2.4 Toluene hydrogenation on 5Ni/HBEA by in situ XAS.....	80
5.3 Results and discussion.....	81
5.3.1 Catalysts characterization.....	81
5.3.2 Reduction of nickel on Beta catalysts results.....	86
5.3.3 In situ XAS measurement during toluene desorption on 5Ni/HBEA.....	97
5.3.4 In situ XAS results of toluene hydrogenation.....	100
5.4 Conclusions.....	104
5.5 References.....	105
VI CONCLUSIONS.....	107
APPENDICES.....	109

CONTENTS (Continued)

	Page
APPENDIX A NITROGEN ADSORPTION-DESORPTION ISOTHERMS OF 3Pd/HBEA, 3Pt/HBEA and 3Pt3Pd/HBEA.....	110
APPENDIX B LINEAR COMBINATION FITTING RESULTS OF 5Ni0.5Pt/HBEA DURING IN SITU REDUCTION FROM ROOM TEMPERATURE TO 300°C	114
APPENDIX C LINEAR COMBINATION FITTING RESULTS OF 5Ni0.5Pt/HBEA DURING IN SITU REDUCTION AT 350°C WITH HOLDING TIME OF 90 MINUTE	120
CURRICULUM VITAE.....	126

LIST OF TABLES

Table	Page
3.1 Relative crystallinity of H-BEA with various gel Si/Al ratios ranging from 8 to 20	34
3.2 Area ratio of the strongest peaks of zeolite MTW and BEA	36
3.3 Acid amount of H-BEA zeolite with gel Si/Al ratios ranging from 8 to 20.....	38
4.1 Textural properties of HBEA and catalysts supported on HBEA.....	54
4.2 Pd L_{III} and L_{II} edges energy from XANES spectra.....	56
4.3 Catalytic selectivity to methylcyclohexane (MCH) and cyclohexane (CyH) of 3Pt3Pd/HBEA	65
5.1 Edge energy and percent of reduction of catalysts at ambient conditions.....	88
5.2 Pre-edge and edge position of 5Ni/HBEA during reduction in hydrogen flow at 350°C recorded from 10 to 90 min.....	96
5.3 Pre-edge and edge position of 5Ni/HBEA during toluene desorption as the temperature increased from room temperature.....	97
5.4 Pre-edge, edge position of 5Ni/HBEA and percent reduction during toluene hydrogenation at 150°C.....	103
5.5 Percent reduction of Ni in 5Ni/HBEA at 200°C.....	104

LIST OF FIGURES

Figure	Page
2.1 A schematic representation of the sample holder. At the right side it is represented the three extra plates that are fixed to the sample holder.	18
2.2 (a) Ethylidyne and (b) π -bonded ethene on a Pt ₆ cluster, as used in the FEFF8 calculations. Pt (dark-gray spheres), C (gray spheres), and H (white spheres).	21
3.1 XRD pattern of synthesized products with gel Si/Al ratios of 8 - 20.	32
3.2 XRD pattern of synthesized products with gel Si/Al ratios of 13, 50, 100, and 200.	35
3.3 Plot of area ratio between the strongest peak of zeolite MTW and BEA (Z/B) versus the gel Si/Al ratio.	37
3.4 SEM images of H-BEA (a) and (b) with gel Si/Al ratio of 13 and (c) sample prepared from gel Si/Al ratio of 200.	39
3.5 Particle size distribution of H-BEA sample with gel Si/Al ratio of 13.	39
3.6 N ₂ adsorption-desorption isotherm of H-BEA sample with gel Si/Al ratio of 13.	41
4.1 XRD profiles of HBEA and HBEA-supported catalysts.	53
4.2 NH ₃ -TPD profiles of HBEA and HBEA-supported catalysts.	55
4.3 XANES spectra of Pd standards measured at ambient condition.	57

LIST OF FIGURES (Continued)

Figure	Page
4.4 XANES spectra of calcined 1Pd/HBEA, 5Pd/HBEA and 3Pt3Pd/HBEA samples comparing with 5Pd/Al ₂ O ₃ standard at ambient condition.....	58
4.5 XANES results of 3Pt3d/HBEA during in situ reduction from room temperature to 300°C.....	59
4.6 XANES results of 3Pt3d/HBEA during increased temperature from 200 to 300°C.....	60
4.7 XANES results of 5Pd/Al ₂ O ₃ during reduction from 23 to 300°C using in situ XAS measurement.....	61
4.8 XANES results of 5Pd/Al ₂ O ₃ during reduction from 200 to 300°C using in situ XAS measurement.....	62
4.9 Toluene conversions on 3Pt3Pd/HBEA, 3Pt/HBEA and 3Pd/HBEA at various reaction temperatures.	64
4.10 (a) Toluene conversion (b) Selectivity for methylcyclohexane on 3Pt3Pd/HBEA at 100 and 200°C during the 5 h period.	67
5.1 Sample holder of in situ XAS cell, (a) show sample holder and (b) show the composition of sample holder; 1 = middle plate, 2 and 3 = cover plates. ...	78
5.2 XRD patterns of calcined 5Ni/HBEA compared with HBEA support.....	81
5.3 XANES profiles of calcined monometallic Ni catalysts compared with NiO standard from ambient condition measurements; raw data plots (a) and normalized data plots (b).	83

LIST OF FIGURES (Continued)

Figure	Page
5.4 XANES profiles of calcined bimetallic Ni catalysts compared with NiO standard from ambient condition measurements; raw data plots (a) and normalized data plots (b).	85
5.5 XANES profiles of reduced monometallic Ni catalysts compared with NiO standard from ambient condition measurements; raw data plots (a) and normalized data plots (b).....	87
5.6 XANES profiles of reduced bimetallic Ni catalysts compared with NiO standard from ambient condition measurements; raw data plots (a) and normalized data plots (b).....	89
5.7 XANES spectra at Ni edge of 5Ni0.5Pt/HBEA from in situ XAS measurement at various reduction temperature	91
5.8 The liner combination fitting of reduced 5Ni0.5Pt/HBEA at 100°C with 10 min holding time and 350°C with 90 min holding time	93
5.9 The degree of reduction of 5Ni/HBEA from Linear combination fitting in Athena program with reduction temperature.	94
5.10 Ni edge on 5Ni0.5Pt/HBEA with reduction temperature of 350°C from 10 to 90 min.	95
5.11 The degree of reduction of 5Ni0.5Pt/HBEA from Linear combination fitting plotting of reaction temperature of 350°C and reduction time.	96

LIST OF FIGURES (Continued)

Figure	Page
5.12 XANES spectra of 5Ni/HBEA catalyst during toluene desorption in N ₂ flow at 21, 100, 200, 250°C and after cool down to room temperature (a) and normalized spectra (b).....	98
5.13 Proposed mechanism of toluene hydrogenation on bifunctional catalyst.....	99
5.14 XANES spectra of calcined 5Ni/HBEA on toluene hydrogenation at 70°C and 110°C.....	101
5.15 XANES spectra of calcined 5Ni/HBEA on toluene hydrogenation at 150°C..	102
5.16 XANES spectra of calcined 5Ni/HBEA on toluene hydrogenation at 200°C..	103

CHAPTER I

INTRODUCTION

1.1 Introduction

This thesis focused on utilization of rice husk silica as a silica source for the syntheses of zeolite beta (BEA) which was used as a support of monometallic and bimetallic catalysts containing palladium (Pd), platinum (Pt) and nickel (Ni). The purity of rice husk silica was improved by leaching out inorganic components such as oxides of calcium, iron and aluminium in the husk with mineral acid before incineration (Kurama and Kurama, 2008 and Khemthong et al., 2007) to give silica with high purity. The obtained amorphous silica was used as a starting material for the BEA syntheses by hydrothermal method. The BEA in proton form (HBEA) is of interest as a catalyst in the conversion of organic chemicals due to its thermal and chemical stability, shape selectivity and high acidity. Combination of HBEA and active metals could further improve the catalytic performance as a bifunctional catalyst, meaning that both components are active for the same reaction. The noble metals including Pt, Pd and Ni were chosen as active metals and the catalysts were tested for toluene hydrogenation. The bifunctional catalysts were prepared by impregnation method and their catalytic activities for toluene hydrogenation were determined in a fixed-bed reactor.

This work also studied the electronic and geometric structure of monometallic and bimetallic catalysts on HBEA using X-ray absorption spectroscopy. This technique

could lead to a better understanding about interaction between the active phase and HBEA support that affects the dispersion of transition metals and the catalytic activity of the prepared catalyst (Chun et al., 1998). The nature of the active metal was also investigated. The changes of the catalysts after pretreatments such as calcination and reduction by hydrogen could be studied by both ambient conditions or with an in situ cell.

1.1.1 Extraction of rice husk silica

Rice husk is abundant in Thailand and its major inorganic component is silica. During production of rice, a large amount of rice husk is left as a waste. It is usually disposed of by combustion, thus giving rice husk ash (RHA). The chemical analysis shows that RHA contains about 90 wt% of silica. The high purity silica could be obtained by leaching the husk before incineration. In this work, rice husk was leached with HCl acid under a efflux condition and calcined at 550°C to give amorphous silica with 98 wt% purity. This silica is used further for the synthesis of zeolite beta.

1.1.2 Synthesis of BEA

BEA is a microporous material with aluminosilicate framework. The general formula of BEA in sodium form (NaBEA) is $\text{Na}_n\{\text{Al}_n\text{Si}_{64-n}\text{O}_{128}\}$, $n < 7$. It has diameters of 0.55×0.55 nm and 0.76×0.64 nm (Baerlocher et al., 2007 and Mintova et al., 2006). According to the beneficial properties of BEA such as its thermal and chemical stability, shape selectivity, and high acidity, the BEA was chosen as a support of metal catalysts.

The amount of acid sites and hydrophilic/hydrophobic properties of the microporous material can be manipulated by controlling the Si/Al ratio. The Si/Al

ratio is an important to characteristic of zeolites. The charge imbalance due to the presence of aluminium in the zeolite framework determines the ion exchange properties and induces potential acidic sites. As the Si/Al ratio increases, the cation content decreases, the thermal stability increases and the surface selectivity change from hydrophilic to hydrophobic. Moreover, the Si/Al ratios ranging could control the phase transition and the physical properties changing of the synthesized zeolite. In this work the BEA was synthesized by hydrothermal method with amorphous RHS and a tetraethylammonium hydroxide (TEAOH) template with gel Si/Al ratios ranging from 8 to 200. The BEA framework of all samples with different Si/Al ratio can be confirmed by X-ray diffraction (XRD). In addition, XRD can determine another by-product such as ZSM-12 zeolite (MTW). The zeolite properties can be studied by various techniques such as nitrogen adsorption-desorption analysis, scanning electron microscope and particle size analysis.

1.1.3 Bifunctional catalysts : Metal/zeolite support

Metal/acidic zeolite is a bifunctional catalyst that each component is capable of catalyzing a different reaction and compromising each other for the overall reaction. This type of catalyst is widely used in petroleum refining, especially in hydrocracking and hydroisomerization. Because transition states of catalytic mechanism occur both on metal and acid sites, the activity and selectivity of bifunctional catalysts can be determined by the characteristics of the metal sites and the zeolitic acid sites. In the other words, zeolite support enhances the catalytic activity and selectivity using the acids sites and the microporous properties. In this study Pt and/or Pd and the HBEA support were effective for toluene hydrogenation. One part of bifunctional catalyst is the zeolite support which is contained acid sites

and help to adsorb toluene molecule on the acid surface. Moreover, the zeolite improves dispersion of metal particles leading to an increase of active sites and hence, catalytic performance. Another part is metal sites that are adsorption sites for hydrogen which can spill over to react with adsorbed hydrocarbon molecules. Thus the bifunctional catalyst consisting of metal supported on acidic zeolite is expected to give a higher catalytic activity than metal supported on non acidic support catalysts.

1.1.4 Catalytic activity on toluene hydrogenation

Because of environmental regulations directed to lower hazardous emissions from vehicle exhaust and a growing demand for high quality diesel fuels, hydrotreating processes are interesting as a center stage in the modern refinery strategies (Sidhpuria et al., 2008). Moreover, decreasing the aromatic content led to an increase of the cetane number in the diesel. In this work, toluene hydrogenation was an example reaction of de-aromatic molecules in diesel composition with monometallic and bimetallic Pt, Pd catalysts supported on HBEA. The reaction testing was done in a fixed-bed reactor and reaction products were continuously detected by gas chromatography. The main product from toluene hydrogenation is methylcyclohexane (MCH) and by-products, from hydrocracking are cyclohexane (CyH) and methane. Comparison the activity and selectivity of monometallic and bimetallic catalysts at various temperatures was the main focusing in this research.

1.1.5 Catalyst characterization by X-ray absorption (XAS)

XAS, covering extended X-ray absorption fine structure (EXAFS) and X-ray absorption near-edge structure (XANES), has become an ideal and powerful tool to monitor species in heterogeneous catalysts. Because the understanding of local atomic structure and the chemical nature of active species in catalyst is important, this

technique is essential for elucidating catalytic phenomena and for designing the optimum catalyst in their specific catalyst application. More advantage of this technique is low detection limit of atomic content in the catalysts. Both EXAFS and XANES measurements in this work were conducted at Beamline8 (BL8) at the Synchrotron Light Research Institute (Public Organization), (SLRI), located in Suranaree University of Technology. Catalysts after calcination and reduction including monometallic and bimetallic Ni and/or platinum on HBEA were prepared and studied at Ni K-edge to determine Ni oxidation state and environment which suggested metal dispersion.

Furthermore, this work focused on monitoring of the electronic and geometric structure change during increasing reduction temperature. This result may help more understanding and suggesting the property effect on activity and selectivity of the catalysts. Moreover, the property changes of the catalysts with toluene adsorption were also monitored. Therefore, in situ XAS cell was designed according to literatures (Hayashi, 1998 and Bernardi et al., 2007) and setup at the BL8 of the SLRI.

The oxidation states of Ni at each stage of preparation and treatment were also the subject of interest in this thesis. These metals were expected to have positive charge after catalyst preparation and could be converted to metallic form after reduction.

1.2 Research objectives

- 1.2.1 To synthesize BEA using rice husk silica with various Si/Al ratio.
- 1.2.2 To characterize BEA with various techniques.
- 1.2.3 To prepare monometallic and bimetallic catalysts containing noble metal (Ni, Pt and Pd) on BEA in proton form using impregnation method.
- 1.2.4 To characterize the prepared catalysts by XRD, XAS, NH₃-TPD and N₂ adsorption-desorption.
- 1.2.5 To test catalytic activity for toluene hydrogenation and study the effect of reaction temperature and time to give high conversion and selectivity.
- 1.2.6 To design, assemble and test in situ XAS cell for studying structural and electronic properties of Ni species on HBEA at BL8 of the Synchrotron Light Research Institute (Public Organization), (SLRI) .

1.3 Scope and limitations of the study

- 1.3.1 Silica source for all syntheses of BEA was from rice husk.
- 1.3.2 The Si/Al ratios of synthesized BEA were varied from 8 to 200.
- 1.3.3 Ni, Pt and Pd were loaded onto BEA by incipient wetness impregnation for monometallic catalysts and co-impregnation for bimetallic ones by vary amount of metal loading.
- 1.3.4 Techniques to characterize the catalysts were those mainly available at Suranaree University of Technology.
- 1.3.5 The toluene hydrogenation was performed in a fixed-bed reactor at Institute of Material Chemistry, Vienna University of Technology,

Austria. It was designed for linearly ramping temperature from 30 to 350°C and pressure range from 0.15 to 0.02 bar. The catalysts for this test were monometallic Pt and Pd and bimetallic PtPd supported on HBEA.

- 1.3.6 The in situ XAS cell was designed for the use at the BL8 of the SLRI. It could be operated up to only 350°C due to the heater limit.

1.4 References

- Baerlocher, Ch., McCusker, L. B., and Olson, D. H. (2007). Atlas of Zeolite Framework Types, 6th ed. Elsevier, Amsterdam, Netherlands.
- Bernardi, F., Alves, M. C. M., Scheeren, C. W., Dupont, J., and Morais, J. (2007). In situ studies of nanoparticles under reaction with sulfur by XAS. **J. Electron Spectrosc.** 156 - 158: 186-190.
- Chun, W. J., Asakura, K., and Iwasawa, Y. (1998). The structure analysis of MoO_x/TiO₂(110) by polarization-dependent total-reflection fluorescence X-ray absorption fine structure. **Catal. Today.** 44: 309-314.
- Hayashi, Y. (1989). Automatic alignment correction system for an ellipsometric monitor. **Rev. Sci. Instrum.** 60: 2800-2801.
- Khemthong, P., Prayoonpokarach, S., and Wittayakun, J. (2007). Synthesis and characterization of zeolite LSX from rice husk silica. **Suranaree J. Sci. Technol.** 12: 367-379.
- Kurama, S. and Kurama, H. (2008). The reaction kinetics of rice husk based ordierite ceramics. **Ceram. Int.** 34: 269-272.

Mintova, S., Valtchev V., Onfroy T., Marichal C., Knozinger H., and Bein T. (2006).

Variation of the Si/Al ratio in nanosized zeolite Beta crystals. **Micropor.**

Mesopor. Mat. 90: 237-245.

Sidhpuria, K. B., Parikh, P.A., Bahadur, P., and Jasra, R. V. (2008). Rhodium

supported H-zeolite for the hydrogenation of toluene. **Ind. Eng. Chem. Res.**

47: 4034-4042.

CHAPTER II

LITERATURE REVIEW

2.1 Zeolite beta (BEA)

2.1.1 Zeolite beta from rice husk silica

In this work rice husk silica was used as a starting material for the syntheses of zeolite beta (BEA). Zeolites are hydrated crystalline aluminosilicates with open three-dimensional framework structures, made up of SiO_4 and AlO_4 tetrahedral linked by sharing their oxygen atom to form regular intracrystalline cavities and channels of atomic dimensions. Zeolites are conventionally prepared by hydrothermal method of the gel containing silica, alumina, cation, template and water. Different types of silica are known to produce different types of zeolites from the same gel mixture (Prasetyoko et al., 2006). Most of the silica sources used in the synthesis of zeolite are commercially available in the form of a solution, a gel, a fumed solid, a colloid, and an organic derivative such as tetraethylorthosilicate.

Several researchers synthesized zeolites from rice husk silica. Bajpai et al. (1981) obtained mordenite, Wang et al. (1998) synthesized ZSM-48 type zeolite using rice husk ash (RHA) as a silica source and Prasetyoko et al. (2006) succeeded in bench-scale experiments aimed at crystallization of zeolite Y, X and ZSM-5. In this work, amorphous silica extracted from rice husk was used as a starting material to prepare BEA which is interesting for many catalytic applications.

BEA was explored as a powerful catalyst in petrochemical applications and fine chemical synthesis, including epoxidation (Van der Waal et al., 1998), transalkylation (Lee et al., 1998), isomerization and acylation (Freese et al., 1999). It is a large pore zeolite with the formula $\text{Na}_n\{\text{Al}_n\text{Si}_{64-n}\text{O}_{128}\}$, $n < 7$ (Meier et al., 1996). The Si/Al ratio may vary from 8 to more siliceous (dealuminated) forms and finally an aluminium-free homologue.

BEA could be prepared by hydrothermal method (Prasetyoko et al., 2006) with a dry gel method and steam assisted crystallization methods (Matsukata et al., 2002). The main reagents in BEA syntheses were a silica source and organic templates. In an original synthesis of BEA patented by Wadlinger et al. (1968), tetraethylammonium hydroxide was used both as a templating and a structure-directing agent. Several other organic templating agents for the same purpose were explored (Prasetyoko et al., 2006).

2.1.2 Transformation of BEA with Si/Al ratio

The physicochemical properties of zeolites are strongly influenced by the framework composition. The claimed Si/Al range for BEA in the original patent was 5 - 100 (Wadlinger et al., 1967). Under the conventional hydrothermal condition, $\text{SiO}_2/\text{Al}_2\text{O}_3$ ratio of BEA was lower than that of the parent gel, indicating that the incorporation efficiency of silicon is lower than aluminum (Mintova et al., 2006). BEA readily crystallized with Si/Al ratios between 10 and 30.

The number of acid sites and the hydrophilic/hydrophobic properties of the microporous materials could be tuned by controlling the Si/Al ratio. Additionally, intensive effort targeted at the expansion of the Si/Al ratio out of this range has been made. A substantial decreased of the Si/Al ratio in the BEA-type structure would

offer a material with properties comparable to zeolite Y that would provide a good comparison of the structural effect on the acidic, catalytic and shape-selective properties of both materials. BEA with a Si/Al ratio lower than 8 was reported. Using relatively dense gel systems and very small amount of template, Borade and Clearfield (1994 and 1996) synthesized BEA with Si/Al = 5.2, which corresponds to 10.3 Al atoms per tetragonal unit cell.

Mintova and coworkers (2006) synthesized BEA in nanocrystal size using basic aluminosilicate precursor solutions upon hydrothermal treatment at 100°C. The synthesis used a colloidal precursor solution having the chemical composition: $0.35\text{Na}_2\text{O}:4.5(\text{TEA})_2\text{O}:x\text{Al}_2\text{O}_3:25\text{SiO}_2:295\text{H}_2\text{O}$, where x was varied between 0 and 0.50. The results revealed that the crystallization kinetics of nanosized BEA were dependent on the amount of Al in the precursor solutions. The nucleation and growth processes were faster in Al-rich systems. The crystallization process of BEA with Si/Al ratios in the initial solutions of 14, 23, and 32 was accomplished within 72 h, whereas longer crystallization times, 140 and 264 h, were necessary to obtain crystalline products with Si/Al ratios of 42 and infinity, respectively.

Chaikittisilp and coworkers (2008) synthesized BEA with the $\text{SiO}_2/\text{Al}_2\text{O}_3$ ratios ranging from 20 to 200 from alkali metal cation-free aluminosilicate gel under basic condition. The homogeneous mixtures with molar compositions of $\text{SiO}_2:x\text{Al}_2\text{O}_3:0.5\text{TEAOH}:y\text{NaX}$ (X: OH, Cl, or Br): $16\text{H}_2\text{O}$ ($x = 0.005 - 0.05$; $y = 0$ or 0.15) were subjected to hydrothermal treatment at 175°C for different periods of time. They found that MTW-type zeolite was crystallized as an impurity phase at higher $\text{SiO}_2/\text{Al}_2\text{O}_3$ ratios (at ≥ 100) and the presence of sodium cations also induced the formation of impurity phases. They concluded that the reactivity of aluminum species

strongly affects the incorporation of aluminum into the framework of BEA, balance of yields of silicon and aluminum could be tuned. In other words, the $\text{SiO}_2/\text{Al}_2\text{O}_3$ ratios could be adjusted by balancing the reactivity of aluminum and silicon sources.

2.1.3 Supported BEA catalysts on hydrogenation of aromatics

Supported noble metal catalysts are known for their high hydrogenation of aromatics at low reaction temperatures and moderate hydrogen pressures, and their low resistance to sulfur poisoning (Bartholomew et al., 1982). These catalysts were typically used in the second reactor of a two-stage process after hydrodesulfurization in the first reactor (Cooper and Donnis, 1996). Interestingly, high intrinsic activity of noble metals could be obtained on acidic, high surface area supports, e.g. a large pore BEA and zeolite Y in proton form (Lee and Rhee, 1998), because it was possible to arrange close proximity of the metal and acid sites. Moreover, the diffusion resistance of liquid resistance onto the pore was minimized in large-pore zeolite.

The noble metal deposited on acidic supports showed the high activity than when they supported on non acidic carriers. This has been related either to the polarization of the metal particle by nearby cations (Jansen and van Santen, 1990), or between the metal and the zeolite protons. In the latter case, the formation of the more reactive metal-proton adducts $[\text{M}_n\text{-H}_z]^{z+}$ has been proposed. However, some studies point out that, in addition to metal centers, the acid sites of the support also played role in aromatic hydrogenation. The hydrogenation of aromatic molecules adsorbed on acid sites by hydrogen spilled-over from the metal surface was confirmed recently for HFAU zeolite-supported noble metal catalysts (Navarro et al., 2000).

2.2 Catalytic hydrogenation of aromatics on bimetallic catalysts

Clean fuel research including desulfurization and dearomatization has become an important subject in environmental catalysis worldwide. The presence of aromatics imparted poor ignition quality and low cetane number to diesel, enhanced smoke point of jet fuel and increase in emission of particulate matters. These particulate matters as well as aromatics emissions were environmental hazards and were known to be responsible for various health problems when inhaled.

Toluene hydrogenation was chosen as the catalytic test reaction in this work because it proceeded at low temperatures, helping to ensure that catalyst clusters remain intact and stable during the reaction because the rates were affected by the electronic nature of the supported metal (Deutsch et al., 1997). The adsorption of toluene on metal particles was strong because of the interaction of the delocalized π -electron with the metal. A support effect that made the metal particles electron deficient has been suggested to make this adsorption stronger and caused the catalytic hydrogenation reaction to proceed at a lower rate. The effect of metal-acid balance in Pt-loading on dealuminate zeolite Y catalysts was studied over the hydrogenation of benzene by Wang and coworkers (1999). Both the catalytic activity and the yield of hydrogenation increased dramatically with Pt loading on a given support at low Pt load, but they increased slowly when Pt loads were higher than 0.5%. At constant Pt loading, the support with more Brønsted acid site favored the production of hydrogenation and improved the overall hydrogenation activity. It was proposed that over noble metal/acid zeolite catalysts the hydrogenation reaction could take place on metal sites as well as on acid sites.

Support metal catalysts modified by addition of a second metal might substantially differ in terms of activity or selectivity from their monometallic counterparts. The final goal of catalytic studies with alloy catalysts was to learn about the functioning of metals and to rationally design catalysts with improved catalytic properties (Rousset et al., 2001).

The hydrogenation was commercially performed using bifunctional catalysts containing of metal supported on either chlorinated alumina or zeolites. Their bifunctionality originates from the acidity of the support and the hydrogenation-dehydrogenation activity of finely dispersed metal particles. The most stable zeolite catalysts for hydrogenation are Pt or Pd supported on zeolite mordenite (MOR) or BEA (Roldán et al., 2008). The final conversion and selectivity depend on a number of parameters including the acidity and pore structure of the zeolite, the nature and dispersion of the supported metal, and the operating conditions such as temperature and contact time (Chica and Corma¹, 1999; Patriceon et al., 2001 and Raybaud et al., 2001).

Bimetallic catalysts based on the association of Pd and Pt have been extensively studied. Koussathana et al. (1991) found that bimetallic Pd-Pt formulations exhibited higher activities than the pure metals toward the hydrogenation of naphthalene and biphenyl. This enhancement of activity was dependent on the support. The structure of the resultant bimetallic species was not well-understood, mainly due to the fact that they were composed of very small and well-dispersed particles. Among others, bimetallic Pt-Pd catalysts have been deeply studied for hydrogenation.

Blomsma et al. (1997) reported that zeolite-supported Pd-Pt bimetallic bifunctional catalysts were more active and selective in the isomerization of heptane

than pure Pt or Pd on the same support. The Pt-Pd system was also studied by Carturan et al. (1984) as a function of the Pd/Pt ratio. They reported that in the styrene hydrogenation, the activity of the bimetallic system displays a remarkable increase up to 30% of Pt whereas in the range of 30 - 100% Pt, the activity is simply the sum of individual activities.

On the other hand, Deganello and coworkers (1995) observed that the addition of Pt reduced both the activity and selectivity of the Pd catalysts in the liquid-phase hydrogenation of 1,3-cyclooctadiene to cyclooctene. In the case of the hydrogenation of phenylacetylene to styrene, Carturan and coworkers (1984) found that the specific activity of Pd-Pt catalysts was smaller than the sum of individual Pd and Pt in the 10 - 100% Pt range.

Other studies have focused on the sulfur tolerance of Pt-Pd alloy deposited on different supports such as Al_2O_3 , $\text{SiO}_2 - \text{Al}_2\text{O}_3$, $\text{Al}_2\text{O}_3 - \text{B}_2\text{O}_3$, or zeolite Y in proton form (Rousset et al., 2001). Industrial application for hydrogenation of aromatics and olefins in hydrocarbon feedstocks on such Pd - Pt alloys were proposed and actually used in plants (Cooper and Donnis, 1996). This high sulfur resistance, greatly enhanced by using acidic supports, was often believed to arise from the formation of electron-deficient metal particles.

Rousset and coworkers (2001) studied the hydrogenation of toluene over γ - Al_2O_3 -supported Pt, Pd, and Pt-Pd clusters. The results showed that the activity of the bimetallic catalysts did not show any synergy between Pd and Pt but rather a perfect additivity of their individual catalytic properties. Pt has been shown to have no electronic influence on the reactivity of Pd atoms.

2.3 X-ray absorption spectroscopy

X-ray absorption spectroscopy (XAS) provides structural information around a specific atom such as coordination number, atomic distances using extended X-ray absorption fine structure (EXAFS). The electronic properties or oxidation state of absorbing atoms was investigated X-ray absorption near edge spectroscopy (XANES). XAS is a powerful tool to obtain structural information of different types of materials lacking long range order: catalysts, inorganic materials, minerals, organometallic complexes and biological samples like enzymes (Hashnain et al., 1999). The local geometry and electronic state of a specific atom could be probed. Materials studied could be either in the gaseous, liquid or solid state. In catalysis, knowledge of the structure of active site and interaction between the catalytic sites and reacting molecules led to an increased understanding of the processes occurring at the active centers (Browne et al., 1991). This could eventually result in the development of better catalysts. Moreover, XAS has become a popular tool in research of heterogeneous catalytic system where small particles of chemically active elements were dispersed on the suitable support. Changes of catalysts in the presence of substrate at various experimental conditions can be studied in in situ XAS cells.

2.3.1 In situ XAS cell design

An in situ XAS cell is used to study the catalysts under reaction conditions similar to those in a plug flow reactor when the catalysts are under a flow of gas substrate. The XAS measurements in the in situ cell allow in observation of changes during the catalysts pretreatment and reaction. It is important that the in situ cell must be gastight, resistant to reactive gases and can be heated to $\sim 500^{\circ}\text{C}$ and cooled down to a desired temperature. Evacuation of the cell for sample pretreatment should be

possible and quick. The cell must be transparent for incoming and transmitted X-ray beam. Sandstrom and Lytle (1979) reported an in situ cell containing boron nitride or beryllium boat which held the sample powder from radiation leaks which could affect the experimental data. Some of the designs consisted of Mylar X-ray windows which were not oxygen tight, while others have dynamic O ring seals which introduced possible leaks. At low temperature, the brass part could not either ensure the leak.

Bernardi and coworkers (2007) designed an in situ XAS cell to investigate an interaction of sulfur on Pt nanoparticle catalysts. The cell design enabled the sample heating to 500°C in the reduction and sulfidation process. The reactor consists of a stainless steel pipe and Kapton® window for the incoming radiation. The cell could be used for XAS measurement in both transmission and fluorescence modes. The cell parts are shown in Figure 2.1. The catalyst in the form of a pellet or in powder, was positioned between the second and third plate. The external plates have Kapton® foil windows. All parts were bolted together in order to ensure a tight gas seal. The sample atmosphere was confined within the sample holder windows and it was isolated from the inner part of the reactor.

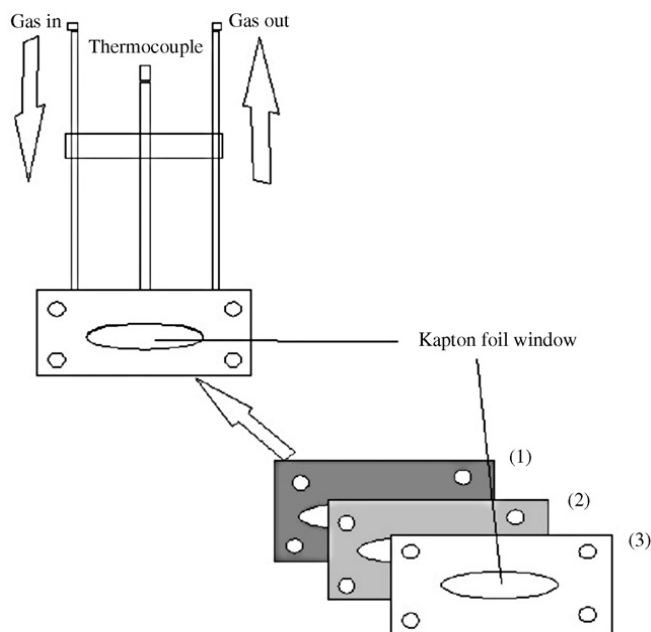


Figure 2.1 A schematic representation of the sample holder. At the right side it is represented the three extra plates that are fixed to the sample holder (from Bernardi et al., 2007).

2.3.2 Electronic and geometric structures of supported metal studied using XAS

Supported metal catalysts consist of active phase (transition metal ions, oxides, or metal complexes) and support (metal oxides, zeolites or porous polymers). The active phase-support interaction affects the dispersion of transition metals and the catalytic activity of the prepared catalyst (Yang et al., 1998). The supported metal catalysts activate hydrocarbon molecules and are therefore widely applied in the chemical industry. The adsorption modes of the reactants, intermediates, and products affect their activity and selectivity. These adsorbates occupy a specific site on the metal surface, which depends on the type of metal, the cluster size, the metal

oxide support, and alloying. Revealing the structures of the adsorption sites provides insight into the mechanisms of how small metal clusters activate hydrocarbon molecules, which, ultimately, enable tuning of the catalytic performance (Bus et al., 2007).

Dispersion of active phase could be enhanced by controlling the metal-support interaction. The best method to control dispersion is by a proper selection of preparation conditions. Pre-treatment gases, pre-treatment temperature, choice of metal precursor and morphology of support are important to control the dispersion of resulting catalysts. Zou and Gonzalez (1992) reported the effect of pre-treatment on the dispersion of Pt/SiO₂ and Pd/SiO₂ catalysts prepared from amine precursors in basic solution. Starting from [Pd(NH₃)₄]²⁺, this complex reacts with H₂ to form highly mobile intermediate species, [Pd(NH₃)₂(H)₂]⁰, which led to agglomeration of Pd particles. On the other hand, a pre-treatment with inert gases such as Ar or N₂ led to highly dispersed Pd/SiO₂ catalysts, due to the formation of strongly bound Pd²⁺ species with SiO₂ support.

Another method to enhance the dispersion of supported metal catalyst is changing of electronic properties of noble metals by introducing non-reducible transition metal ions (Yermakov et al., 1976; Tzou et al., 1986; Ichikawa et al., 1986 and Fukuoka et al., 1987). Yermakov et al. (1976) suggested that easily reducible Pt metal could be chemically anchored to the SiO₂ support by introducing non-reducible or partially reducible metal ions (Mo or W). In this system, non-reducible metals like Mo or W act as an anchoring site for the reducible metal. Tzou and coworkers (1986) showed that small Pt and Rh particles in Y zeolite could be prepared by the addition of Fe and Cr ions. The Fe or Cr ions are electrostatically bound to the zeolite oxygen

atoms, which act as anchoring sites and prevent the migration of Rh and Pt atoms. These reports emphasized the importance of pretreatment conditions and chemical anchoring in obtaining enhanced metal-support interaction in the preparation steps. Despite the importance of these interactions, the effects of metal-support interaction on the preparation of highly dispersed catalyst were still ill-defined.

Bus and Bokhoven (2007) used in situ XAS to study the structure of the Pt and Au supported on SiO₂ and TiO₂ under various conditions. The white line of L₂ and L₃ edges in the XANES spectra of Pt and Au probed the shape and the electron density of the 5d valence band. XAS results showed that the structure of the Pt and Au nanoclusters were differed from that of the bulk materials. Preparation of SiO₂- and TiO₂-supported PtAu catalysts from a Pt₂Au₄(C=CBu[†])₈ precursor resulted in well-mixed bimetallic clusters. Au was preferentially located on the surface of the small clusters. X-ray absorption near-edge spectroscopy (XANES) showed that the electronic structure of Pt and Au differed from that in the monometallic clusters. Furthermore, the white-line intensity increased for Au and decreased for Pt.

Furthermore, Bus, and coworkers (2007) used in situ XAS to study ethylene adsorption on supported Pt and Au under various temperatures and pressures. The ability of in situ XAS could detect the structure of the adsorbate sites on supported Pt catalysts that activate hydrocarbons. Furthermore, the catalytic activity of Pt alloyed with Au was distinctly different from that of the pure metal. This different catalytic activity could originate from geometry and electronic effects inducing different modes of adsorption as experimentally observed (Yeates et al., 1987). The ethene-induced changes in the XAS spectra as a function of temperature and pressure were correlated to changes in the adsorption mode of the hydrocarbon.

At low temperature, ethene was adsorbed in on-top (π) and bridged ($\text{di-}\sigma$) sites on small platinum clusters in Figure 2.2. Below room temperature, the adsorbed ethene was dehydrogenated to an ethylidyne species, which was adsorbed in threefold Pt sites. On larger clusters the dehydrogenation proceeded at higher temperature indicating a different reactivity. EXAFS results showed that changes in the geometrical structures were mainly due to (co)adsorbed hydrogen.

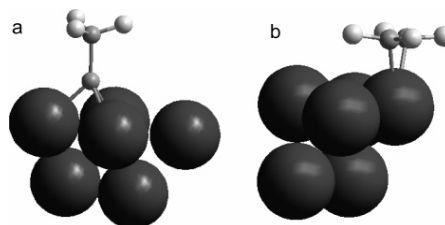


Figure 2.2 (a) Ethylidyne and (b) π -bonded ethene on a Pt₆ cluster, as used in the FEFF8 calculations. Pt (dark-gray spheres), C (gray spheres), and H (white spheres) from Bus et al., 2007.

2.4 References

- Bajpai, P. K., Rao, M. S., and Gokhale, K. V. G. K. (1981). Synthesis of mordenite type zeolite using silica from rice husk ash. **Ind. End. Chem.Prod. Res. Dev.** 20: 721-726.
- Bartholomew, C. H., Agrawal, P. K. and Katzer, J. R. (1982). Sulfur poisoning of metals. **Adv. Catal.** 31: 135-235.
- Bernardi, F., Alves, M. C. M., Scheeren, C. W., Dupont, J. and Morais, J. (2007). In situ studies of nanoparticles under reaction with sulfur by XAS. **J. Electron. Spectrosc.** 156 - 158: 186-190.

- Blomsma, E., Martens, J. A., and Jacobs, P. A. (1997). Isomerization and hydrocracking of heptane over bimetallic bifunctional PtPd/H-Beta and PtPd/USY Zeolite Catalysts. **J. Catal.** 165: 241-248.
- Borade, R. B. and Clearfield, A. (1994). Synthesis of zeolite Beta from dense system containing a minimum of template. **Catal. Lett.** 26: 285-289.
- Borade, R. B. and Clearfield, A. (1996). Preparation of aluminum-rich Beta zeolite. **Micropor. Mater.** 5: 289-297.
- Browne, V. M., Fox, S. G., and Hollins, P. (1991). Infrared spectroscopy as an in situ probe of morphology. **Catal. Today.** 9: 1-14.
- Bus, E. and van Bokhoven, J. A. (2007). Electronic and Geometric Structures of Supported Platinum, Gold, and Platinum–Gold Catalysts. **J. Phys. Chem. C.** 111: 9761-9768.
- Bus, E., Ramaker, D. E., and van Bokhoven, J. A. (2007). Structure of Ethene Adsorption Sites on Supported Metal Catalysts from in Situ XANES Analysis. **J. Am. Chem. Soc.** 129: 8094-8102.
- Carturan, G., Cocco, G. Facchin, G., and Navazio, G. (1984). Phenylacetylene hydrogenation with Pd, Pt and Pd/It alloy catalysed dispersed on amorphous supports: effect of Pt/Pd ratio on catalytic activity and selectivity. **J. Mol. Catal.** 26: 375-384.
- Chaikittisilp, W., Yokoi, T., and Okubo, T. (2008). Crystallization behavior of zeolite beta with balanced incorporation of silicon and aluminum synthesized from alkali metal cation-free mixture. **Micropor. Mesopor. Mat.** 116: 188-195.
- Chica, A. and Corma A. (1999). Hydroisomerization of pentane, hexane, and heptane for improving the octane number of gasoline. **J. Catal.** 187: 167-176.

- Cooper, B. H. and Donnis, B. B. L. (1996). Aromatic saturation of distillates: an overview. **Appl. Catal. A.** 137: 203-223.
- Deganello, G., Duca, D., Liotta, L. F., Martorana, A., Venezia, A. M., Benedetti, A., and Fagherazzi, G. (1995). Pumice-supported Pd-Pt bimetallic catalysts: synthesis, structural characterization, and liquid-phase hydrogenation of 1.3-cyclooctadiene. **J. Catal.** 151: 125-134.
- Deutsch, S. E., Xiao, F. S., and Gates B. C. (1997). Near absence of support effects in toluene hydrogenation catalyzed by MgO-Supported Iridium clusters. **J. Catal.** 170: 161-167.
- Bus, E., Ramaker, D. E., and van Bokhoven, J. A. (2007). Structure of ethene adsorption sites on supported metal catalysts from in situ XANES analysis. **J. Am. Chem. Soc.** 129: 8094-8102.
- Freese, U., Heinrich, F., and Roessner, F. (1999). Acylation of aromatic compounds on H-Beta zeolites. **Catal. Today.** 49: 237-244.
- Fukuoka, A., Ichikawa, M., Hriljac, J. A., and Shriver, D. F. (1987). Promoter effect of iron on olefin hydroformylation catalyzed by silica-supported rhodium-iron bimetallic carbonyl clusters: Rh-Fe³⁺ bimetallic activation of catalytic carbon monoxide insertion. **Inorg. Chem.** 26: 3643-3645.
- Hashnain, S. S., Helliwell, J. R., and Kamitsubo, H., (1999). XAFS conference proceedings and JSR. **J. Synchrotron Radiat.** 6-3: 121-122.
- Ichikawa, M., Fukushima, T., Yokoyama, T., Kosugi, N., and Kuroda, H. (1986). EXAFS evidence for direct Rh-Fe bondings in SiO₂-supported Rh-Fe bimetallic catalysts. **J. Phys. Chem.** 90: 1222-1224.

- Jansen, A. P. J. and van Santen, R. A. (1990). Hartee-Fock-Slater calculation on cation-induced changes in the adsorption of CO on Ir₄ clusters. **J. Phys. Chem.** 94: 6765-6772.
- Koussathana, M., Vamvouka, D., H. Economou, and Verykios, X. (1991). Slurry-phase hydrogenation of aromatic compounds over supported noble metal catalysts. **Appl. Catal.** 77: 283-301
- Lee, J. K. and Rhee, H. K. (1998). Sulfur tolerance of zeolite beta-supported Pd-Pt catalysts for the isomerization of n-hexane. **J. Catal.** 177: 208-216.
- Lee, Y. K., Park, S. H., and Rhee, H. K. (1998). Transalkylation of toluene and 1,2,4-trimethylbenzene over large pore zeolites. **Catal. Today.** 44: 223-233.
- Matsukata, M., Osaki, T., Ogura, M., and Kikuchi, E. (2002). Crystallization behavior of zeolite beta during steam-assisted crystallization of dry gel. **Micropor. Mesopor. Mat.** 56: 1-10.
- Meier, W. M., Olson, D. H., and Baerlocher, Ch. (1996). Atlas of Zeolite Structure Types, fourth ed. International Zeolite Association, Netherlands.
- Mintova, S., Valtchev, V., Onfroy, T., Marichal, C., Knözinger, H., and Bein T. (2006). Variation of the Si/Al ratio in nanosized zeolite Beta crystals. **Micropor. Mesopor. Mater.** 90: 237-245.
- Navarro, B. M., Pawelec, B., Trejo, J. M., Mariscal, R., and Fierro. J. L. G. (2000). Hydrogenation of aromatics on sulfur-resistant PtPd bimetallic catalysts. **J. Catal.** 189: 184-194.
- Patrigeon, A., Benazzi, E., Travers, C., and Bernhard, J. Y. (2001). Influence of the zeolite structure and acidity on the hydroisomerization of n-heptane. **Catal. Today.** 65: 149-155

- Prasetyoko, D., Ramli, Z., Endud, S., Hamdan, H., and Sulikowsk, B. (2006). Conversion of rice husk ash to zeolite beta. **Waste Management**. 26: 1173-1179.
- Raybaud, P., Patrigeon, A., and Toulhoat, H. (2001). The origin of the C₇-hydroconversion selectivities on Y, β, ZSM-22, ZSM-23, and EU-1 zeolites. **J. Catal.** 197: 98-112.
- Roldán, R., Beale, A. M., Sánchez, M. S., Salguero, F. J. R., Sanchidrián, C. J., Gómez, J. P., and Sankar, G. (2008). Effect of the impregnation order on the nature of metal particles of bi-functional Pt/Pd-supported zeolite Beta materials and on their catalytic activity for the hydroisomerization of alkanes. **J. Catal.** 254: 12-26.
- Rousset, J. L., Stievano, L., Cadete Santos Aires, F. J., Geantet, C., Renouprez, A. J. and Pellariny, M. (2001) Hydrogenation of toluene over γ-Al₂O₃-supported Pt, Pd, and Pd–Pt model catalysts obtained by laser vaporization of bulk metals. **J. Catal.** 197: 335-343.
- Sandstrom, D. R. and Lytle, F. W. (1979). Developments in Extended X-Ray Absorption Fine Structure Applied to Chemical Systems. **Ann. Rev. Phys. Chem.** 30: 215-238.
- Tzou, M. S., Jiang, H. J., and Sachtler, W. M. H. (1986). Chemical anchoring of platinum in zeolites. **Appl. Catal.** 20: 231-238.
- Van der Waal, J. C., Rigutto, M. S., and van Bekkum, H. (1998). Zeolite titanium beta as a selective catalyst in the epoxidation of bulky alkenes. **Appl. Catal. A Gen.** 167: 331-342.

- Wadlinger, R. L., Kerr, G. T., and Rosinski, E. J. (1967). Synthesis zeolite beta. US Patent 3308069.
- Wang, H. P., Lin, K. S., Huan, Y. J., Li, M. C., and Tsaur, L. K. (1998). Synthesis of zeolite ZSM-48 from rice husk ash. **J. Hazard. Mater.** 58: 147-152.
- Wang, J., Li, Q. Z., and Yao J. D. (1999). The effect of metal-acid balance in Pt-loading dealuminated Y zeolite catalysts on the hydrogenation of benzene. **Appl. Catal. A: Gen.** 184: 181-188.
- Yangl, J. C., Shula, Y. G., Louisb, C., and Che. M. (1998). In situ EXAFS study of the nucleation and crystal growth of Ni particles on SiO₂ support. **Catal. Today.** 44: 315-325.
- Yeates, R. C. and Somorjai, G. A. (1987). Surface structure sensitivity of alloy catalysis: catalytic conversion of n-hexane over Au-Pt(111) and Au-Pt(100) alloy crystal surfaces. **J. Catal.** 1987. 103: 208-212.
- Yermakov, Yu. I. (1976). Supported catalysts obtained by interaction of organometallic compounds of transition elements with oxide supports. **Catal. Rev.** 13: 77-120.
- Yermakov, Yu. I., Kuznetsov, B., and Ryndin, Yu. A. (1976). Hydrogenolysis of ethane on supported (Mo + Pt)/SiO₂ catalysts. **J. Catal.** 42: 73-78.
- Zou, W. and Gonzalez, R. D. (1992). The chemical anchoring of noble metal amine precursors to silica. **Catal. Today.** 15: 443-453.

CHAPTER III

SYNTHESIS OF ZEOLITE BETA WITH PRETEATED RICE HUSK SILICA AND ITS TRANSFORMATION TO ZSM-12

Abstract

Silica with 98% purity was prepared from rice husk by acid leaching and used as a silica source for the syntheses of zeolite beta (BEA) under hydrothermal conditions with gel Si/Al ratios of 8, 13, 15, 20, 50, 100, 150, and 200. Based on powder X-ray diffraction patterns, samples with gel Si/Al ratios of 8 - 20 contained only the pure phase of BEA and the highest relative crystallinity was observed in the BEA a with gel Si/Al ratio of 13. This sample was further characterized by scanning electron microscopy, particle size analyzer and N₂ adsorption analysis. The BEA particles were sphere shaped with the average particle size of 1.5 μm and a surface area of 670 m²/g. The samples with gel Si/Al ratios ranging from 50 to 200 showed mixed phases of BEA and ZSM-12 (MTW), and the latter phase was more dominant as the Si/Al ratio increased.

3.1 Introduction

Rice husk is composed of both organic (about 75 - 80 %) and inorganic components (about 20 - 25%) (Kurama et al., 2008). After the combustion to remove organic content, the ash contained silica with a purity of about 90% (Sun et al., 2001). The purity of rice husk silica (RHS) could be improved by leaching out inorganic components in the husk such as oxides of calcium or aluminium with mineral acid before incineration (Kurama et al., 2008 and Khemthong et al., 2007). The RHS could be used as a silica source for preparation of a number of porous materials such as MCM-41 (Grisdanurak et al., 2003), zeolite LSX (Khemthong et al., 2007) and zeolite ZSM-5 (Vempati et al., 2006 and Mohamed et al., 2008). This work focuses on the utilization of RHS as a silica source for the synthesis of zeolite beta in proton form (HBEA).

The general formula of BEA in sodium (NaBEA) form is $\text{Na}_n \{ \text{Al}_n \text{Si}_{64-n} \text{O}_{128} \}$, $n < 7$. It has a 3-dimensional large pore with a diameter of 0.76×0.64 nm (Baerlocher et al., 2007). The NaBEA could be synthesized by hydrothermal method with various silica sources and organic templates (Kim et al., 2004) then the procedure followed by exchanging with ammonium aqueous solution to form HBEA. The HBEA is of interesting as a catalyst in the conversion of organic chemicals due to its thermal and chemical stability, shape selectivity, and high acidity.

In the case of an aluminosilicate zeolite every instance of aluminum substitution into the lattice (ideally) creates an acid site. Zeolite framework composition is variously reported as the silicon to aluminum (Si/Al) ratio or the silica to alumina ($\text{SiO}_2/\text{Al}_2\text{O}_3$) ratio. These quantities are inversely proportional to acid site density. Acid site density is important in catalysis; for example, secondary reactions can be

more important on a catalyst with a high acid site density, and the acid site density must be considered in the design of experiments probing acid strength.

The acidity is an important property of catalytic supports for metal such as platinum and palladium, because it enhances the electron-deficiency of the metal. The amount of acid sites and the hydrophilic/hydrophobic properties of the microporous material can be manipulated by controlling the Si/Al ratio.

This chapter includes the syntheses of HBEA with amorphous RHS and a tetraethylammonium hydroxide (TEAOH) template by the hydrothermal method with gel Si/Al ratios ranging from 8 to 200. The synthesized products were characterized by powder X-ray diffraction (XRD) to confirm the formation of the BEA structure, compare the relative crystallinity and determine the crystal size. The acid amount in BEA was determined by X-ray fluorescence (XRF). The sample with only the pure BEA phase and the highest relative crystallinity was further analyzed with N₂-adsorption measurement, scanning electron microscopy (SEM), and a laser diffraction particle size analyzer (DPSA).

3.2 Experimental

3.2.1 Materials and chemicals

Rice husk was obtained from a local rice mill in Lampang Province, Thailand. Chemicals for the RHS preparation and BEA syntheses were hydrochloric acid (37% HCl, Carlo Erba), tetraethylammonium hydroxide (40 wt% TEAOH, Alfa), sodium chloride (NaCl, Ajax Fine Chem), potassium chloride (KCl, Ajax Fine Chem), sodium hydroxide (98% NaOH, Prolabo), and sodium aluminate (55 - 56 wt% NaAlO₂, Riedel-de Haen).

3.2.2 Preparation of rice husk silica (RHS)

RHS (with 98% purity) was prepared by a procedure described elsewhere (Wittayakun et al., 2008). Briefly, the rice husk was leached in 3 M HCl under the reflux conditions for 6 h to remove traces of other inorganic content besides silica, washed until the pH of the rinsing solution was ~ 7 , and pyrolyzed at 550°C. The obtained silica was in amorphous phase as indicated by XRD, similar to that in the literature (Wittayakun et al., 2008).

3.2.3 Synthesis of BEA

Zeolite beta in sodium form (NaBEA) was synthesized by a method modified from the literature (Cambor et al., 1998) with a gel Si/Al ratio varied from 8 to 200 and TEAOH was used as a template reagent to assist the formation of the zeolite framework. The RHS was dissolved in a NaOH solution before the addition of TEAOH. Then a solution of sodium aluminate with the desired Si/Al ratio was added and the mixture was stirred for 4 h. The obtained gel was crystallized in a teflon-lined autoclave at 135°C for 3 days and quenched in cold water. The product was separated by centrifugation, washed until the pH of the rinsing solution was ~ 9 , and dried at 100°C for 24 h. Finally, the template was removed by calcination at 550°C for 6 h. All samples were characterized by XRD (Bruker AXS Diffractometer D5005) and only samples with pure BEA phase were converted to proton form (HBEA). The Na-BEA zeolite was three times exchanged with 20wt% ammonium nitrate (NH_4NO_3) solution, each time for 8 h at 80°C to produce NH_4BEA . After separation by centrifugation, the NH_4BEA was washed with distilled water, dried at 110°C overnight and calcined in air at 400°C for 3 h to convert to HBEA.

3.3.4 Characterization of zeolite beta

The samples, after the template removal, were analyzed by XRD using Cu- K_{α} (1.54 Å) radiation, 2θ scan from 3 to 50°. The relative crystallinity of the samples with a pure Na-BEA phase was determined by comparing the total area of the major XRD peaks (Cambior et al., 1998 and Buurman et al., 1996) and the sample with the highest total peak area would give a relative crystallinity of 100%.

The Si/Al ratios were determined by X-ray fluorescence (XRF, EDS Oxford Instrument ED 2000). The samples and synthetic calibration standards for XRF analysis were prepared by borate-fusion technique (Tangkawanit et al., 2005). The flat sample disks were bombarded with X-ray generated with a high voltage of 40 kV and current of 30 mA. The quantities of oxides of silicon and aluminum were determined with a standard procedure and the acidities were calculated based on XRF measurements.

The morphology of the HBEA with highest the crystallinity was studied by SEM (JEOL JSM-6400) and the particle size distribution (PSD) was measured by a laser diffraction particle size analyzer (DPSA, Malvern Instruments, Mastersizer 2000). The DPSA method measures particles in a wide range from 0.02 μm to 2.0 mm. The measurements were conducted by dispersed the sample powder in distilled water with refractive index for light equal to 1.33. In the calculation of particle size, the Mie theory which describes the interaction between laser light and matter (by means of exact solution of Maxwells equations) was used.

The N_2 adsorption-desorption isotherm was obtained by a Micromeritics ASAP 2010 (Autosorb-1 series). Before measurement, each sample was degassed at 300°C for 3 h. The BET surface area was determined in the P/P_0 range of 0.01 - 0.3.

3.3 Results and discussion

3.3.1 XRD Characterization

After calcination, the synthesized products with gel Si/Al ratios ranging from 8 to 200 were characterized by XRD. The products with pure BEA phase were transformed to HBEA and characterized again with XRD. The gel Si/Al ratios that gave pure BEA phase were 8, 13, 15, and 20 and their spectra of the HBEA are shown in Figure 3.1. The spectrum contained large peaks of BEA at 7.8 and 22.4° along with small peaks similar to those of BEA synthesized from the commercial silica source and the simulated BEA spectrum (Wittayakun et al., 2004).

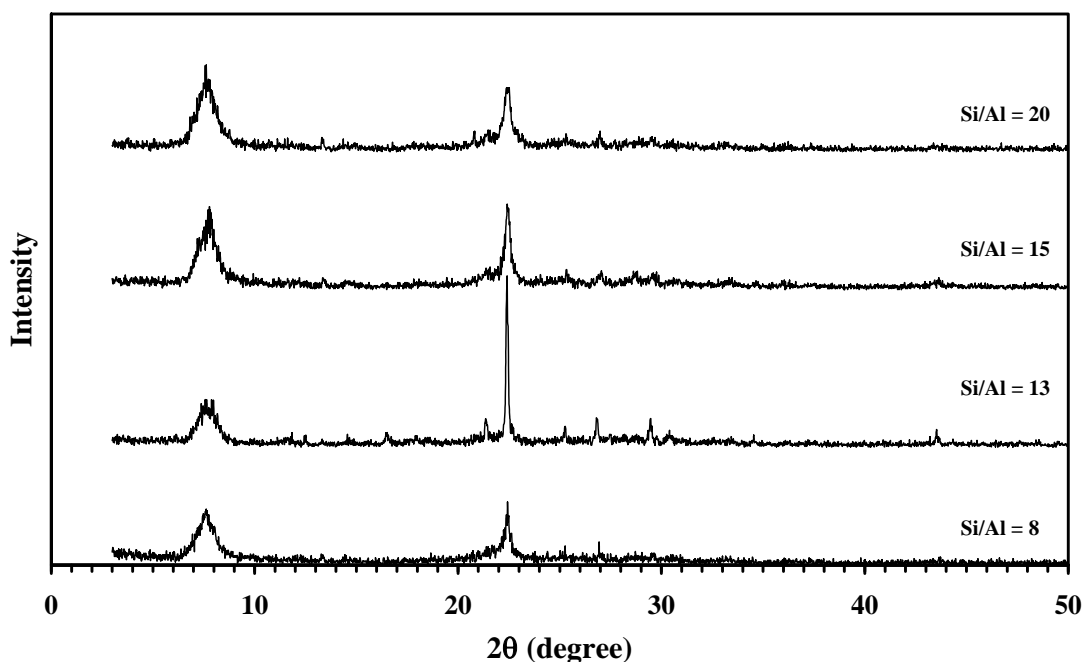


Figure 3.1 XRD pattern of synthesized products with gel Si/Al ratios of 8 - 20.

The relative crystallinities of HBEA with gel Si/Al ratios ranging from 8 to 20 are displayed in Table 3.1. The highest crystallinity was obtained from the sample

with the ratio of 13. The relative crystallinity of HBEA decreased with increasing of gel Si/Al ratio. In addition, Table 3.1 also shows the crystal size of these HBEA calculated by Scherrer's equation: $t = K\lambda/(B \cos\theta)$ where t was the averaged dimension of crystallites; K is the Scherrer constant, somewhat arbitrary value that falls in the range 0.9 - 1.0 (it was assumed to be 0.9 in this work); λ is the X-ray wavelength; and B was the integral breadth of a reflection (in radians 2θ) located at 2θ . The crystal size was largest in the sample with gel Si/Al ratio of 13.

Table 3.1 Relative crystallinity of HBEA with various gel Si/Al ratios ranging from 8 to 20

Gel Si/Al ratio	Total peak area	Relative crystallinity ^a	XRD Crystal size ^b (nm)
8	276.6	83	86
13	346.4	100	189
15	306.7	90	71
20	320.5	93	64

^acalculated from total area of peaks at $2\theta = 7.8$ and 22.4° , relative to the highest value (gel Si/Al ratio of 13)

^bcalculated from peak area at $2\theta = 22.4^\circ$ of XRD pattern by Scherrer equation

The XRD pattern of samples with gel Si/Al ratios ranging from 50 to 200 are shown in Figure 3.2 with that of one HBEA exemplary XRD spectrum from the sample with the gel Si/Al ratio of 13. The samples with gel Si/Al ratios ranging from

50 to 200 showed mixed phases containing characteristic peaks of the BEA and ZSM-12 zeolite (MTW) (Treacy et al., 2001; Gopal et al., 2001 and Wei et al., 2001). The phase change was indicated by a splitting of the BEA peak at 7.5° , a fading of the peak at 22.4° , and an emerging of a new peak at $\sim 21^\circ$. The phase change from BEA to ZSM-12 became more significant with a higher gel Si/Al ratio. In addition, an unknown phase with XRD peaks in the region of $14 - 16^\circ$ was also observed. At the ratio of 100 or more, the characteristic of ZSM-12 was dominant and the main peaks at 7.5 , 7.6 , 8.9 , 20.7 , and 22.5° were clearly observed (Baerlocher et al., 2007). The mixed phase of the BEA and MTW was reported previously in the synthesis of MTW with the Si/Al gel ratios of 25 and 30 and crystallization temperature of 160°C (Gopal et al., 2001).

To determine the degree of phase change from BEA to MTW in the samples with gel Si/Al ratios of 50 - 200, the ratio of the peak area of the most intense XRD peaks of BEA ($2\theta = 22.4^\circ$) to that of MTW ($2\theta = 21.0^\circ$) were determined and are displayed in Table 3.2.

Their ratios were plotted versus the Si/Al ratios in Figure 3.3 and a linear correlation was observed. The plot confirmed that the phase change increased as the Si/Al ratio increased. From the extrapolation, pure phase BEA should be obtained in the samples with the gel Si/Al ratio of less than 35. Note that the MTW peaks at 7.5 and 7.6° were not used because they overlapped with BEA peaks.

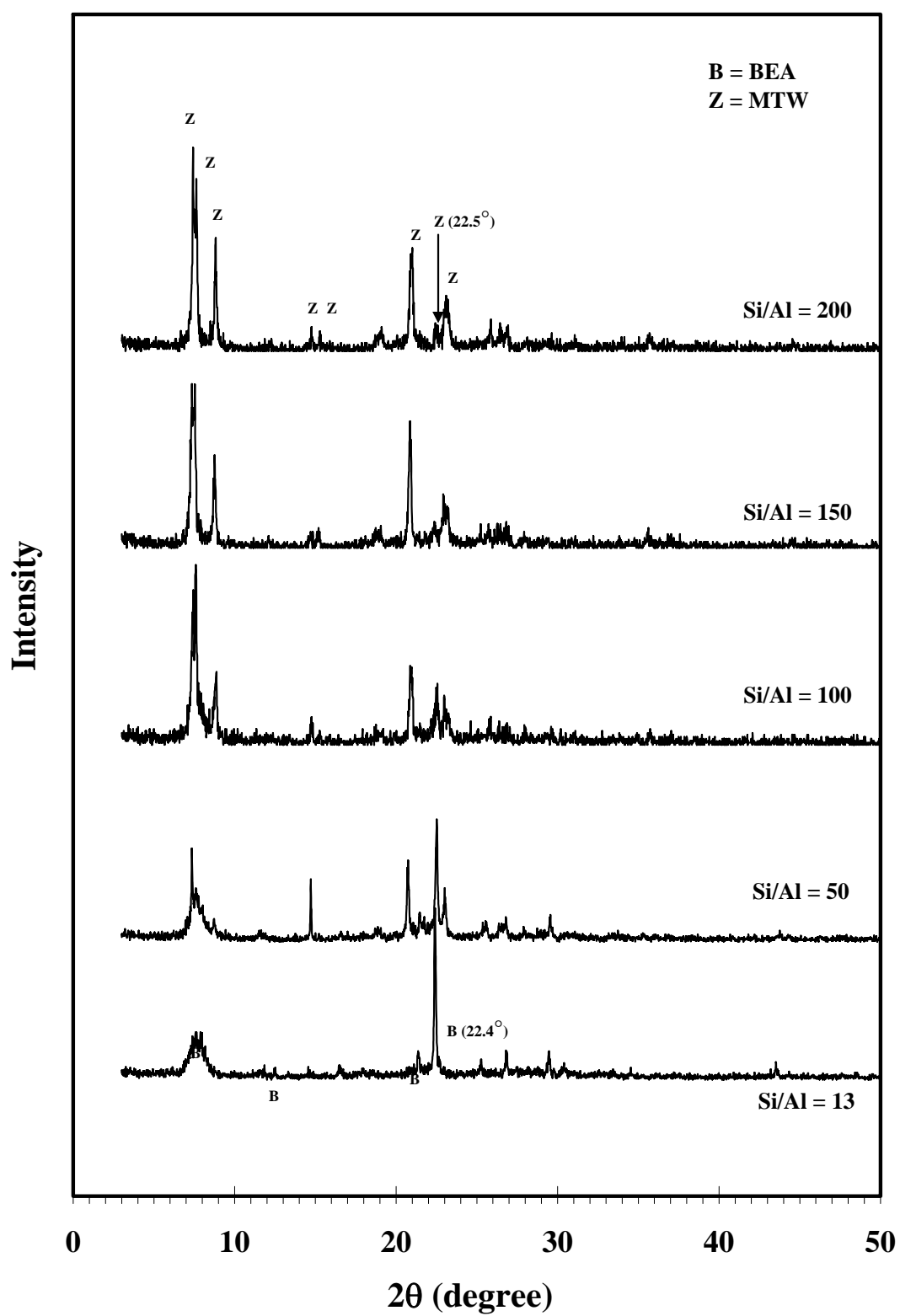


Figure 3.2 XRD pattern of synthesized products with gel Si/Al ratios of 13, 50, 100, and 200.

Table 3.2 Area ratio of the strongest peaks of zeolite MTW and BEA

Gel Si/Al ratio	Peak area at $2\theta = 21.0^\circ$ (ZSM-12)	Peak area at $2\theta = 22.4^\circ$ (Beta)
50	32.7	40.7
100	51.5	27.2
150	60.1	15.4
200	68.1	11.2

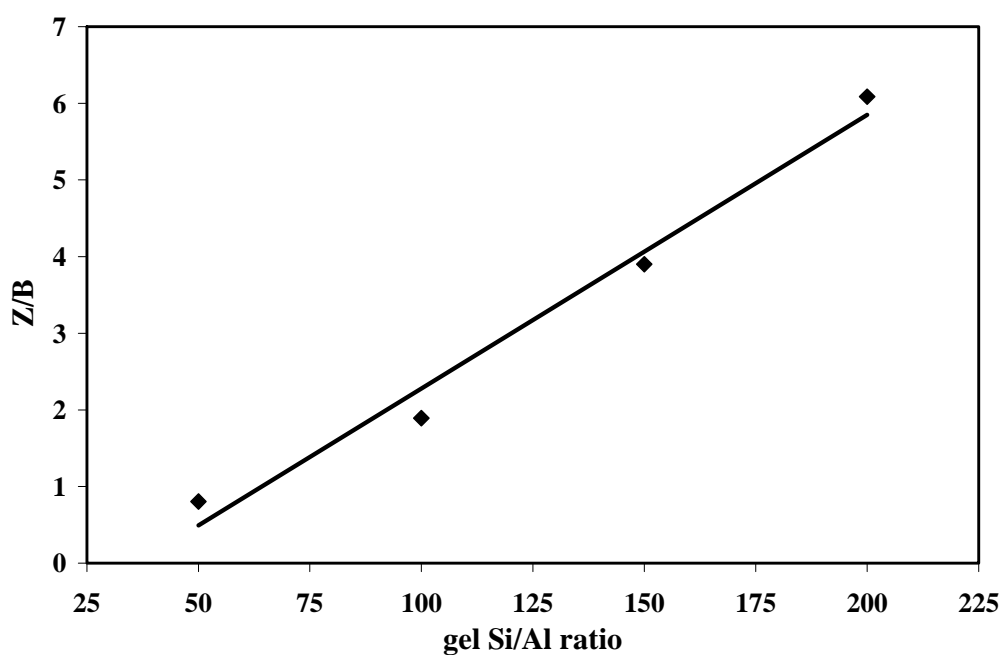


Figure 3.3 Plot of area ratio between the strongest peak of zeolite MTW and BEA (Z/B) versus the gel Si/Al ratio.

3.3.2 Acid amount of HBEA zeolite with pure phase

Table 3.3 shows the acid amount of HBEA synthesized with gel Si/Al ratio from 8 to 20 determined by XRF. The amount increased with aluminum content

in the samples. The acidity in zeolite is important as a catalytic function in heterogeneous catalyst. Although the HBEA with the Si/Al ratio of 13 did not have the highest acid amount, 1.17 mmol/g, it had the highest crystallinity and this ratio was considered to be the most suitable ratio for BEA synthesis with rice husk silica. The next part focused on further characterization of the BEA with the gel Si/Al ratio of 13.

3.4.3 Characterization of HBEA with gel Si/Al ratio of 13

The common properties of catalytic support are pure phase and high crystallinity which allow morphology control. The sample with the gel Si/Al ratio of 13 was interesting because it contained BEA in pure phase with the highest crystallinity; hence, it was further characterized by SEM, N₂ adsorption analysis, and laser diffraction particle size analysis (DPSA).

Table 3.3 Acid amount of HBEA zeolite with gel Si/Al ratios ranging from 8 to 20

Gel Si/Al ratio	Acid amount (mmol/g) ^a
8	2.60
13	1.17
15	1.04
20	0.94

^aCalculated by using % Al content from XRF results

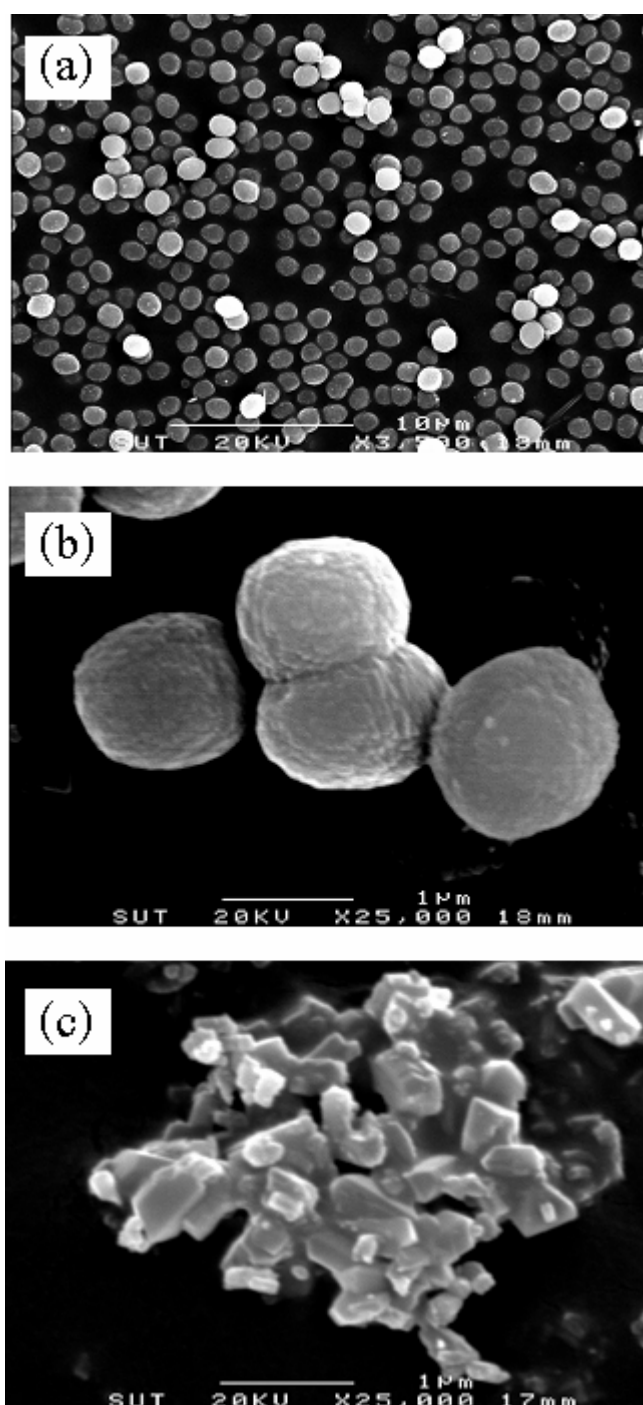


Figure 3.4 SEM images of HBEA (a) and (b) with gel Si/Al ratio of 13 and (c) sample prepared from gel Si/Al ratio of 200.

Figure 3.4 (a) and (b) shows the SEM micrograph of HBEA. The particles had a spherical shape and uniform size with a diameter about 1.5 μm . This size was similar to that of the commercial BEA which was synthesized by the same method (Liu et al., 2006). The morphology was much different from the sample synthesized with the gel Si/Al ratio of 200 which contained MTW as a major component. As shown in Figure 3.4 (c), MTW had shapes that were difficult to describe with crystals coalesced to form an aggregate.

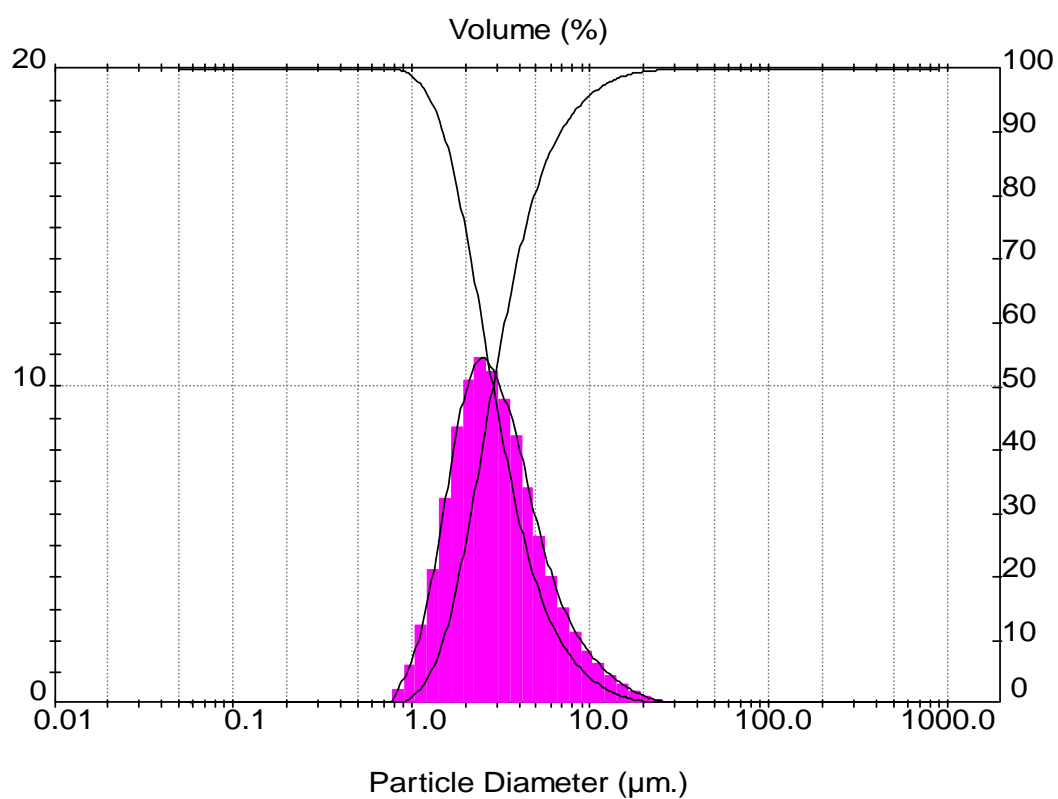


Figure 3.5 Particle size distribution of HBEA sample with gel Si/Al ratio of 13

Particle size distribution of HBEA sample with gel Si/Al ratio of 13 from DPSA analysis was the particle size distribution and the statistics of distribution calculated from the results using the derived diameters, an internationally agree method of defining the mean and other moments of particles size (BS2955, 1993). The percentage of volume sample that was under a certain particle size band (% under) at 10, 50, and 90% were 1.49, 2.79, and 6.29 μm , respectively. The width of distribution was 1.72 μm . The particle size distribution in all ranges by DPSA is displayed in a histogram in Figure 3.5, revealing that the obtained product were homogeneous in size. The average particle size from DPSA was approximately 3.52 μm . This average was larger than the particle size from SEM because several particles were fused together to form large particles.

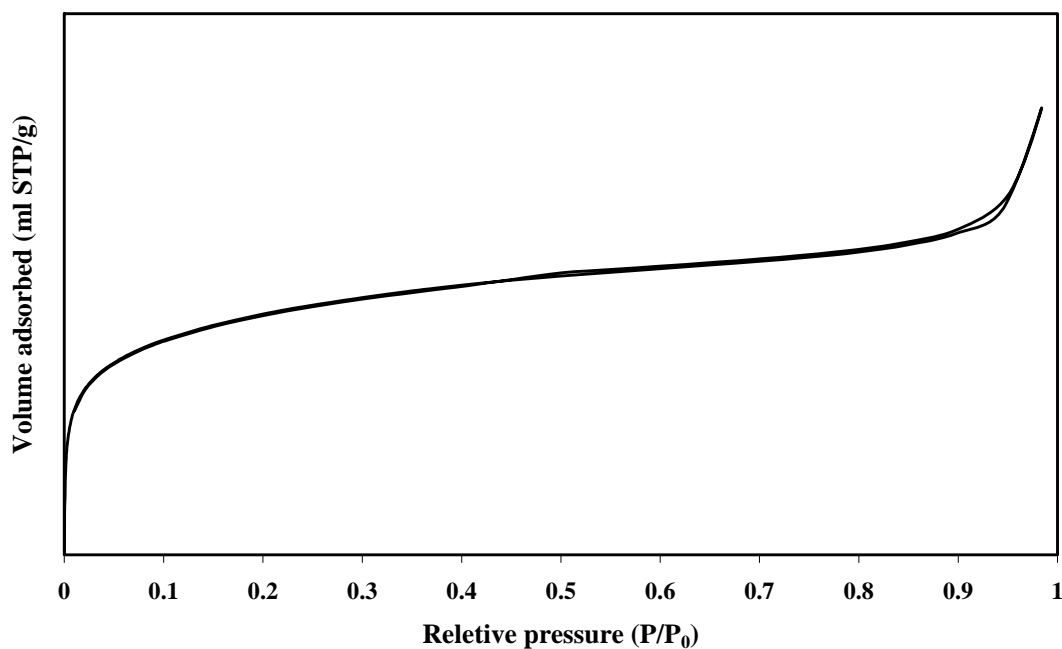


Figure 3.6 N_2 adsorption-desorption isotherm of HBEA with gel Si/Al ratio of 13

The N₂ adsorption-desorption isotherm of the BEA with the gel Si/Al ratio of 13 is shown in Figure 3.6. It could be classified as Type I which is a characteristic of microporous material, such as zeolite. The adsorbed amount of nitrogen gas (N₂) increased dramatically after the exposure to N₂ at a low relative pressure corresponding to quick adsorption of N₂ on the external surface and a concave to nearly constant volume due to monolayer adsorption. The slopes at a higher relative pressure were not completely flat indicating that multi-layer adsorption also occurred. The BET surface area of this sample was 670 m²/g and the micropore volume was 0.26 cm³/g.

3.4 Conclusions

Amorphous silica rice husk could be used as a silica source for HBEA synthesis by the hydrothermal method at 135°C and completed by crystallization for 3 days. The XRD results showed that the products with gel Si/Al ratios of 8 - 20 contained only the pure phase of BEA. The highest crystallinity and the largest crystal size were observed in the sample with the gel Si/Al ratio of 13. The samples with the gel Si/Al ratios of 50 - 200 showed a mixed phase of BEA and MTW. The phase of MTW became more significant with a higher Si/Al ratio and was almost pure at the ratio of 200. Analysis of HBEA with the gel Si/Al ratio of 13 by SEM showed a spherical morphology with the approximate particle size 1.5 μm. The surface area was 670 m²/g and acid amount was 1.17 mmol/g.

3.5 References

- Baerlocher, Ch., McCusker, L. B., and Olson, D. H. (2007). Atlas of Zeolite Framework Types, 6th ed. Elsevier, Amsterdam, Netherlands.
- Buurman, P., Vanlagen, B., and Velthorst, J. (1996) Manual for soil and water analysis, Backhuys, Netherlands.
- BS2955. (1993). Glossary of terms relating to particle technology. British Standards Institution.
- Cambor, M. A., Corma, A., and Valencia, S. (1998). Characterization of nanocrystalline zeolite Beta. **Micropor. Mesopor. Mat.** 25: 59-74.
- Gopal, S., Yoo, K., and Smirniotis, P. G. (2001). Synthesis of Al-rich ZSM-12 using TEOH as template. **Micropor. Mesopor. Mat.** 49: 149-156.
- Grisdanurak, N., Chiarakorn, S., and Wittayakun, J. (2003) Utilization of Mesoporous Molecular Sieves Synthesized from Natural Source Rice Husk Silica to Chlorinated Volatile Organic Compounds (CVOCs) Adsorption. **Korean J. Chem. Eng.** 20: 950-955.
- Khabuanchalad, S., Khemthong, P., Prayoonpokarach, S., and Wittayakun, J. (2008). Transformation of zeolite NaY synthesis from rice husk silica to NaP during hydrothermal synthesis. **Suranaree J. Sci. Tech.** 15: 225-231.
- Khemthong, P., Wittayakun, J., and Prayoonpokarach, S. (2007). Synthesis and characterization of zeolite LSX from rice husk silica. **Suranaree J. Sci. Tech.** 14: 367-739.
- Kim, D. S., Chang, J. S., Hwang, J. S., Park, S. E., and Kim, J. M. (2004). Synthesis of zeolite beta in fluoride media under microwave irradiation. **Micropor. Mesopor. Mat.** 68: 77-82.

- Kurama, S. and Kurama, H. (2008). The reaction kinetics of rice husk based cordierite ceramics. **Ceram. Int.** 34: 269-272.
- Liou, T. H. (2001). Preparation and characterization of nano-structured silica from rice husk. **Ind. Mater. Sci Eng.** 364: 313-323.
- Liu, Y., Guo, W., Zhao, X. S., Lian, J., Dou, J., and Kooli, F. (2006). Zeolite beta catalysts for *n*-C7 hydroisomerization. **J. Porous Mat.** 13: 359-364.
- Mohamed, M. M., Zidan, F., and Tabet, I. M. (2008). Synthesis of ZSM-5 zeolite from rice husk ash: Characterization and implications for photocatalytic degradation catalysts. **Micropor. Mesopor. Mat.** 108: 193-203.
- Tangkawanit, S. and Rangsiwatananon, K. (2005). Synthesis and kinetic study of zeolite from loburi perlite. **Suranaree J. Sci. Tech.** 12: 61-68.
- Treacy, M. M. J. and Higgins, J. B. (2001). Collection of simulated XRD Powder Patterns for Zeolites. 4th ed. Elsevier. (p.586). Amsterdam, Netherlands.
- Vempati, R. K., Borade, R., Hegde, R. S., and Komarneni, S. (2006). Template free ZSM-5 from siliceous rice hull ash with varying C contents. **Micropor. Mesopor. Mat.** 93: 134-140.
- Wittayakun, J., Grisdanurak, N., Kingler, G., and Vinek, H. (2004). Adsorption Behavior of NO and CO and Their Reaction over Cobalt on Zeolite Beta. Korean Journal Chemical Engineering. **Korean J. Chem. Eng.** 21: 950-955.
- Wittayakun, J., Khemthong, P., and Prayoonpokrach S. (2008). Synthesis and characterization of zeolite Y from rice husk silica. **Korean J. Chem. Eng.** 25: 861-864.
- Wei, X. and Smirniotis, P. G. (2006). Synthesis and characterization of mesoporous ZSM-12 by using carbon particles. **Micropor. Mesopor. Mat.** 89: 170-178.

CHAPTER IV

CATALYTIC ENHANCEMENT OF PLATINUM

SUPPORTED ON ZEOLITE BETA FOR TOLUENE

HYDROGENATION BY ADDITION OF PALLADIUM

Abstract

This chapter focused on preparation, characterization and catalytic performance of a bimetallic platinum-palladium catalyst for toluene hydrogenation. The catalyst with 3 wt% loading of each metal was prepared by co-impregnation on zeolite beta in proton form and denoted as 3Pt3Pd/HBEA. The structure of HBEA was retained after catalyst preparation and metal occupied strong acidic sites of the zeolite. By comparing to monometallic 3Pt/HBEA, the 3Pt3Pd/HBEA had smaller Pt particle size indicating a better dispersion on the support. The catalytic performance of the bimetallic catalyst at various temperatures indicated that the presence of Pd enhanced toluene hydrogenation of Pt catalyst at high temperature. The most suitable temperature for toluene hydrogenation on 3Pt3Pd/HBEA was 150°C where a complete toluene conversion was obtained with methylcyclohexane as the only product.

4.1 Introduction

Aromatic compounds are important components of gasoline because of their antiknock properties and some of them are raw materials for petrochemical products (Antos et al., 1995). However, there are upper limits from environmental regulations for these compounds and their concentrations can be controlled by methods such as catalytic hydrogenation by noble metals. In this work we focused on the use of bimetallic platinum-palladium catalysts supported on zeolite beta (BEA) for toluene hydrogenation. The chemical equation is displayed in scheme 1 showing methylcyclohexane (MCH) as the hydrogenation product and cyclohexane and methane as cracking by-products (Crowl and Louvar, 2000).

Platinum (Pt) is known as a suitable catalyst for several kinds of reactions such as hydrogenation, hydrogenolysis, isomerization and oxidation (Bartholomew and Farrauto, 2006). Its performance can be improved by dispersion on a support with high surface area. A catalyst that both metal and support are active for a reaction is called bifunctional catalyst. This type of catalyst is interesting because the performance of metals can be improved. Various types of zeolites which are aluminosilicate crystalline materials are good examples of active supports. They have acidic sites for adsorption of reactants and uniform pores or cavities for shape and size selectivity of organic molecules. Bifunctional catalysts containing metal on zeolites are widely used in petroleum refining, especially in hydrocracking and hydroisomerization. One example is bifunctional catalysts containing Pt on HBEA which were tested for n-heptane hydroisomerization. The increase of Pt content and/or Si/Al ratio of HBEA from 11.7 to 24.5 improved the yield and selectivity (Talebi et al., 2008).

Modification of the bifunctional catalyst by incorporating another metal can enhance the performance or improve stability. Stable catalysts for hydroisomerization are those containing Pt- or Pd-supported on zeolites such as mordenite (MOR) or BEA (Roldán et al., 2008). The final conversion and selectivity depend on a number of parameters including acidity and pore structure of the zeolite, the nature and dispersion of the supported metal, and the operating conditions such as temperature and contact time (Talebi et al., 2008).

Although, aromatic hydrogenation was known to be a metal-catalyzed reaction, the performance of Pt or Pd catalyst for aromatic hydrogenation reactions could be enhanced on acidic support (Chou and Vannice, 1987 and Lin and Vannice, 1993). Wang and coworkers found a remarkable improvement of the mechanical mixture of Pt/Al₂O₃ and zeolite Y over Pt/Al₂O₃ catalyst for the hydrogenation of benzene, toluene and *o*-xylene in spite of the fact that the zeolite Y itself was inactive for these reactions (Wang et al., 1999). It was proposed that the adsorbed aromatic molecules on acid sites could be hydrogenated by the spillover hydrogen which migrated from the surface of Pt/Al₂O₃ particles to the surface of zeolite particles.

Bimetallic catalysts based on the association of palladium have been extensively studied. Koussathana et al. (1991) found that the bimetallic Pt-Pd formulations gave higher activities than the monometallic ones and was dependent on the support. On the other hand, Carturan et al. (1984) found that the specific activity of Pt-Pd catalysts was lower than the sum of individual Pd and Pt in the 10 - 100% Pt range on the hydrogenation of phenylacetylene to styrene. Because the size, the structure, or the composition of supported bimetallic is difficult to control for active phases obtained by chemical methods, it is generally not straight forward to compare the catalytic

properties of bimetallic catalyst to those of a monometallic one. To obtain comparable results, Rousset and coworkers (2001) compared the monometallic and bimetallic systems having approximately the same size, morphology and overall uniformity. They observed that the activity of monometallic Pt was higher than bimetallic Pt-Pd and monometallic Pd catalysts.

Pawelec et al. (2002) studied simultaneous hydrogenation of toluene and naphthalene in the presence of dibenzothiophene on supported Pt-Pd catalysts on zeolite beta. They found that the activity of bimetallic catalysts was higher than the monometallic Pt at steady state and the conversion increased with metal loading. In addition, the bimetallic catalysts showed less deactivation by coking. Thomas et al. (2002) found that Pt-Pd catalysts on zeolite FAU and amorphous silica-alumina were more active for toluene hydrogenation in the presence of sulfur than monometallic catalysts. The support acidity also had influence on the Pt-Pd catalysts.

In this paper, we report the characterization and catalytic behavior of bimetallic Pt-Pd catalysts prepared by co-impregnation on HBEA and compared with monometallic ones. The catalysts were characterized by X-ray diffraction (XRD), N₂ adsorption-desorption analysis and NH₃ temperature-programmed desorption (NH₃-TPD). The catalytic behaviors were studied over toluene hydrogenation in a continuous flow fixed-bed reactor.

4.2 Experimental

4.2.1 Catalyst preparation

The support material for this work was zeolite beta in proton form (HBEA). Zeolite beta in sodium form (NaBEA) was synthesized with gel Si/Al ratio of 13 and

subsequently transformed to HBEA with a conventional ion exchange method (Talebi et al., 2008 and Loiha et al., 2009). Monometallic Pt and Pd catalysts were prepared by the incipient wetness impregnation with a solution of dihydrogen hexachloroplatinate ($\text{H}_2\text{PtCl}_6 \cdot 6\text{H}_2\text{O}$, 40%, supplied by the Right Chemical) and palladium (II) acetate ($\text{Pd}(\text{acac})_2$ 98%, supplied by Strem Chemicals) onto the HBEA. The loading of both metals were 3 wt% and these catalysts were referred to as 3Pt/HBEA and 3Pd/HBEA, respectively. Bimetallic catalysts were also prepared by co-impregnation with a solution containing both metal precursors with a concentration to produce 3 wt% loading of each metal and this catalyst was referred to as 3Pt3Pd/HBEA. Both mono- and bi-metallic catalysts were dried in air at 100°C for 3 h, calcined at 400°C for 3 h and characterized by X-ray diffraction (XRD), N_2 adsorption-desorption analysis and NH_3 temperature-programmed desorption (TPD).

4.2.2 Characterization techniques

The crystalline phase of samples were analyzed by powder XRD on a Bruker axS D5005 with $\text{Cu-K}\alpha$ (1.54 Å) with a step size of 0.02° in the 2θ range of 3 - 80°. Metal particle sizes were calculated from the line broadening of the highest peak intensity of metal Pt or Pd using Scherrer equation (Pawelec et al., 2006) in equation (1);

$$t = K\lambda / (B \cos\theta) \quad \dots(1)$$

where t is the averaged dimension of crystallites; K is the Scherrer constant, somewhat arbitrary value that falls in the range 0.9 - 1.0 (it was assumed to be 0.9 in this work); λ is the X-ray wavelength; and B is the width at half height of maximum peak in radians.

N_2 adsorption-desorption analysis of the calcined catalysts were carried out on a Micromeritics ASAP 2010. The samples were degassed in vacuum with a pressure of 10^{-3} mmHg at 300°C until physisorbed gas was completely removed. The analysis was carried out at liquid nitrogen temperature and the specific surface areas were determined from BET method in the relative pressure of 0.1 - 0.3.

The acidity of HBEA and HBEA-supported catalysts were determined by NH_3 -TPD. Each sample was pretreated with heat at 400°C in He (20 mL/min flow rate) for 90 min to eliminate physisorbed species and reduced in flowing H_2 for 3 h at 400°C before cooling to 100°C . Then a constant flow of 5 mL/min of NH_3 was introduced over the samples for 30 min to achieve saturation. After purging with He for 30 min to remove physisorbed species, the temperature was increased at a rate of $10^\circ\text{C}/\text{min}$ to 400°C . The amount of ammonia desorbed from the sample was recorded by a quadrupole mass spectrometer (Balzers QME 200). The number of acid sites was calculated from the peak area compared to a reference material (ZSM-5) with known number of acid sites that was analyzed with the same conditions (Föttinger et al., 2003).

X-ray absorption near edge structure (XANES) was used to characterize only Pd species on HBEA in Pd L_{III} and L_{II} edges by using transmission mode at BL8 of the Synchrotron Light Research Institute (Public Organization) (SLRI). The analysis of Pt species was not included because its energy range was not available. The storage ring of the SLRI was operated with the electron energy of 1.2 GeV and current between 90 - 140 mA. The monochromator consisted of a double channel-cut InSb crystal, and the energy calibration was made at Pd L_{III} and L_{II} edge using a Pd foil as a standard. The XANES spectra were acquired in an energy range

of 3150 - 3250 eV, with 0.2 eV step and with an acquisition time of 1 s/point. The measurements were done in two conditions. The first condition was referred to as ambient condition which was under helium flow at atmospheric pressure. The ambient condition was used to study Pd species on HBEA after calcination at 400°C for 4 h comparing with standards of palladium acetate ($\text{Pd}(\text{acac})_2$), palladium chloride (PdCl_2) and palladium oxide (PdO) in form of 5 wt% Pd on alumina (Al_2O_3). The second condition was carried out in an in situ XAS cell in which the XANES data were collected continuously under a reduction condition at various temperatures under hydrogen flow. The in situ XANES measurement mode was used to study the percent of reduction of Pd on HBEA during the reduction. The XAS cell was constructed according to the literatures with modifications (Odzak's et al., 2001; Bernadi et al., 2007 and Yang et al., 1998). The detail of XAS cell design and setup were explained in Chapter V. A small amount of catalyst powder of Pd on zeolite beta was painted on Kapton® tape and attached on the sample holder of the in situ XAS cell. The reduction procedure was initiated by the introduction of a H_2 gas flow with temperature increased from room temperature to 300°C in 45 min and hold at the final temperature for 2 h. The XAS spectra were recorded at 25, 100, 200, 250, 300, and once more after cooling down to room temperature. Finally, the system was cooled down to room temperature under the H_2 flow and the spectra were recorded once more.

4.2.3 Toluene hydrogenation testing

The catalytic performance for toluene hydrogenation was studied in a fixed-bed reactor using a quartz tube (6 mm i.d.) connected to a gas chromatograph (Hewlett Packard, 5890 series II). The catalyst (70 mg) was mixed with quartz sand

(1:1 by weight), loaded in the reactor and subsequently reduced in situ prior to the reaction by a H₂ stream at a flow rate of 50 mL/min at 400°C for 3 h. The reaction was performed at temperature range of 30 - 350°C, pressure range of 1.15 - 1.20 bar, H₂ flow rate of 50 mL/min, and H₂/toluene mole ratio of 28.

The conversions of toluene (*Tol*) were calculated from equation 2 where *Tol_{initial}* and *Tol_{final}* are number of moles of toluene before and after the reaction, respectively. The selectivities of methylcyclohexane (*MCH*) were calculated using equation 3 where *MCH* and *CyH* are amount and all products (equation 3), where is cyclohexane (equation 3).

$$\text{Conversion (\%)} = \frac{\textit{Tol}_{\textit{initial}} - \textit{Tol}_{\textit{final}}}{\textit{Tol}_{\textit{initial}}} \times 100 \quad \dots(2)$$

$$\text{MCH Selectivity (\%)} = \frac{\textit{MCH}}{\textit{MCH} + \textit{CyH}} \times 100 \quad \dots(3)$$

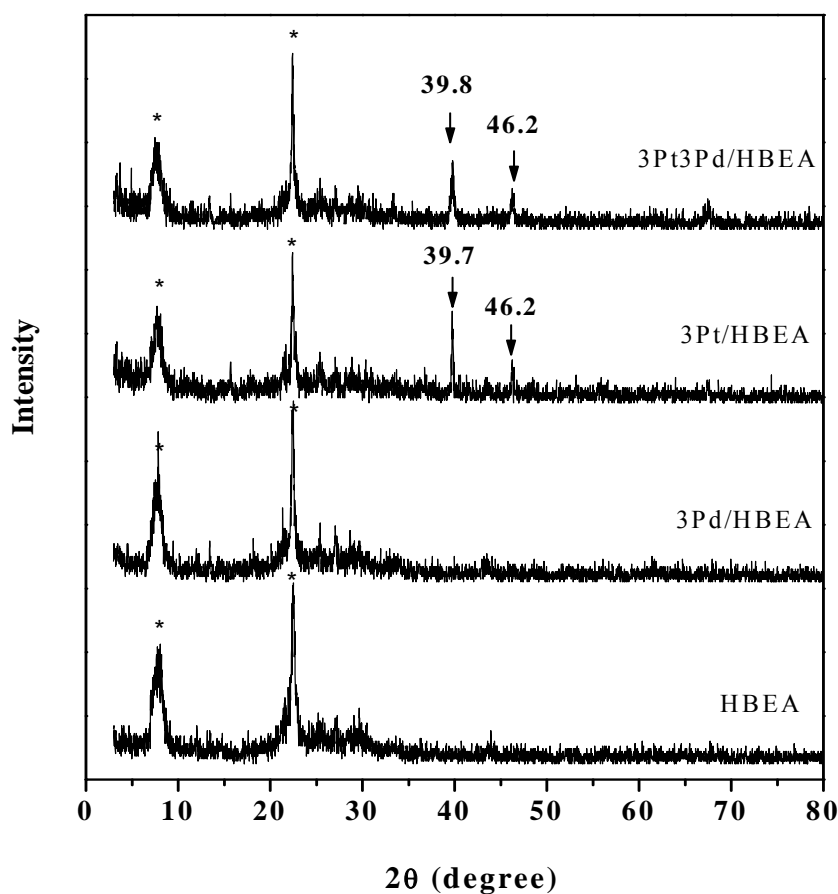
4.3 Results and discussion

4.3.1 XRD patterns of HBEA and HBEA-supported catalysts

XRD patterns of HBEA and HBEA-supported catalysts are shown in Figure 4.1. The spectrum of HBEA had characteristic peaks at 7.4 and 22.4° similar to those in literatures (Talebi et al., 2008 and Loiha et al., 2009). These peaks were also observed in all catalyst samples indicating that the metal loading did not changed crystalline structure of the HBEA support. Additional two peaks at 39.8 and 46.2° were observed on 3Pt3Pd/HBEA and similar two peaks at 39.7 and 46.2° were observed on 3Pt/HBEA. These peaks were assigned to Pt according to the database JCPDS 04-802 (1998) which has 2θ peaks at 39.76 and 46.2°. The sharp peaks

indicated that the Pt formed large particles on HBEA implying a poor dispersion as a result of weak metal-support interaction. The peaks at 39.8 or 39.7° were used to determine the crystal size by Scherrer equation and the results are presented in Table 4.1. The crystal sizes of Pt on Pt/HBEA and PtPd/HBEA were 55.6 and 33.4 nm, respectively. It was possible that the presence of Pd from co-impregnation prevented clustering of Pt to form large particles. In other work by Kim et al., XRD spectra of bimetallic Pt-Au with Pt loading from 1.1 to 3.75 wt% supported on Al₂O₃, a more acidic support than HBEA, only showed broad Pt peaks because of a good dispersion with particle size in the range of 2 - 3 nm due to a strong metal-support interaction (Kim et al., 2009).

The main reflection peak of Pd at 40.12° according to the database JCPDS 46-1043 (1998) was not observed in both of Pd/HBEA and PtPd/HBEA indicating a good dispersion of Pd in both catalysts.



* referred to characteristic peaks of HBEA.

Figure 4.1 XRD profiles of HBEA and HBEA-supported catalysts.

4.3.2 BET surface area of HBEA and HBEA-supported catalysts

The specific surface areas of HBEA and HBEA-supported catalysts from N_2 adsorption-desorption with BET method are presented in Table 4.1. Full isotherms of the catalysts are in Appendix A. A slight decrease of the HBEA surface area was observed after the metal deposition by impregnation suggesting that the blocking of zeolite channels by metal particles was not significant.

Table 4.1 Textural properties of HBEA and catalysts supported on HBEA.

Sample	Metal size (nm) ^a		Acidity from NH ₃ -TPD (mmol/g)	BET surface area (m ² /g)
	Pt	Pd		
HBEA	-	-	1.05	513
3Pd/HBEA	-	-	1.00	510
3Pt3Pd/HBEA	33.4	-	0.95	454
3Pt/HBEA	56.6	-	0.85	462

^a calculated by using the Scherrer equation from XRD peak at 39.8° for 3Pt3Pd/HBEA and 39.7° for 3Pt/HBEA.

4.3.3 Acidity of HBEA and HBEA-supported catalysts from NH₃-TPD

The number of acid sites of HBEA and HBEA-supported catalysts were determined by NH₃-TPD. The amount of ammonia desorbed and the desorption temperature were considered as a measure of total acidity and acid strength of catalysts (Fúnez et al., 2008). The NH₃-TPD profiles of all samples are shown in Figure 4.2. A broad desorption peak was observed in the temperature range of 150 - 350°C and peak position did not vary substantially with the different metal loading similar to the desorption curves of HBEA reported in literature (Fúnez et al., 2008). The desorption temperature below 250°C and between 250 and 400°C corresponded to ammonia on weak and strong acid sites, respectively. The acidities in the unit of mmol of ammonia per gram of catalyst calculated from peak area are reported in Table 4.1. The amount of ammonia adsorbed on HBEA-supported catalysts was

lower than that on HBEA. The decrease was obvious at the temperature range of 275 - 350°C indicating the occupation of strong acid sites by metal.

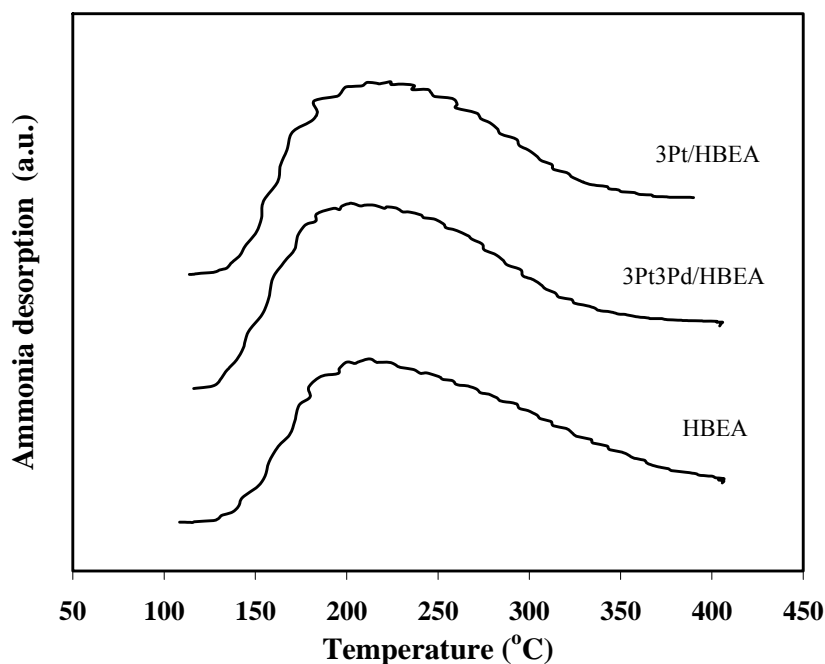


Figure 4.2 NH₃-TPD profiles of HBEA and HBEA-supported catalysts.

4.3.4. Characterization of Pd/HBEA by XANES

4.3.4.1 Calcined Pd/HBEA at ambient condition

The XANES spectra of Pd species in both monometallic and bimetallic on HBEA after calcined at 400°C for 4 h were compared with those of Pd foil, Pd(acac)₂, PdCl₂ and 5Pd/Al₂O₃ standards. The edge energy of Pd L_{III} and L_{II} were observed but the calibration was done according to the L_{III} edge of the Pd foil which is a dominant peak. The energy of both L_{III} and L_{II} edges are reported in Table 4.2. The energy of L_{III} of all samples was slightly higher than that of Pd foil but the L_{II} edge energy were lower.

Table 4.2 Pd L_{III} and L_{II} edges energy from XANES spectra

Sample	L_{III} edge (eV)	L_{II} edge (eV)
Pd foil	3173.00	3203.71
Pd(acac) ₂	3174.89	3203.71
PdCl ₂	3174.39	3203.71
5Pd/Al ₂ O ₃	3174.80	3203.71

The XANES spectra of the Pd standards are shown in Figure 4.3. The Pd(2+) in Pd(acac)₂ and PdCl₂ standards showed the absorption intensity of Pd L_{III} edge higher than Pd L_{II} edge. In contrast, the intensity of Pd L_{II} edge of 5Pd/Al₂O₃ was higher than the Pd L_{III} edge. Because the edge positions of Pd in 5Pd/Al₂O₃ were similar to those in Pd(acac)₂ and PdCl₂, the form of Pd in 5Pd/Al₂O₃ was Pd(2+) and it was likely in the form of PdO. This result agreed with the literature that the edge energy of the Pd L_{III} edge of Pd(2+) was higher than that of Pd(0) by using the X-ray transmission mode of measurement (Liu et al., 2004). On the other hand, the X-ray fluorescence (XRF) spectra were not observed the energy shift in Pd L_{III} edge among different Pd compounds (Liu et al., 2004). The energy of Pd L_{II} edge of Pd(2+) standards were similar position to that of Pd foil. From these results, the 5Pd/Al₂O₃ was used further as a standard to compare with the Pd species on the samples supported on HBEA. However, only the Pd L_{III} edge could be used to compare the energy shift of Pd species on the samples.

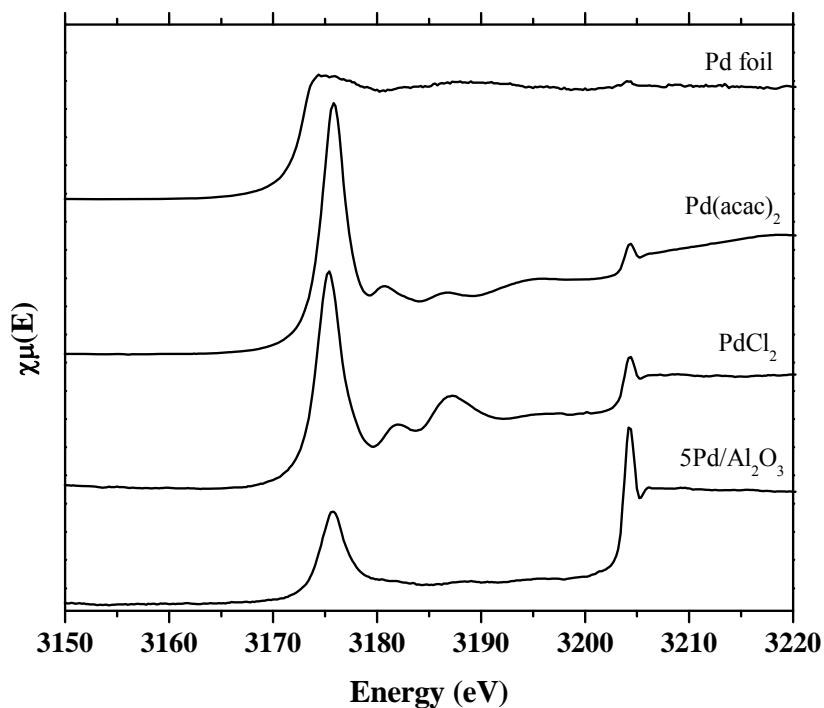


Figure 4.3 XANES spectra of Pd standards measured at ambient condition

The monometallic catalysts with 1 and 5 wt% of Pd on HBEA which were labeled as 1Pd/HBEA and 5Pd/HBEA respectively and the bimetallic catalyst with 3 wt% Pd and 3 wt% Pt as 3Pt3Pd/HBEA were characterized by XANES and the results were compared with 5Pd/Al₂O₃ standard (see Figure 4.4). The spectra of all samples showed a strong peak of Pd L_{II} edge at the same energy of standard indicating that the Pd species on HBEA after calcination was in PdO form with the oxidation state of +2. Because the Pd L_{III} edge was not observed or had low intensity, the calcination temperature and time was sufficient to transform the Pd precursor to PdO. The spectrum of 5Pd/HBEA had low intensity because of strong absorption by Pd atoms.

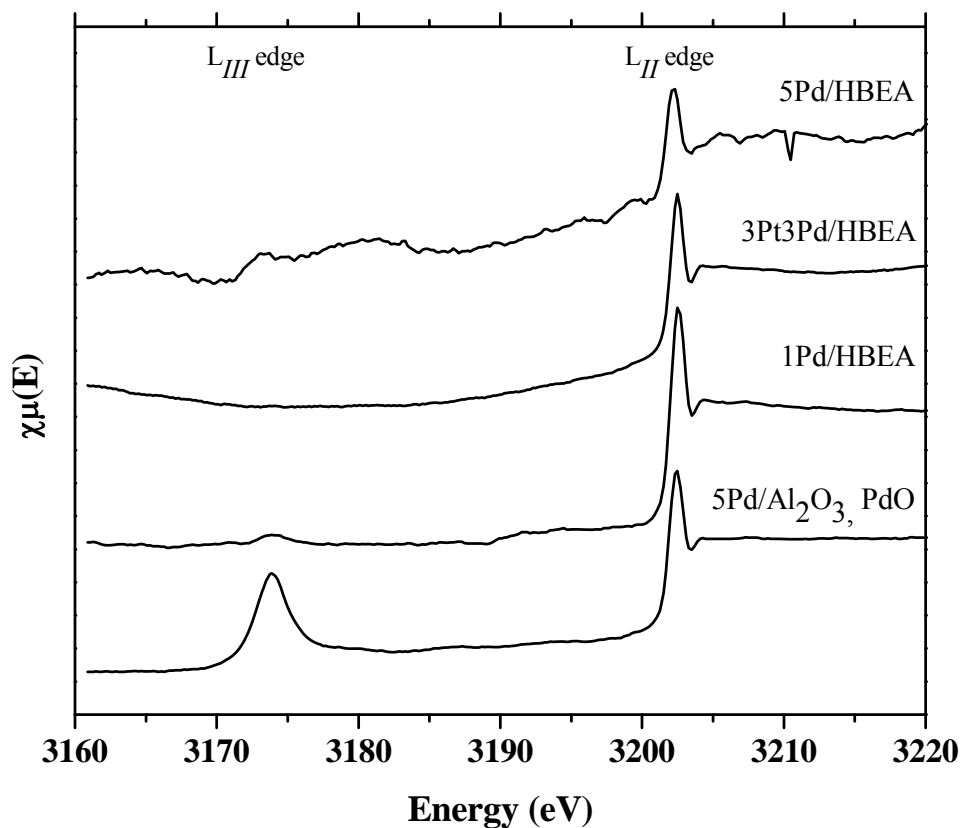


Figure 4.4 XANES spectra of calcined 1Pd/HBEA, 5Pd/HBEA and 3Pt3Pd/HBEA samples comparing with 5Pd/Al₂O₃ standard at ambient condition.

4.3.4.2 Reduced Pd on HBEA by in situ XANES measurement

The XANES spectra of 3Pt3Pd/HBEA reduced from 21 to 300°C are shown in Figure 4.5. Only the Pd L_{II} edge was observed which was similar to that of calcined 3Pt3Pd/HBEA (Figure 4.4). The spectrum after reduced at 300°C for 2h and cooled down in H₂ flow to 40°C showed the same edge position with that at room temperature (21°C). However, the signals other than the L_{II} edge were poor. This result indicated that the change of Pd in 3Pt3Pd/HBEA could not be observed.

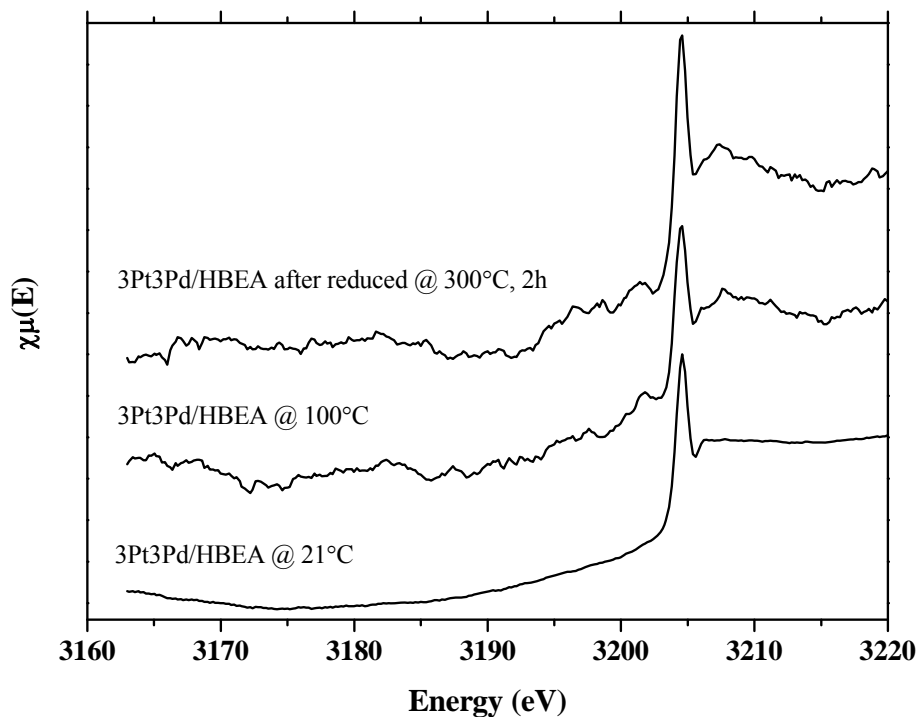


Figure 4.5 XANES results of 3Pt3Pd/HBEA during in situ reduction from room temperature to 300°C

The XANES spectra of 3Pt3Pd/HBEA during the in situ reduction with increasing temperature from 200 to 300°C are shown in Figure 4.6. The spectrum quality was too poor to interpret and the degree of reduction could not be calculated. However, after reduced at 300°C for 2 h and cooled down to 40°C the spectrum was similar to that before the reduction (see Figure 4.5). The poor data quality during the temperature change (to 200, 250, and 300°C) indicating that the in situ measurement could only be done at low temperature.

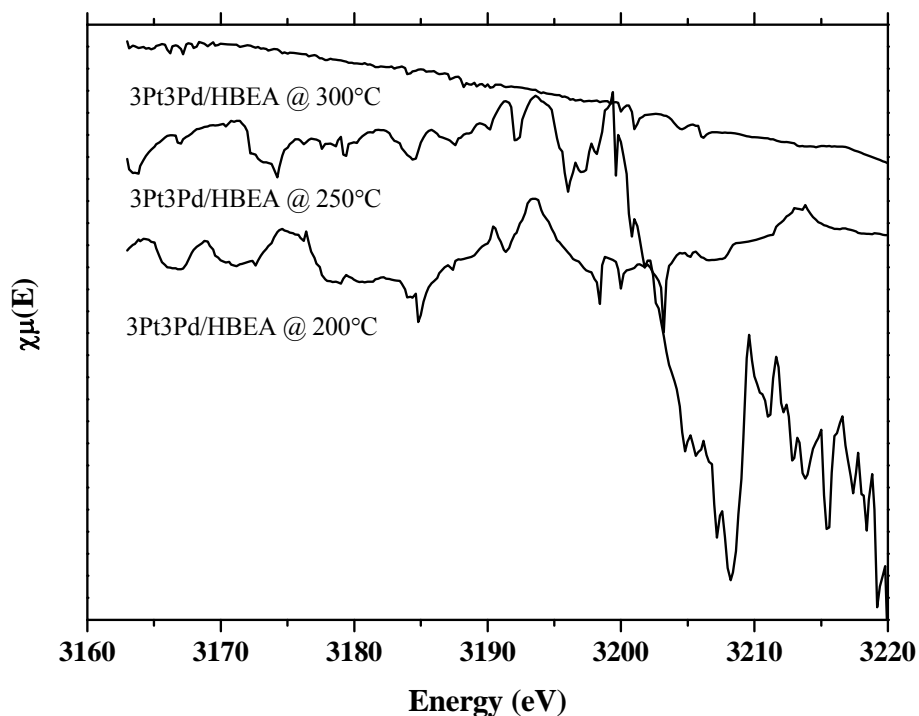


Figure 4.6 XANES results of 3Pt3Pd/HBEA during increased temperature from 200 to 300°C

To confirm the above hypothesis, the in situ reduction of 5Pd/Al₂O₃ from 23 to 300°C was studied. Figure 4.7 shows the XANES spectra of 5Pd/Al₂O₃ during in situ reduction at 23, 100°C and spectra after reduced at 300°C and cooled down to temperature. Peak positions of Pd L_{III} and L_{II} edges from these conditions were similar to that of the calcined one. The L_{II} edge was well defined while the L_{III} edge was not cleared because of low absorption intensity. These results indicated that the change of Pd forms in this catalyst could not be observed by this technique. The in situ spectra at 200, 250, and 300°C during the temperature increase did not show any characteristic of Pd edges (Figure 4.8) similar to those of

3Pt3Pd/HBEA. Thus, the poor data was a result of from measurement technique, not from the sample nature.

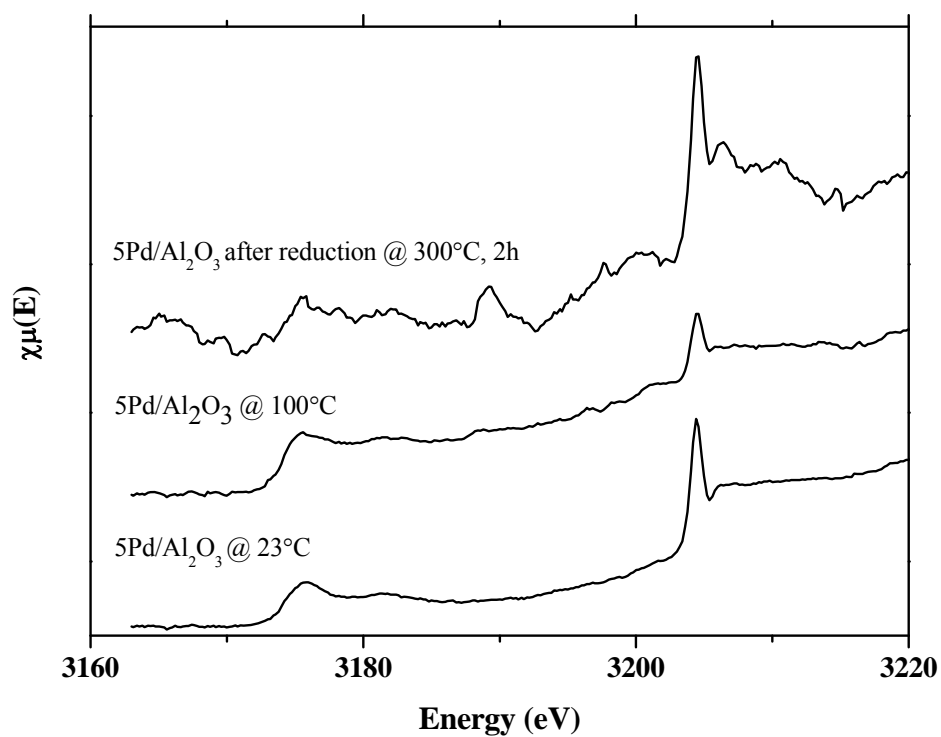


Figure 4.7 XANES results of 5Pd/Al₂O₃ during reduction from 23 to 300°C using in situ XAS measurement

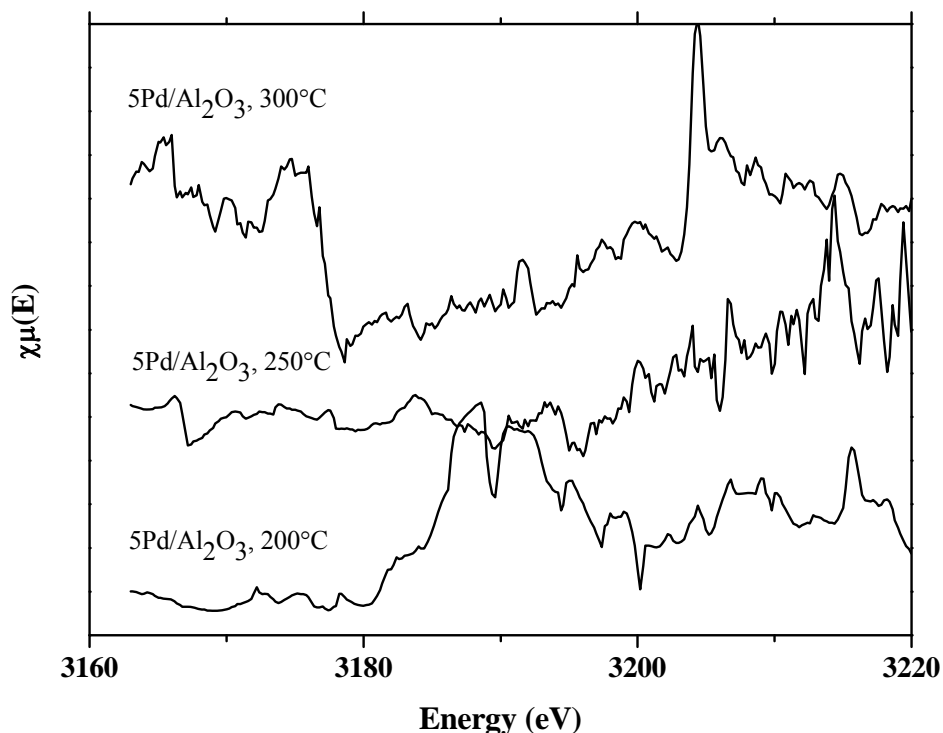


Figure 4.8 XANES results of 5Pd/Al₂O₃ during reduction from 200 to 300°C using in situ XAS measurement

4.3.5 Effect of temperature on catalytic conversion

Toluene hydrogenation over monometallic and bimetallic catalysts was carried out from 30 to 350°C and the conversions are plotted in Figure 4.9. The monometallic 3Pt/HBEA gave high toluene conversions (80 - 100 %) at the temperature range of 30 - 200°C with a complete conversion at 100 - 150°C. This catalyst was deactivated quickly at higher reaction temperatures by coking. The monometallic 3Pd/HBEA gave lower toluene conversions than the 3Pt/HBEA at all temperature with the maximum conversion of 58% at 200°C. In the bimetallic

3Pt3Pd/HBEA, the conversion was higher than 3Pd/HBEA in the temperature 30 - 250°C. High toluene conversion (80 - 100%) was obtained in the 70 - 250°C range with a complete conversion at 150°C.

Thomas et al. (2002) also studied toluene hydrogenation of bimetallic PtPd with different loading from this work on zeolite FAU but only in the temperature range of 110 - 150°C. Without the presence of sulfur, the toluene conversion at the temperature less than 150°C on 0.3Pt0.5Pd/FAU was lower than that on 0.3Pt/FAU but higher than that on 0.5Pd/FAU. Near complete toluene conversions on 0.3Pt/FAU and 0.3Pt0.5Pd/FAU were achieved at 110 and 148°C, respectively. In this work, the toluene conversion on 3Pt3Pd/HBEA at the temperature above 150°C was higher than that on 3Pt/HBEA indicated that the presence of Pd minimized deactivation from coking. The temperatures that provided maximum activity on each catalyst were in the following order: 100°C, 3Pt/HBEA < 150°C, 3Pt3Pd/HBEA < 220°C, 3Pd/HBEA. The influence of Pd on a catalytic performance of the bimetallic catalyst at the temperature above 150°C could be explained from TPD investigation that desorption temperature of hydrogen from Pd was higher than that from Pt. Therefore, hydrogen could be supplied from Pd for hydrogenation of toluene which adsorbed on Pt (Rousset et al., 2001). In addition, the presence of Pd in the bimetallic 0.3Pt0.5Pd/FAU improved the catalysts stability by increasing sulfur tolerance (Thomas et al., 2002).

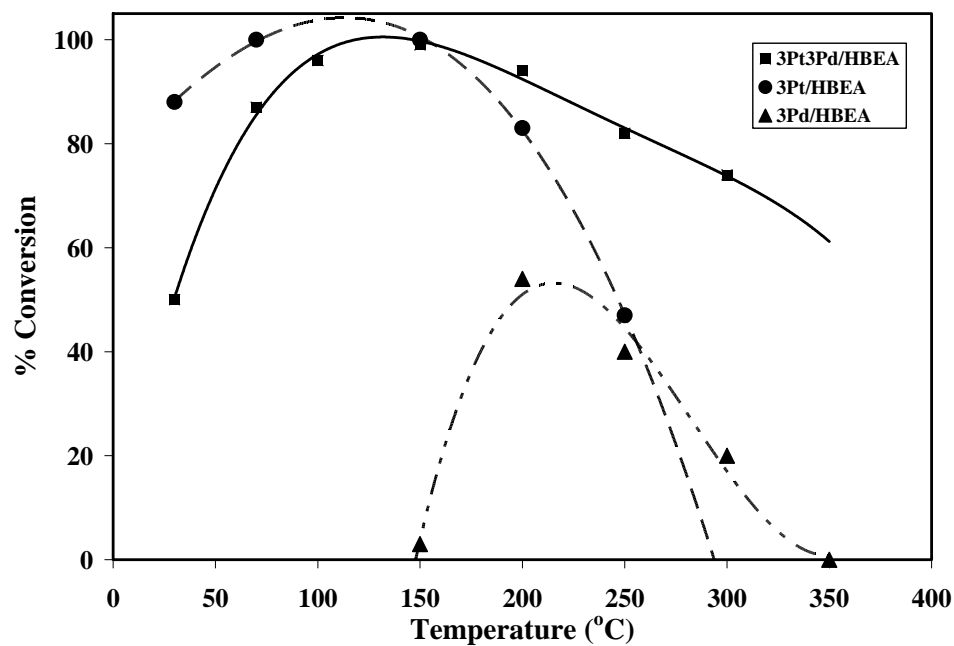


Figure 4.9 Toluene conversions on 3Pt3Pd/HBEA, 3Pt/HBEA and 3Pd/HBEA at various reaction temperatures.

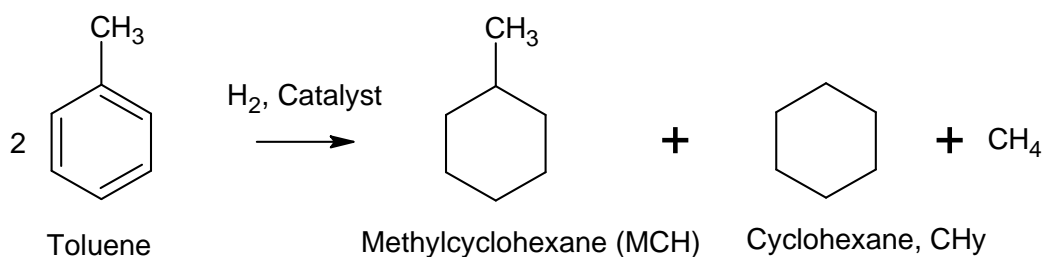
Reactions that can occur along with hydrogenation of aromatic compounds are isomerization and cracking. Adjusting reaction conditions or modification of catalyst could improve selectivities. For example, Wang and coworkers demonstrated that the selectivity for cyclohexane from benzene hydrogenation on bifunctional Pt/USY varied upon a change of temperature, metal loading and zeolite acidity (Wang et al., 1999).

Table 4.3 Catalytic selectivity to methylcyclohexane (MCH) and cyclohexane (CyH) of 3Pt3Pd/HBEA.

Temperature (°C)	MCH selectivity (mole %)			CyH selectivity (mole %)		
	Pt/HBEA	Pd/HBEA	PtPd/HBEA	Pt/HBEA	Pd/HBEA	PtPd/HBEA
100	100	–	100	0	–	0
150	94	84	100	6	16	0
200	84	83	82	16	17	18
250	50	68	53	50	32	47

(–) refer to the results which was not observed (conversion = 0).

In this study, the selectivity of toluene hydrogenation on these catalysts was explained by Scheme 4.1 following the observed products of methylcyclohexane (MCH) and cyclohexane (CHy).



Scheme 4.1 The chemical reaction of toluene hydrogenation.

MCH was a major product from all catalysts (see Table 4.3) but the selectivities decreased with an increase of the temperature. Only MCH was detected

at 100°C on monometallic 3Pt/HBEA and bimetallic 3Pt3Pd/HBEA while no products were detected on 3Pd/HBEA at the same temperature. At higher temperature, the MCH selectivity on monometallic catalysts decreased because of the increase of cracking products, CyH and methane. The selectivity for MCH on 3Pt/HBEA was higher than that on 3Pd/HBEA at 100 - 200°C but it was reversed at 250°C. Although the bimetallic 3Pt3Pd/HBEA provided 100% MCH selectivity at both 100°C and 150°C, the conversion was higher at 150°C. Thus, the most suitable temperature for toluene hydrogenation on 3Pt3Pd/HBEA was 150°C. The selectivity for methylcyclohexane as high as 100% was also reported on rhodium supported on montmorillonite but the conversion was 41% (Sidhpuria et al., 2009).

In addition, the toluene conversion and MCH selectivity on 3Pt3Pd/HBEA at 150°C remained constant at 100% during the testing period of 5 h (see Figure 4.10) indicating that catalyst was not deactivated. The catalyst was also stable at 200°C and Figure 4.10b confirmed that the selectivity at 150°C was higher than that at 200°C throughout the test.

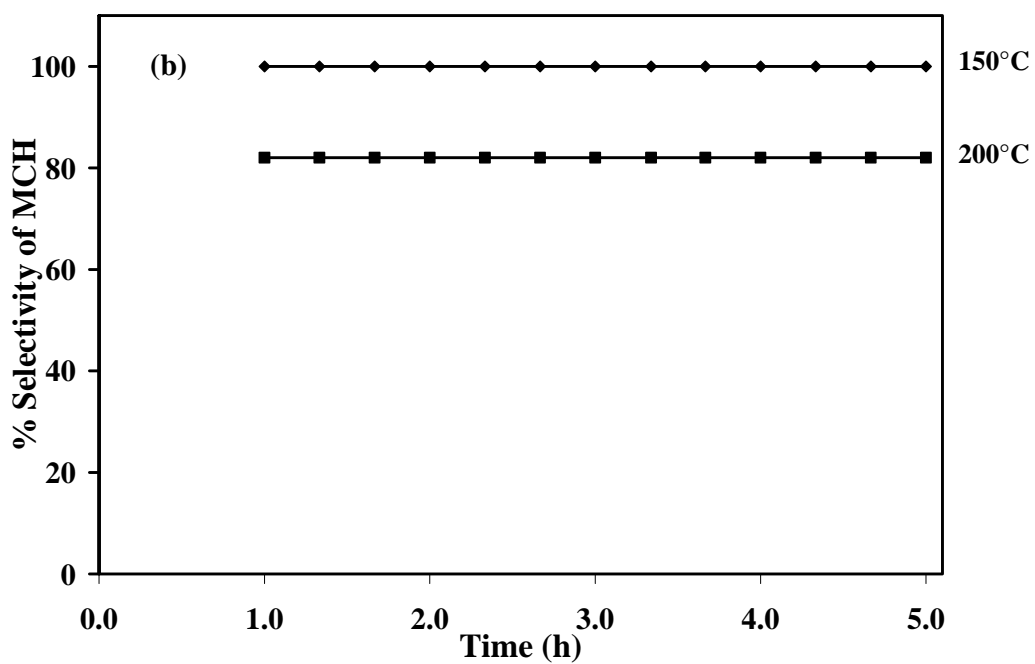
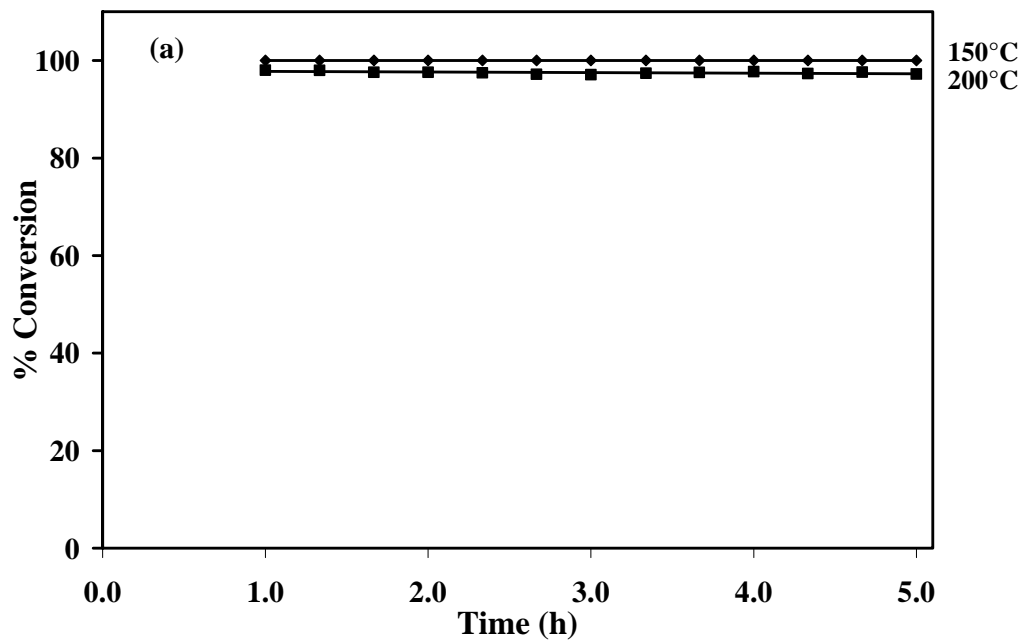


Figure 4.10 (a) Toluene conversion (b) Selectivity for methylcyclohexane on 3Pt3Pd/HBEA at 100 and 200°C during the 5 h period.

4.4 Conclusions

Bimetallic 3Pt3Pd/HBEA catalyst was prepared by co-impregnation and the structure of HBEA was maintained. The peaks of Pt were observed by XRD and the Pt particle size on 3Pt3Pd/HBEA was smaller than that on 3Pt/HBEA probably due to the presence of Pd. NH₃-TPD indicated that the metals occupied strong acidic sites of HBEA. The changes of Pd form during the reduction could not be observed by in situ XANES. The catalytic performance of bimetallic 3Pt3Pd/HBEA over toluene hydrogenation was studied and the presence of Pd enhanced both toluene conversion and selectivity for methylcyclohexane. The most suitable temperature for toluene hydrogenation on 3Pt3Pd/HBEA was 150°C in which a complete toluene conversion and 100% selectivity for methylcyclohexane were achieved.

4.5 References

- Antos, G. J., Aitani, A. M., and Parera, J. M. (1995). Catalytic Naphtha Reforming Science and Technology. (p. 5). Marcel Dekker Inc. New York.
- Bartholomew, C. H. and Farrauto, R. J. Fundamentals of Industrial Catalytic Processes, 2nd Ed. (pp. 157, 489, 667). John Wiley&Sons, Inc. New Jersey.
- Bernardi, F., Alves, M. C. M., Scheeren, C. W., Dupont, J., and Morais, J. (2007). In situ studies of nanoparticles under reaction with sulfur by XAS. **J. Electron Spectrosc.** 156-158: 186-190.
- Carturan, G., Cocco, G., Facchin, G., and Navazio, G. (1984). Phenylacetylene hydrogenation with Pd, Pt and Pd-Pt alloy catalysts dispersed on amorphous supports: effect of Pt/Pd ratio on catalytic activity and selectivity. **J. Mol. Catal.** 26: 375-384.

- Chou, P. and Vannice, M. A. (1997). Benzene hydrogenation over supported and unsupported palladium : I. Kinetic behavior. **J. Catal.** 107: 129-139.
- Crowl, D. A. and Louvar, J. F. (2000). Chemical Process Safety Fundamentals with Applications. (p.44). Prentice Hall. New Jersey.
- Föttinger, K., Kinger, G., and Vinek, H. (2003). 1-Pentene isomerization over FER and BEA. **Appl. Catal. A: Gen.** 249: 205-212.
- JCPDS--International Centre for Diffraction Data. (1998). Powder Diffraction File. Pennsylvania.
- Fúnez, A., Lucas, A. D., Sánchez, P., Ramos, M. J., and Valverde, J. L. (2008). Hydroisomerization in liquid phase of a refinery naphtha stream over Pt–Ni/H-beta zeolite catalysts. **J. Chem. Eng.** 136: 267-275.
- Kim, K. J., Boo, S. I., and Ahn, H. G. (2009). Preparation and characterization of the bimetallic Pt–Au/ZnO/Al₂O₃ catalysts: Influence of Pt–Au molar ratio on the catalytic activity for toluene oxidation. **Ind. Eng. Chem.** doi:10.1016/j.jiec.2008.09.005
- Koussathana, M., Vamvouka, D., Economou, H., and Verykios, X. (1991). Slurry-phase hydrogenation of aromatic compounds over supported noble metal catalysts. **Appl. Catal.** 77: 283-301.
- Lin, S. D. and Vannice, M. A. (1993). Hydrogenation of Aromatic Hydrocarbons over Supported Pt Catalysts .I. Benzene Hydrogenation. **J. Catal.** 143: 539-553.
- Loiha, S., Prayoonpokarach, S., Songsiriritthigun, P., and Wittayakun, J. (2009). Synthesis of zeolite beta with pretreated rice husk silica and its transformation to ZSM-12. **Mater. Chem. Phys.** 115: 637-640.

- Liu, Z., Handa, K., Kaibuchi, K., Tanaka, Y., and Kawai, J. (2004). The charge transfer effect in Pd compounds (II): evidence from the L3 X-ray absorption near edge structure spectroscopy. **Spectrochim. Acta. B.** 59: 901-904.
- Liu, Z., Yuge, K., and Kawai, J. (2004) High resolution $L\alpha$ X-ray fluorescence spectra of palladium compounds. **Spectrochim. Acta. B.** 59: 93-99.
- Odzak J. F., Argo, A. M., Lai, F. S., Gatesa, B. C., Pandya, K., and Feraria, L. (2001). A flow-through x-ray absorption spectroscopy cell for characterization of powder catalysts in the working state. **Rev. Sci. Instrum.** 72: 3943-3945.
- Pawelec, B., La Parola, V., Navarro, R. M., Murcia-Mascarós, S., and Fierro, J.L.G. (2006). On the origin of the high performance of MWNT-supported PtPd catalysts for the hydrogenation of aromatics. **Carbon.** 44: 84-98.
- Pawelec, B., Mariscal, R., Navarro, R. M., Bokhorst, S. V., Rojas, S., and Fierro, J.L.G. (2002). Hydrogenation of aromatics over supported Pt-Pd catalysts. **Appl. Catal. A: Gen.** 225: 223-237.
- Roldán, R., Beale, A. M., Sánchez, M. S., Salguero, F. J. R., Sanchidrián, C. J., Gómez, J. P., and G. Sankar. (2008). Effect of the impregnation order on the nature of metal particles of bi-functional Pt/Pd-supported zeolite Beta materials and on their catalytic activity for the hydroisomerization of alkanes. **J. Catal.** 254: 12-26.
- Rousset, J. L., Stievano, L., Cadete Santos Aires, F. J., Geantet, C., Renouprez, A. J., and Pellarin, M. (2001). Hydrogenation of Toluene over γ -Al₂O₃-Supported Pt, Pd, and Pd–Pt Model Catalysts Obtained by Laser Vaporization of Bulk Metals. **J. Catal.** 197: 335-343.

- Sidhpuria, K. B., Patel, H. A., Parikh, P. A., Bahadur, P., Bajaj, H. C., and Jasra, R. V. (2009). Rhodium nanoparticles intercalated into montmorillonite for hydrogenation of aromatic compounds in the presence of thiophene. **Appl. Clay Sci.** 42: 386-390.
- Talebi, G., Sohrabi, M., Royaei, S. J., Keiski, R. L., Huuhtanen, M., and Imamverdizadeh, H. (2008). Synthesis and activity measurement of the some bifunctional platinum loaded Beta zeolite catalysts for n-heptane hydroisomerization. **J. Ind. Eng. Chem.** 14: 614-621.
- Thomas, K., Binet, C., Chevreau, T., Cornet, D., and Gilson, J-P. (2002). Hydrogenation of Toluene over Supported Pt and Pd Catalysts: Influence of Structural Factors on the Sulfur Tolerance. **J. Catal.** 212: 63-75.
- Wang, J., Li, Q., and Yao, J. (1999). The effect of metal-acid balance in Pt-loading dealuminated Y zeolite catalysts on the hydrogenation of benzene. **Appl. Catal. A: Gen.** 184: 181-188.
- Yang, J. C., Shul, Y. G. Louis, C., and Che, M. (1998). In situ EXAFS study of the nucleation and crystal growth of Ni particles on SiO₂ support. **Catal. Today.** 44: 315-325.

CHAPTER V

**THE APPLICATION OF IN SITU XAS CELL ON
REDUCTION, TOLUENE DESORPTION, TOLUENE
HYDROGENATION OF NICKEL SUPPORTED ON
ZEOLITE BETA**

Abstract

In this chapter focused on a design, setup and application of in situ X-ray absorption cell for the study of structural and electronic properties of metal supported catalysts. Monometallic nickel (Ni) or bimetallic nickel-platinum (NiPt) supported on zeolite beta in proton form (HBEA), referred to as Ni/HBEA or NiPt/HBEA catalysts were characterized by the in situ XAS to monitor metal-support interaction and changes of the Ni during a reduction, toluene desorption and toluene hydrogenation. Data from X-ray absorption near edge spectroscopy (XANES) at Ni K-edge provided structural and electronic information of the metal. Measurements in ambient conditions indicated that the calcined catalysts contained Ni with 5 wt% loading had octahedral geometry but Ni in the catalyst with low loading had tetrahedral or square planar. After reduction the catalysts with 1 wt% Ni loading was not reducible and the reducibility increased with metal loading, temperature and time. With high metal loading, Ni possibly located outside the zeolite pores because large crystal size was detected from X-ray diffraction. With low metal loading, Ni could reside in both

zeolite channels and on the surface. In toluene adsorption on calcined 5Ni/HBEA, there was no Ni-C interaction because there was no change in Ni pre-edge. Thus, toluene adsorbed on HBEA acid sites. Moreover, toluene might be oxidized by oxygen from NiO because the coordination number of Ni decreased during the in situ XANES measurement. In toluene hydrogenation on calcined 5Ni/HBEA, the NiO was slowly reduced by hydrogen as indicated by an appearance of Ni(0) edge. Although some products were detected, the catalyst performance was not fully studied.

5.1 Introduction

X-ray absorption spectroscopy (XAS) is a powerful tool to obtain information of different types of materials lacking long range order such as catalysts, inorganic materials, minerals, organometallic complexes. The local geometry of a specific atom such as coordination number and bond distances can be probed by Extended X-ray absorption fine structure (EXAFS). The formation about electronic properties such as oxidation state can be obtained from X-ray absorption near edge spectroscopy (XANES). In catalysis, knowledge of the structure of the active site and the interaction between catalytic sites and reacting molecules can lead to an understanding of the occurring processes and development of better catalysts. In situ investigations of catalyst systems under reaction conditions can be performed routinely on atoms having absorption edges at energies above 3 - 4 keV (Van der Eerdena et al., 2000)

There are many researches about the application of in situ XAS technique to investigate the structure, electrical and dispersion properties of supported metal catalysts. Previous studies showed that the conditions of Ni deposition on an oxide

support may influence the nature of the supported phase (Burattin et al., 1997). Carriat et al. (1998) studied the influence of the Ni deposition modes on the dispersion of the Ni²⁺ precursors which were investigated in a preparation of Ni/SiO₂ catalyst using in situ XAS technique. The modification of the coordination sphere of silica supported Ni²⁺ ions versus the Ni deposition mode was mainly followed by XAFS measurements. For samples activated at 700°C, this spectroscopy showed the presence of several categories of atoms in the first (oxygen backscatterers) and second (Ni and Si backscatterers) shells. A distribution of long ($d \sim 2.04 \text{ \AA}$) and short ($d \sim 1.75 \text{ \AA}$) Ni-O distances was found, corresponding to hexacoordinated (Ni²⁺_{6c}) and isolated tricoordinated (Ni²⁺_{3c}) ions, respectively. Modeling of the structure of the Ni²⁺_{3c} site indicated a distorted site with two short and one long Ni-O distance. Impregnation with ethylenediammine Ni nitrate was advantageous as it led after thermal activation at 700°C to NiO particles smaller than those produced from impregnation with Ni nitrate and therefore to smaller Ni particles after the subsequent reduction step.

Several studies to obtain the enhanced dispersion of active phase by controlling the metal-support interaction were reported. Yang et al. (1998) proposed the presence of transition ion-support interactions at the interface which could be controlled by changing preparation methods. As the model, Ni/SiO₂ catalysts were used to prove the effect of ion-support interaction on the nucleation and growth of Ni particle on a support using one- and two-step impregnation. The catalyst structures during nucleation and growth behavior of Ni particles with increasing of temperature were continuously monitored by in situ EXAFS spectroscopy. They found that the bulk NiO was formed in the impregnated Ni/SiO₂ catalyst whereas the small particles of Ni

could be prepared by the two-step method. The formation of small particle was attributed to the strong ion-support interaction between nickel nuclei and nickel reservoir.

Another work of Bus and coworkers (2007) used in situ XAS to study ethylene adsorption on supported Pt and Au under various temperatures and pressures using XANES technique. They found that the ethene-induced changes in the XAS spectra as a function of temperature and pressure were correlated to changes in the adsorption mode of the hydrocarbon.

Bernardi and coworkers (2007) modified in situ XAS cell as a reactor that enables sample heating up to 500°C under sulfur reactive environment. The results were obtained with PtPd and Pt nanoparticles submitted subsequently to the reduction and sulfidation reactions. The environment modifications in the short range order around the Pt atoms as the catalysts could be monitored with temperature variation.

The aim of this work was to design and setup an in situ XAS cell to use at BL8, the Synchrotron light research institute (Public organization) (SLRI) and used the cell for an investigation on changes of structural and electronic properties of Ni catalyst supported on zeolite beta in proton form (HBEA) support both monometallic and bimetallic catalysts. The experiment were divided into 3 parts including of reduction, toluene desorption, and toluene hydrogenation of Ni/HBEA catalysts operating into in situ XAS cell. The structural and electronic properties were investigated with continuously increasing temperature using XANES measurement. Moreover, dispersion of Ni metals on the acidic support of BEA with various metals loading was monitored under ambient condition.

5.2 Experimental

5.2.1 Catalyst preparation

5.2.1.1 Sample preparation: Impregnation method

The support material for this work was zeolite beta in proton form (HBEA). Zeolite beta in sodium form (NaBEA) was synthesized with Si/Al ratio of 13 (Loiha et al., 2009) and subsequently transformed to HBEA with NH_4NO_3 using a conventional ion exchange method.

Monometallic Ni catalysts were prepared by the incipient wetness impregnation method with a solution of nickel acetate tetrahydrate ($\text{Ni}(\text{acac})_2 \cdot 4\text{H}_2\text{O}$, 40%, supplied by the Right Chemical) onto the HBEA. The loading of Ni metal were 1, 3, and 5 wt% and these catalysts were referred to as 1Ni/HBEA, 3Ni/HBEA, and 5Ni/HBEA, respectively.

Bimetallic catalysts were prepared by co-impregnation with a solution containing the same Ni precursor and dihydrogen hexachloroplatinate hexahydrate ($\text{H}_2\text{PtCl}_6 \cdot 6\text{H}_2\text{O}$, 40%, supplied by the Right Chemical) as a Pt precursor. The loading of Pt was fixed at 0.5 wt%, the loading of Ni were 1 and 5 wt% and the catalysts prepared were referred to as 1Ni0.5Pt/HBEA and 5Ni0.5Pt/HBEA. Both mono- and bi-metallic catalysts were dried in a hot air oven at 100°C for 3 h and calcined in a muffle furnace at 400°C for 3 h. After calcination, the samples were characterized by powder X-ray diffraction (Bruker axs D5005) measurement using $\text{Cu-K}\alpha$ (1.54 Å). The samples were subsequently reduced in situ prior to use in the reaction and characterization by XAS by a H_2 stream at a flow rate of 50 ml/min at 350°C for 2 h.

5.2.1.2 Characterization by X-ray absorption spectroscopy (XAS)

The XANES and EXAFS spectra of monometallic and bimetallic Ni on HBEA catalysts were obtained in a transmission mode at BL8 of the SLRI using both in situ cell and ambient measurements. The storage ring was operated with the electron energy of 1.2 GeV and current between 90 - 140 mA. The monochromator consisted of a double channel-cut Ge(2 2 1) crystal, and the energy calibration was made at Ni K-edge using a Ni foil as a standard. The XAS spectra were acquired in an energy range of 8200 - 9200 eV, with 0.3 eV step in the XANES and 1 eV step in the EXAFS region, with an acquisition time of 1 s/point. Three scans were averaged to get a better signal to noise ratio.

5.2.2 Reduction of Ni/HBEA and NiPt/HBEA

5.2.2.1 Ambient XAS measurement

After calcination, the supported mono- and bimetallic Ni-containing catalysts were reduced in H₂ flow with a rate of 50 ml/min at 350°C for 2 h. Then the reduced catalysts powder were ground and pressed with a hydraulic pressure of 10 tons to form a pellet. Consequently, all samples were pressed on a plastic frame and covered by a Kapton® tape before installing on a sample holder. The XANES spectra of the reduced catalysts were collected in a transmission mode and the Ni K-edge was monitored for all catalysts. The energy calibration at the Ni K-edge was done using a Ni foil standard. The XAS spectra were acquired in a range of 8200 - 9200 eV, with 0.3 eV step in the XANES and 1 eV step in the EXAFS region, with an acquisition time of 1 s/point.

5.2.2.2 In situ XAS measurement

5.2.2.2.1 In situ XAS cell setup

The in situ XAS cell setup was modified from the literatures (Odzak's et al., 2001; Bernadi et al., 2007 and Yang et al., 1998). The cell consisted of three parts as shown in Figure 5.1. The cell chamber consisted of a stainless steel, 190 mm height and 115 mm diameter, with two 115 mm, two 75 mm, and two 55 mm ports. Two of those had bored flanges with 55 mm thick Kapton® windows for the incoming radiation. Measurements in transmission mode could be accomplished.

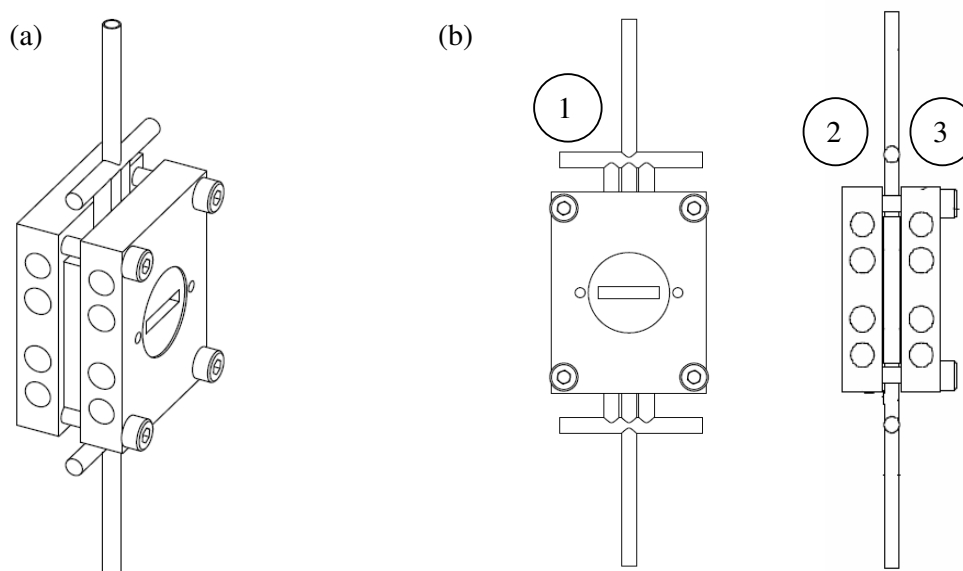


Figure 5.1 Sample holder of in situ XAS cell, (a) show sample holder and (b) show the composition of sample holder; 1 = middle plate, 2 and 3 = cover plates.

The sample holder (Figure 5.1(a) and (b)) made of stainless steel, was placed at the center of the chamber. Two tubes connected to the sample holder allowing the reactive gas to pass through a sample during the XAS measurements. One of them was connected to a gas inlet and the other to an exhaust system. Besides the holder itself, there were two extra plates (Figure 5.1(b)) that were used to maintain the sample in place. One of the plates was placed the heating elements inside and another one was placed the Chromel–Alumel thermocouple inside to measure the temperature at the sample holder, positioned at about 2 mm from the sample position. A power supply controlled the catalyst temperature during the experiments with accuracy of $\sim 1^\circ\text{C}$. The sample holder cavity had a capacity of about 30 mg of catalyst and the catalyst, in the form of a pellet or powder, was positioned between the second and third plate. The external plates have Kapton® foil windows and all parts were bolted together in order to ensure a tight gas seal. The sample atmosphere was confined within the sample holder windows and it was isolated from the inner part of the chamber.

5.2.2.2.2 In situ XAS measurement during reduction of 5Ni0.5Pt/HBEA under hydrogen flow at various temperatures

The catalyst powder of 5Ni0.5Pt/HBEA was press to form a pellet with a hydraulic pressure of 10 tons. The sample was put into the sample cell holder of in situ XAS cell which was carefully sealed two sides by Kapton® tape. The reduction procedure was initiated by the introduction of a H_2 gas flow with temperature increased from room temperature to 350°C in 1h and hold at the final temperature for 2 h. Finally, the system was cooled down to room temperature under

the H₂ the flow. XAS spectra were acquired at 25, 100, 200, 300, 350°C and once more after cooling down to room temperature. The spectra were analyzed in accordance with the standard procedure of data reduction (Bernardi et al., 2007).

5.2.3 Toluene desorption on 5Ni/HBEA by in situ XAS

The 5Ni/HBEA catalyst was pressed to form a pellet using hydraulic pressure of 10 tons. The pellet was exposed to vapor of boiling toluene at ~80°C in a close container for 1 h to ensure adsorption saturation then it was purged with a N₂ flow to remove toluene physisorption for 1 h. The pretreated sample was put into the sample cell holder of the in situ XAS cell and again, both sides were sealed by Kapton® tape. Then the desorption measurement was performed in the in situ cell by purging with N₂ with an increasing of temperature. XANES spectra at Ni K-edge were acquired at 21, 100, 200, 250°C and after cool down to room temperature.

5.2.4 Toluene hydrogenation on 5Ni/HBEA by in situ XAS

The 5Ni/HBEA catalyst for toluene hydrogenation was prepared in a similar way as described in section 5.3.3. The sample was put in the sample holder and place at a position for radiation. The gas inlet lines of the holder were connected with lines of toluene and hydrogen (99.999%), which were fed continuously through the sample during the measurement. Both gas inlet and outlet lines were heated to 120°C to ensure that toluene remained in gas phase throughout the measurement and to prevent toluene condensation on the sample surface. XANES measurement was aimed to monitor changes of NiO during the increase of reaction temperature from room temperature to 200°C. Furthermore, after being cooled down to room temperature, the XANES and EXAFS spectra of Ni K-edge were acquired again to compare changes of the catalyst before and after the reaction.

5.3 Results and discussion

5.3.1 Catalysts characterization

5.3.1.1 XRD results

XRD spectrum of 5Ni/HBEA before reduction is showed in Figure 5.2 comparing with that of HBEA. The main characteristic peaks of zeolite beta at 7.8 and 22.4° were observed in both samples.

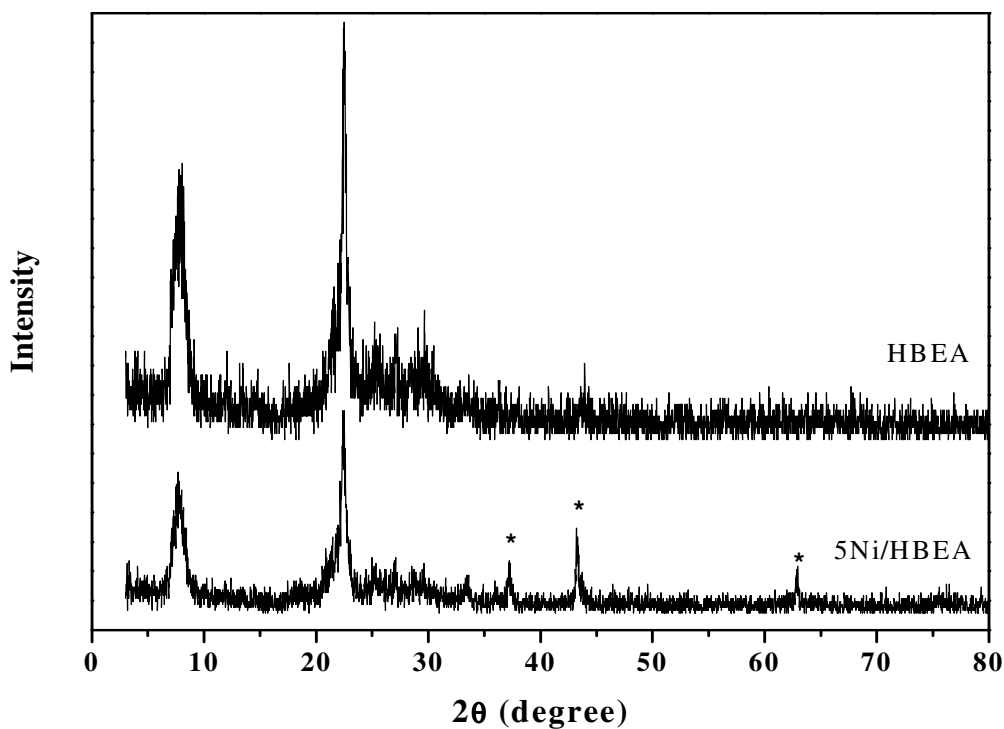


Figure 5.2 XRD patterns of calcined 5Ni/HBEA compared with HBEA support

After calcinations, characteristic peaks of NiO species were observed on 5Ni/HBEA at 37.2 , 43.2 , and 62.9° . These peaks were indexed to the cubic structure of crystalline NiO (Wu et al., 2004) corresponding to the (111), (200), and

(220) crystal, respectively. Thus the presence of 5Ni/HBEA did not destruct the HBEA structure. Moreover, the reflection peaks of NiO indicated that the catalyst preparation by the impregnation method produced metal particles on surface of HBEA with the crystal size, calculated from Scherrer formula, of 28.63 nm.

5.3.1.2 XANES results of calcined Ni catalysts

After calcinations the monometallic and bimetallic catalysts containing Ni on HBEA were characterized by XAS at ambient conditions. The spectra of monometallic samples including 1Ni/HBEA, 3Ni/HBEA, and 5Ni/HBEA comparing to that of the NiO standard are shown in Figure 5.3. The XANES profiles of 5Ni/HBEA and 3Ni/HBEA were similar to NiO that of the standard. However, a slight shift of absorption white line to higher energy was observed. The absorption intensity of catalysts increased with the amount of metal loading. At low Ni content, monometallic of 1 wt% Ni on HBEA (1Ni/HBEA) showed same white line position with NiO but strong decreasing of post edge after white line profile was observed. Moreover, pre-edge of 1 wt% Ni catalyst was strongly decreased.

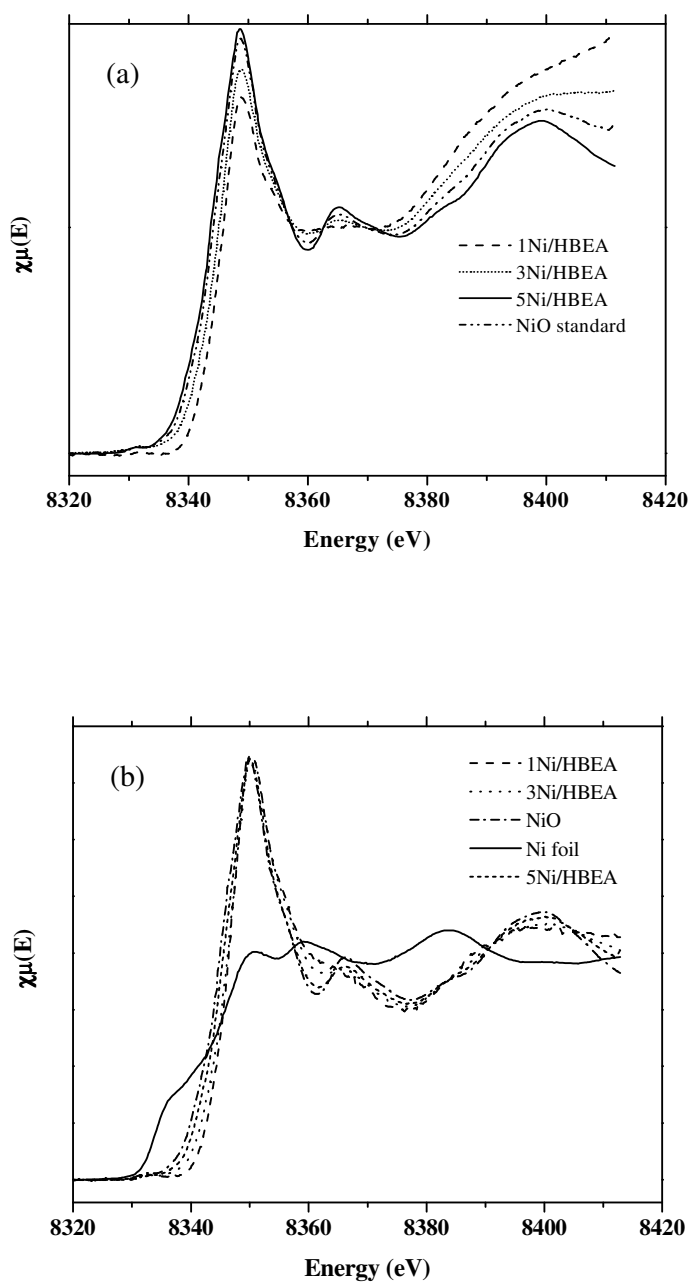


Figure 5.3 XANES profiles of calcined monometallic Ni catalysts compared with NiO standard from ambient condition measurements; raw data plots (a) and normalized data plots (b).

The XANES profiles of bimetallic 1Ni0.5Pt/HBEA and 5Ni0.5Pt/HBEA comparing with that of NiO standard are shown in Figure 5.4. The similar results to those of monometallic ones were observed. The 5Ni 0.5Pt/HBEA showed XANES feature similar to NiO standard but the edge slightly shifted to a higher energy. In contrast, 1Ni0.5Pt/HBEA showed a different feature from NiO standard that the pre-edge peak disappeared, the edge energy shifted to higher value than that of 5Ni0.5Pt/HBEA and the intensity of post edge peaks had low intensity.

The change of pre-edge, white line intensity and XANES features may imply structural changes on Ni atom. Fernando de Souza and coworkers (2003) reported a distinction between 4-, 5-, and 6-coordinated of Ni species from XAS spectra which obtained under high resolution conditions, by analyzing the dependence of the position and the intensity of the pre-edge features. For the catalytic system, a lower intensity of the main edge compared to the octahedral geometry is an indication of lower coordination at the Ni atom and also that the absence of a high-intensity preedge peak eliminates the possibility of square-planar geometry (Fernando de Souza et al., 2003). This means that the 6- and 4- coordinated square-planar configurations can be excluded. In this work, the change of the Ni geometry on zeolite beta support depends on amount of metal loading (Figure 5.3).

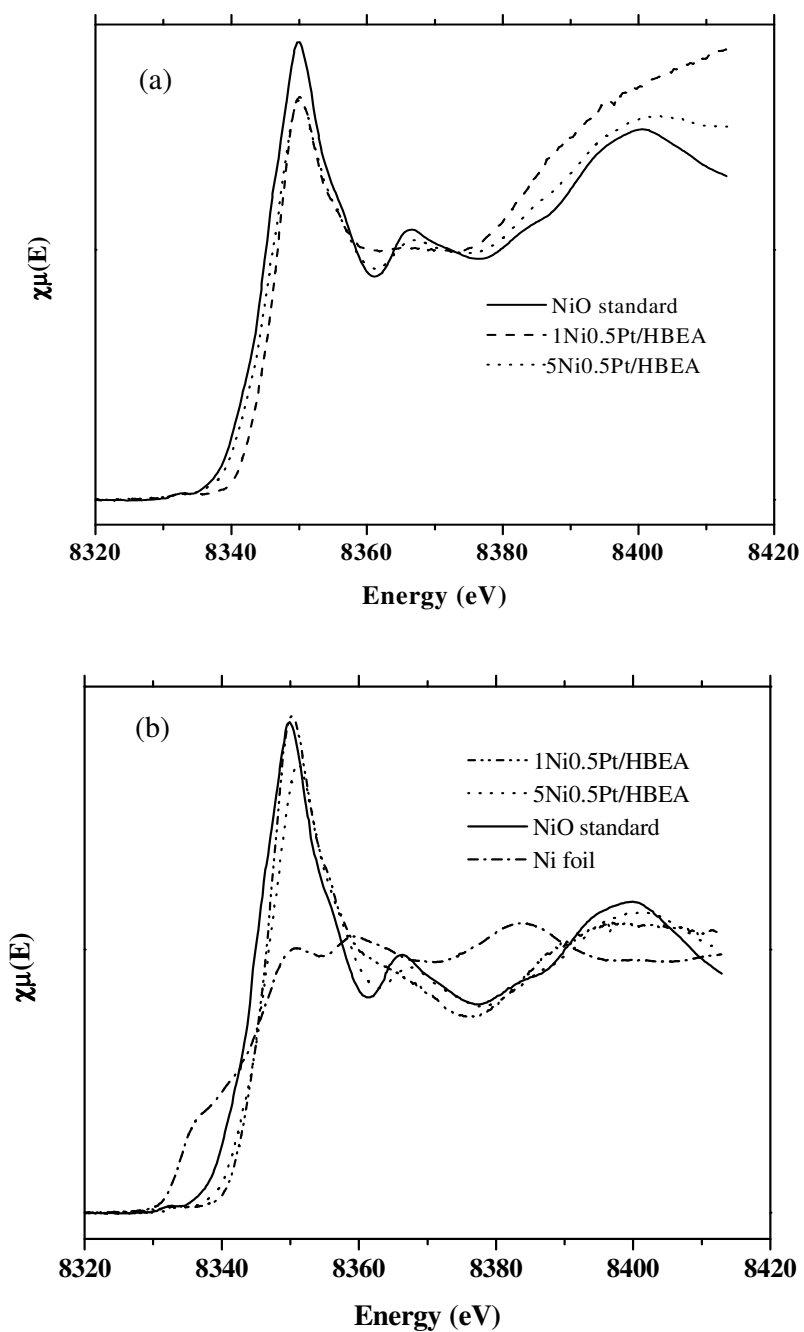


Figure 5.4 XANES profiles of calcined bimetallic Ni catalysts compared with NiO standard from ambient condition measurements; raw data plots (a) and normalized data plots (b).

At low Ni loading (1 wt%) for both monometallic and bimetallic catalysts on zeolite beta, 1Ni/HBEA and 1Ni0.5Pt/HBEA, the XANES profiles indicated a low coordination number of Ni(II) ion possibly tetrahedral or square-planar (Fernando de Souza et al., 2003) because of low white line intensity and flat post-edge. The samples with a higher Ni content, 3Ni/HBEA showed a similar feature to tetrahedral geometry causing with the presence of pre-edge and low white line intensity when compared with NiO octahedral standard. In case of 5Ni/HBEA, the feature clearly showed NiO in octahedral geometry similar to the standard.

5.3.2 Reduction of nickel on Beta catalysts results

5.3.2.1 Ex-situ XANES of reduced Ni catalysts

XANES of calcined monometallic and bimetallic Ni catalysts were reduced at 350°C for 2 h. The samples were pressed to form a pellet by hydraulic pressure of 10 tons before placing on the cell holder for XAS measurement.

Figure 5.5 shows the XANES spectra of monometallic Ni/HBEA with Ni loading of 1, 3, and 5 wt%. A new edge position of Ni(0) species was clearly observed on 5Ni/HBEA at 8333.08 eV along with the same white line peak as in NiO at 8350 eV. This indicated that the reduction of this catalyst was not complete. The edge positions of these samples are listed in Table 5.1. The post-edge of all catalysts the strongly decreasing profiles are also observed. In case of low metal loading of wt% Ni catalysts, the edge energy was slightly shifted to higher value.

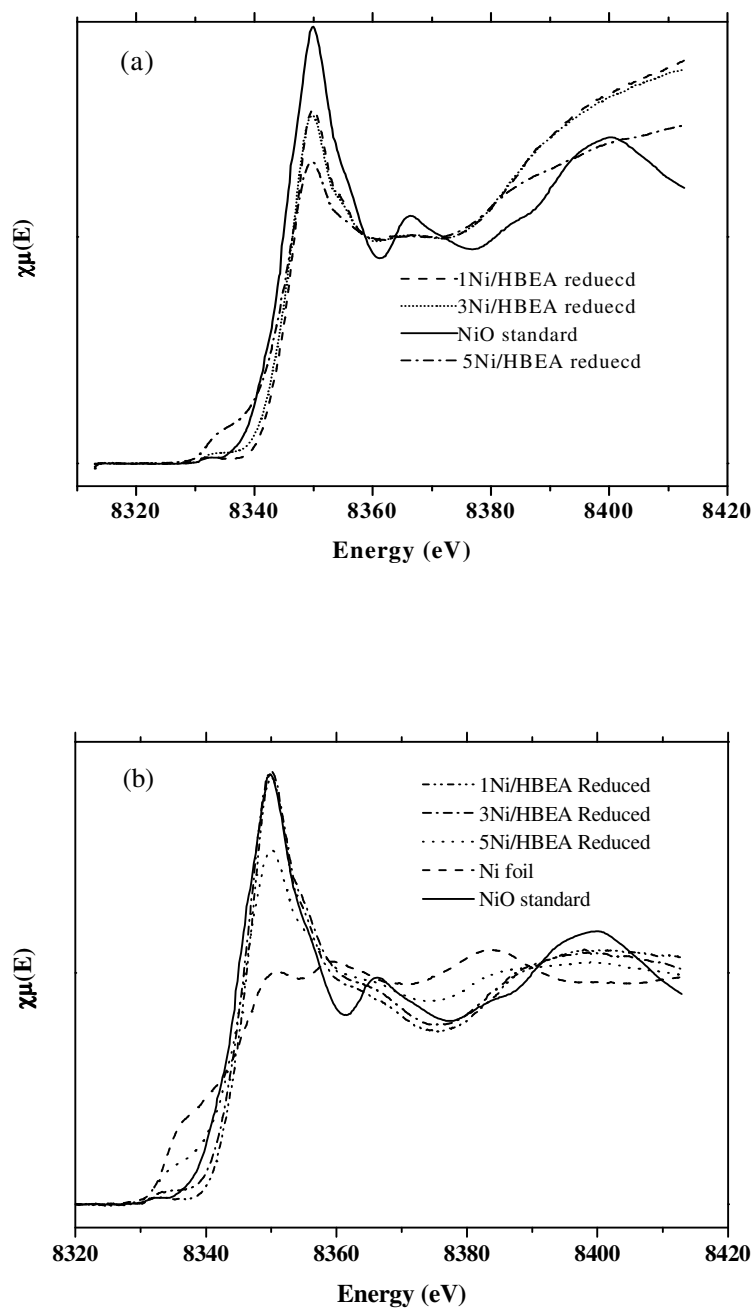


Figure 5.5 XANES profiles of reduced monometallic Ni catalysts compared with NiO standard from ambient condition measurements; raw data plots (a) and normalized data plots (b).

XANES results of reduced bimetallic catalysts were showed in Figure 5.6. 5Ni0.5Pt/HBEA showed similar edge to that of 5Ni/HBEA with character of Ni(0) at 8333.08 eV. In contrast, the nickel edge in 1Ni0.5Pt/HBEA was not changed indicating that nickel in this catalyst could not be reduced..

Table 5.1 shows the energy shift from NiO, edge energies, white line position of monometallic and bimetallic catalysts containing Ni from XAS spectrum as well as the percent reduction calculated from linear combination fitting from Athena program. The degree of reduction of 5Ni0.5Pt/HBEA was 44% and the degree of reduction of 5Ni/HBEA was 41%. In contrast, both the catalyst with Ni loading of 1 and 3 wt% were not reduced. When the loading was low, all Ni ions had good dispersion with a strong interaction with HBEA and could not be reduced (Bartholomew and Farrauto, 2006). As the loading increased, some amount of ions had weaker interaction with the HBEA ad could aggregate to form larger particles resulting in a poorer dispersion. These ions are more easily reduced.

Table 5.1 Edge energy and percent of reduction of catalysts at ambient conditions.

Sample	Energy shift (eV)	Edge energy (eV)	White line (eV)	Percent of reduction (Ni wt%) ^a
1Ni/HBEA	-0.24	8344.6	8350	0.0
3Ni/HBEA	0.19	8346.4	8350	0.0
5Ni/HBEA	0.14	8348.1	8350	40.8 (\pm 1.9)
1Ni0.5Pt/HBEA	-0.09	8347.3	8350	0.0
5Ni0.5Pt/HBEA	0.23	8347.7	8350	44.2 (\pm 2.2)

^a calculated by using Linear combination fitting from Athena program.

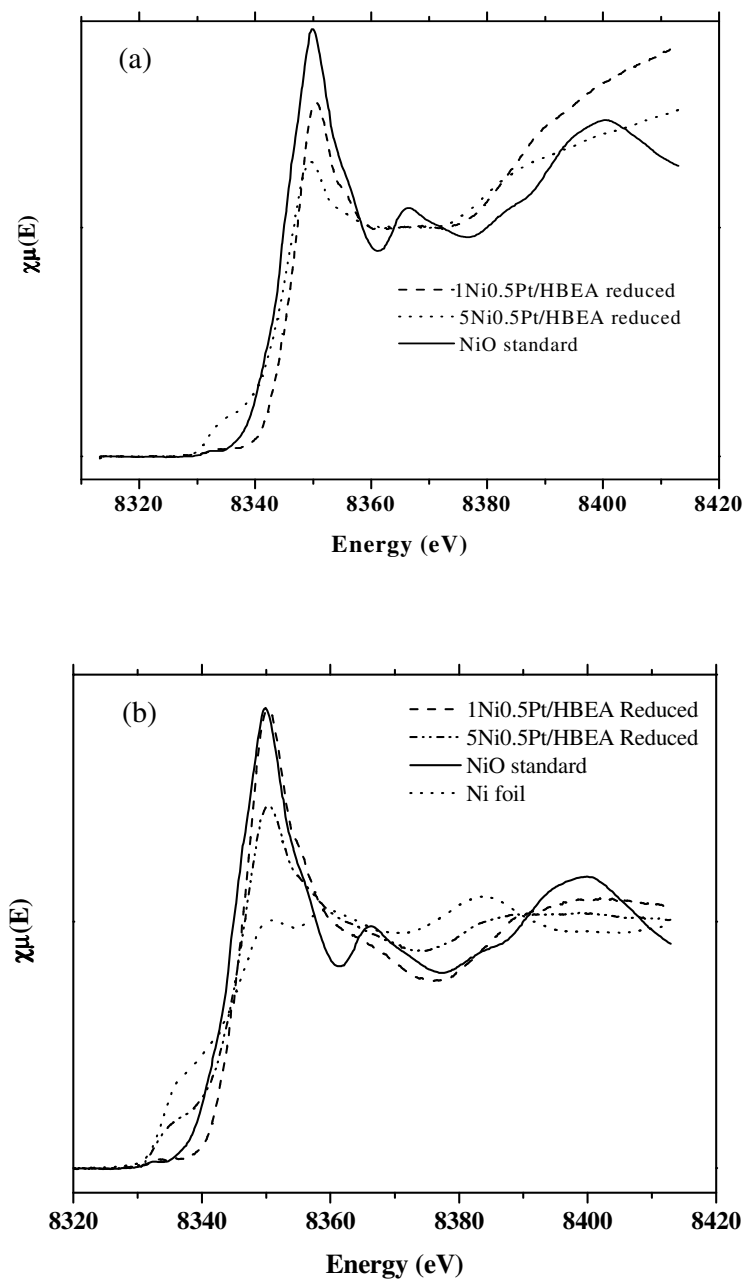


Figure 5.6 XANES profiles of reduced bimetallic Ni catalysts compared with NiO standard from ambient condition measurements; raw data plots (a) and normalized data plots (b).

Consequently, the further investigation was focused on a continuous monitoring of the structural changes in Ni catalysts on HBEA during reduction with an increase of temperature in the in situ X-ray absorption cell. The XAS measurements in both XANES and EXAFS regions were performed to confirm the ionic valence of Ni species, geometrical changes and tendency of the degree of reduction. The reduction conditions included a continuously increase of reduction temperature from 21 to 350°C with H₂ flow rate of 50 ml/min.

5.3.2.2 In situ XANES results of reduced 5Ni0.5Pt/HBEA

Figure 5.7 shows XANES spectra of the 5Ni0.5Pt/HBEA catalyst from the in situ XAS measurement with varying reduction temperature from 21 to 350°C. The profile at 21°C was similar to the pattern of NiO standard whose pre-edge was clearly observed with the white line position at 8350.8 eV. After increasing the temperature to 100°C, the pre-edge decreased and the white line was observed at the same position. The results indicated changing of NiO geometry from octahedral to lower symmetry or lower coordination number (Fernando de Souza et al., 2003). The most possible structure change was to tetrahedral geometry because the edge position was the same indicating that Ni remained in the form of Ni(II) but the lower intensity of main edge and pre-edge implied changing from the octahedral structure as in NiO standard (Fernando de Souza et al., 2003). However, the strong distortion of the main edge position also implied the possible geometry of square-planar in the structure.

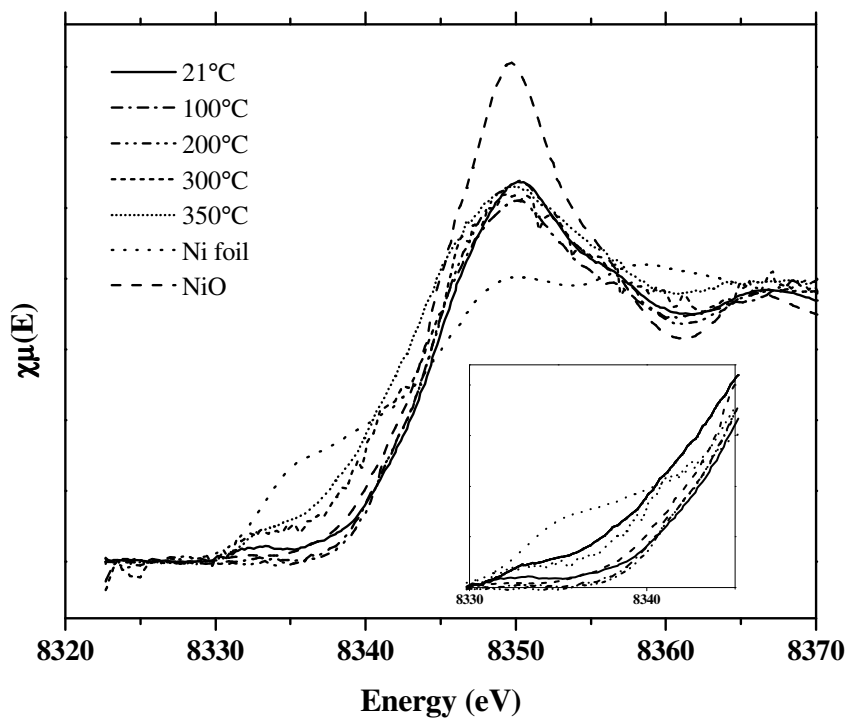
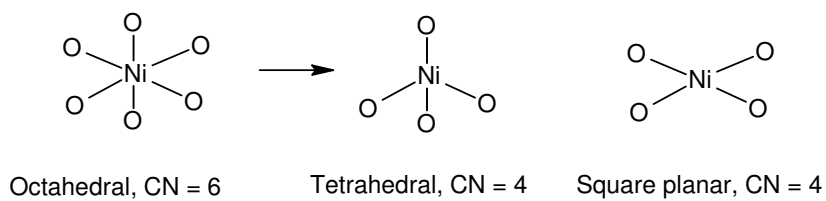


Figure 5.7 XANES spectra at Ni edge of 5Ni0.5Pt/HBEA from the in situ XAS measurement at various reduction temperatures.

The change of geometry of Ni during the reduction from octahedral to tetrahedral or square planar involves the change of coordination number (CN) with surrounding oxygen from 6 to 4 as shown in Scheme 1.



Scheme 1 the geometry change of NiO structure from coordination number of 6 to 4.

At 200°C, a clear geometry change of NiO occurred as a shoulder emerged before the white line region of the XANES profile. This result indicated a change of NiO geometry to a mixture of tetrahedral and square-planar (Fernando de Souza et al., 2003). The results of 300°C have strongly geometry change because the strength line of the XANES was detected. This result is interesting for further study on the effect of temperature to the geometry change. At 300°C, a pre-edge of Ni(0) at 8333 eV was observed with higher intensity than that at 200°C, similar white line intensity but the intensity after the edge was flat. The spectrum at 350°C was similar to that at 300°C showing a pre-edge at 8333 eV and the white line position at 8345 eV. Therefore, the 5Ni/HBEA could be reduced partially at 350°C with 50 ml/min H₂ flow.

The percentage of reduced Ni at various temperatures was calculated from linear combination fit function from the Athena program. The raw data of XANES spectra were calibrated by Ni foil standard and normalized by using Athena program before the fit by linear combination function. Two standards of Ni foil and NiO were used as standards for fitting as Ni(0) and Ni(II) species, respectively. Examples of the linear combination fitting results are shown to exhibit the raw data, fit data and components of the fit data. The graphs from further fitting results are put in Appendix B and C and only the percentages of reduction are shown in tables. Note that the phase of Ni(acac)₂ from the precursor was not found in all calculation and it was excluded from all the graphs and tables.

The linear combination fitting results of reduced Ni at the temperature of 100 and 350°C are shown in Figure 5.8. The degree of reduction was

about 40% for the temperature of 100°C and about 70% for the temperature of 350°C with holding time of 1.5 h.

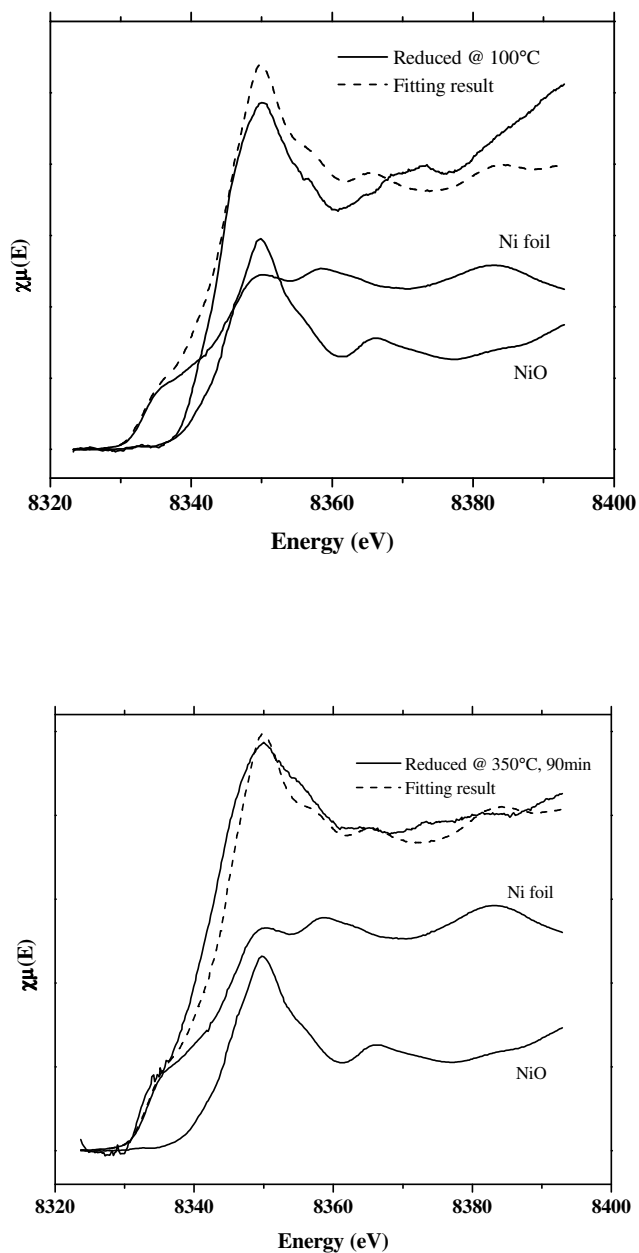


Figure 5.8 The linear combination fitting of reduced 5Ni0.5Pt/HBEA at 100°C with 10 min holding time and 350°C with 90 min holding time.

The percentage of reduced Ni in 5Ni0.5Pt/HBEA at various temperatures are shown in Figure 5.9. The degree of reduction increased with temperature and reached about 47% at 350°C. The reduction was about 69% after 1.5 h indicating that a longer reduction time is needed for this catalyst at this temperature.

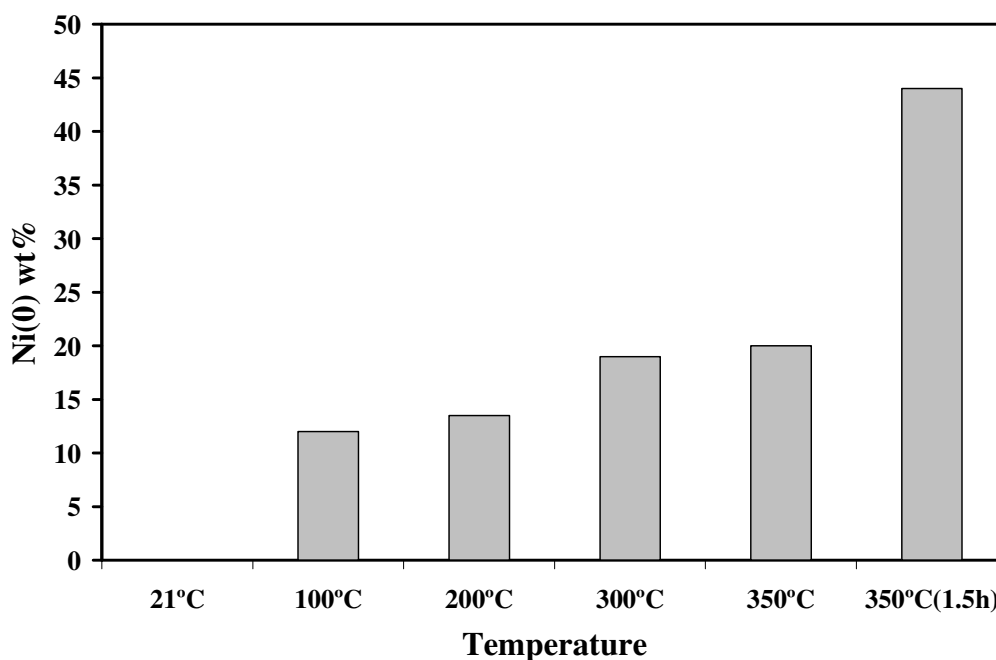


Figure 5.9 The degree of reduction of 5Ni0.5Pt/HBEA from Linear combination fitting in Athena program with reduction temperature.

The trend of the degree of reduction with time may lead to a suitable time to complete reduction. Figure 5.10 showed XANES spectra of 5Ni/HBEA during a reduction under hydrogen flow at 350°C recorded from 10 to 90 min. From the spectra, increases of pre-edge and shifts in edge energy were observed. The position of pre-edge and edge from Figure 5.10 are shown in Table 5.2. The percent of

reduced Ni at 350°C calculated from linear combination fit function from the Athena program are plotted in Figure 5.11. The degree of reduction increased with time and reached a maximum after 60 min. The results indicated that the higher degree of nickel reduction was not possible at this temperature.

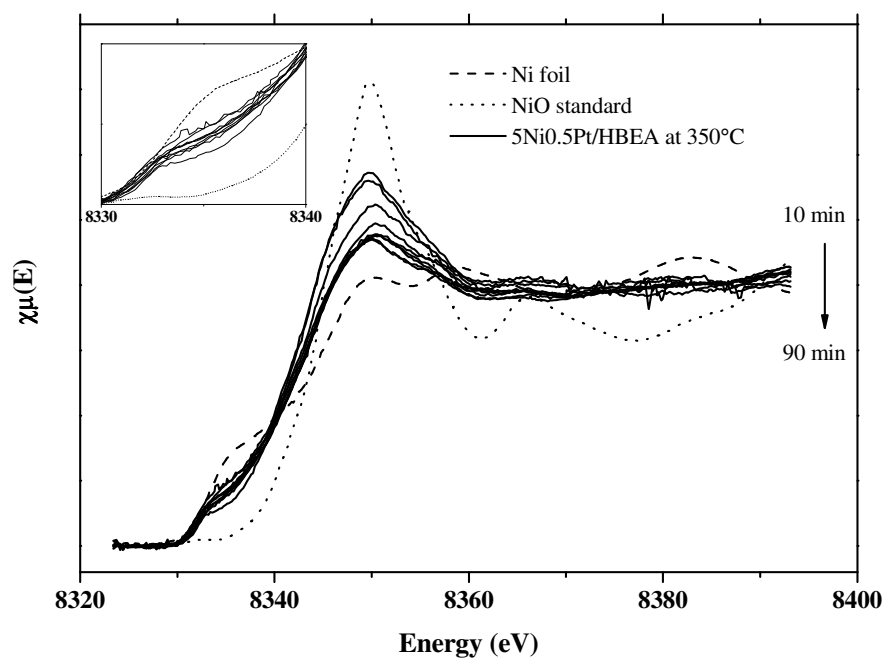


Figure 5.10 Ni edge on 5Ni0.5Pt/HBEA with reduction temperature of 350°C from 10 to 90 min.

Table 5.2 Pre-edge and edge position of 5Ni0.5Pt/HBEA during reduction in hydrogen flow at 350°C recorded from 10 to 90 min.

Time (min)	Pre-edge position (eV)	Edge position (eV)
10	8329.77	8340.79
20	8331.43	8343.04
40	8331.72	8343.79
60	8332.54	8343.08
70	8334.00	8345.02
80	8332.62	8343.92
90	8333.11	8342.65

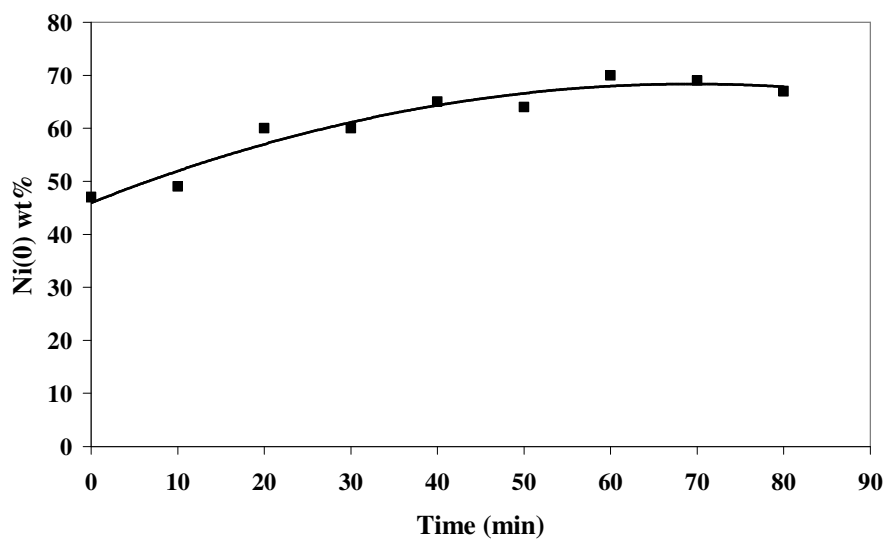


Figure 5.11 The degree of reduction of 5Ni0.5Pt/HBEA from Linear combination fitting plotting of reaction temperature of 350°C and reduction time.

5.3.3 In situ XAS measurement during toluene desorption on 5Ni/HBEA

Figure 5.12 shows XANES spectra of calcined 5Ni/HBEA from in situ measurements during toluene desorption from room temperature (21°C) to 250°C. The catalyst was used after calcination without reduction, and thus, the active form was presumably NiO. Moreover, after cool down the sample to room temperature the spectrum was also recorded to compare the structure change at high temperature of 250°C and room temperature.

Table 5.3 Pre-edge and edge position of 5Ni/HBEA during toluene desorption as the temperature increased from room temperature.

Temperature	Pre-edge position	Edge position
21	-	8344.46
100	8332.02	8343.56
200	8331.23	8344.34
250	8332.44	8344.23
21 (after cooled down)	8333.10	8343.96

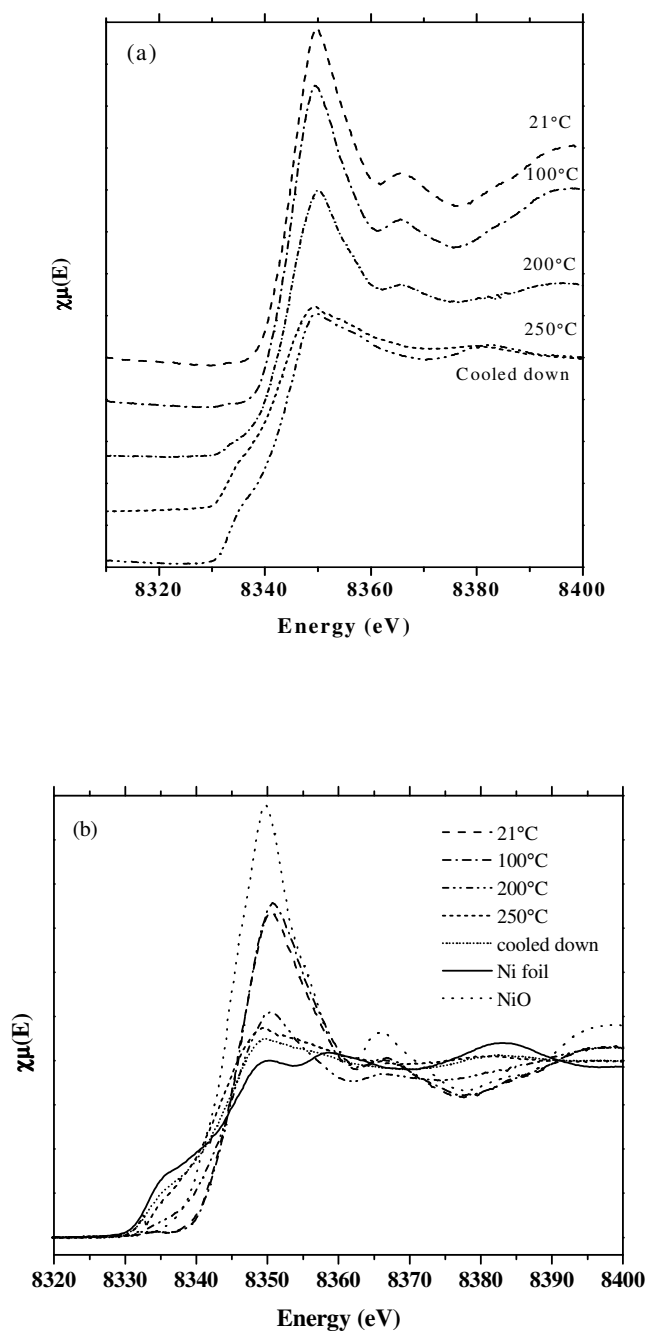


Figure 5.12 XANES spectra of 5Ni/HBEA catalyst during toluene desorption in N_2 flow at 21, 100, 200, 250°C and after cool down to room temperature (a) and normalized spectra (b).

The XANES spectrum of 5NiO/HBEA at 21 and 100°C showed similar features to that of NiO standard which had octahedral geometry with 6 oxygen atoms surrounding the nickel atom. These results implied that the electronic properties of NiO/HBEA did not change during the toluene adsorption and desorption at these temperatures. At 100°C the structure of Ni was still octahedral and the intensity of pre-edge and white line slightly decreased while other features remained the same. Little change of NiO structure indicated that toluene was not adsorbed on Ni but it adsorbed on acid sites of HBEA supported. The adsorption of toluene on zeolite beta was reported in the literatures (Yoshimoto et al., 2007). The results confirmed catalytic mechanism of toluene hydrogenation on bifunctional catalysts proposed in the literatures (Wang et al., 1999 and Lin et al., 1993) that toluene molecules did not adsorb on Ni atoms but they preferred to adsorb on acid sites of zeolite. The proposed toluene hydrogenation mechanism on bifunctional Ni/HBEA catalysts is illustrated in Figure 5.13. Therefore, the Ni atoms would not be deactivated by toluene adsorption which could polymerize to coking. As a result, hydrogen molecules could adsorb easily on Ni sites and available for hydrogenation mechanism.

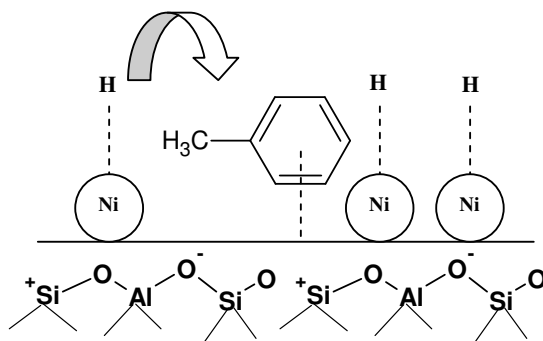


Figure 5.13 Proposed mechanism of toluene hydrogenation on bifunctional catalyst.

At 200°C the XANES spectrum of 5NiO/HBEA in Figure 5.12 showed the edge feature that was different from that of NiO. The intensity of pre-edge decreased indicating that a distortion of NiO structure from octahedral to lower coordination number. This result might cause by loss of oxygen from Ni-O bond, thus the distortion might cause by mixture of 5-, 4- coordination of the structure (Fernando de Souza et al., 2003). Therefore, oxygen atom from Ni-O bond could be released at 200°C and it was the cause of structural change of Ni. However, the edge positions did not change significantly implying that Ni atom remained in form of Ni(II). The spectrum with reaction temperature at 250°C showed more decrease of the pre-edge indicating more change in coordination number from oxygen loss. Furthermore, the XANES spectrum of the sample after cooling down to room temperature was similar to that of the sample at 250°C. This result means that the structural change was not reversible.

5.3.4 In situ XAS results of toluene hydrogenation

Toluene hydrogenation on calcined 5Ni/HBEA was studied in the in situ XAS cell and changes of XANES spectra were continuously monitored with an increase of reaction temperature. Results are shown in Figure 5.14. The first spectrum was recorded at 70°C and the next one was recorded when the temperature was increased to 110°C. More spectra were recorded at this temperature every 10 min for 5 times. All spectra showed similar features to that of NiO standard without an increase of the pre-edge intensity. Because the XANES spectra did not change, there was no change in nickel structure. This is explained by the adsorption behavior of toluene that is more preferable to occur on the zeolite not Ni sites. Although the calcined catalyst was exposed to hydrogen flow, the temperature was too low for the

reduction of nickel oxides. Thus, the form of Ni was still NiO which was not active for hydrogenation due to the difficulty of hydrogen adsorption on metal oxide.

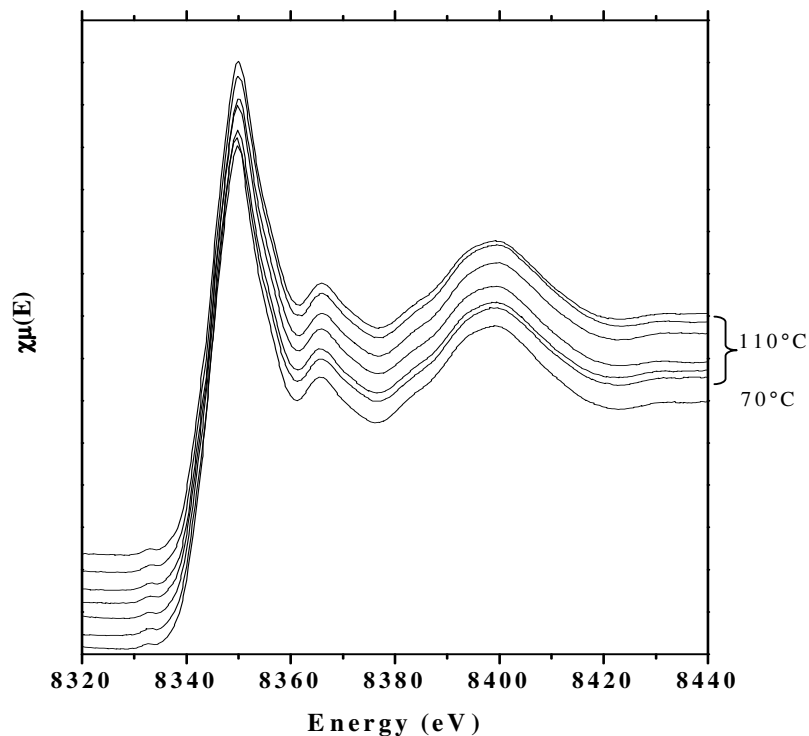


Figure 5.14 XANES spectra of calcinated 5Ni/HBEA on toluene hydrogenation at 70 and 110°C.

The in situ XAS measurement during toluene hydrogenation was also carried out at 150°C. The results are shown in Figure 5.15. At the beginning the XANES spectra showed a characteristic of Ni(O) with a new edge at 8333 eV. This new edge was more evident when the holding time was longer. At this temperature hydrogen could reduce NiO to Ni(O) and the resulting metallic sites became adsorption sites for hydrogen. Then the spill-over hydrogen from Ni sites could react with

toluene adsorbed on the zeolites to form hydrogenation products as described in Scheme 5.1. The edge positions of Ni(0) and Ni(II) as well as the percent reduction are listed in Table 5.3. The amount of metallic Ni calculated from Linear combination fit in Athena program increased with the time.

After the last measurement at 150°C, the temperature was raised to 200°C with the ramp of 10°C/min under hydrogen and toluene flow. The intensity of Ni(0) edge increased indicating that more reduction occurred. The position of white line and post edge character in all measurement at 200°C were similar to that of the Ni foil standard indicating that the calcined catalyst converted to Ni(0) upon the reaction condition. The percent reduction of Ni at 200°C is shown in Table 5.4. The range of 78 - 86 % was obtained.

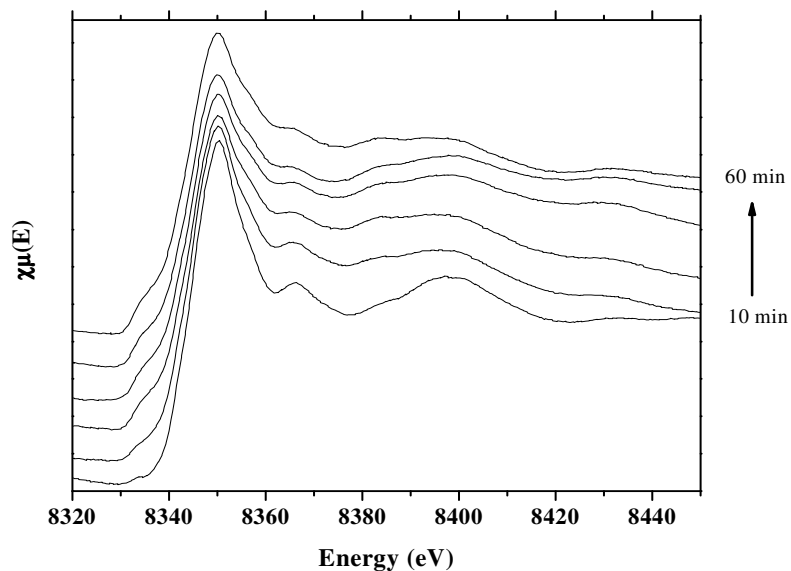


Figure 5.15 XANES spectra of calcined 5Ni/HBEA on toluene hydrogenation at 150°C.

Table 5.4 Pre-edge, edge position of 5Ni/HBEA and percent reduction during toluene hydrogenation at 150°C.

Time (min)	Ni(0) edge position (eV)	Ni (II) edge position (eV)	Percent of reduction
0	-	8344.97	-
10	8331.89	8343.76	15.2
20	8331.81	8344.18	15.8
30	8331.66	8344.03	18.9
40	8331.45	8344.37	23.8
50	8331.55	8344.11	28.0
60	8332.05	8344.11	37.4

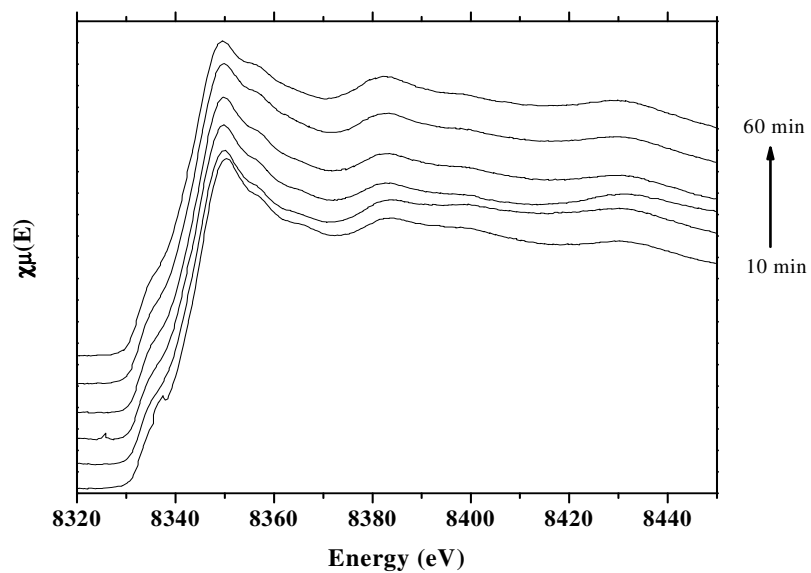


Figure 5.16 XANES spectra of calcined 5Ni/HBEA on toluene hydrogenation at 200°C.

Table 5.5 Percent reduction of Ni in 5Ni/HBEA at 200°C.

Time (min)	Percent reduction
0	-
10	80.3
20	77.6
30	78.5
40	80.9
50	85.5
60	86.4

5.4 Conclusions

Monometallic Ni/HBEA and bimetallic NiPt/HBEA were prepared by impregnation. The calcined 5Ni/HBEA showed characteristic peaks of HBEA and peaks corresponding to crystalline NiO with the size of 28.63 nm. The crystal size indicated the occupation of Ni atom outside BEA channels.

From XANES results, the oxidation state of Ni of all catalysts was 2+. Nickel in the catalysts with low metal loading had lower coordination than that with high loading. The catalysts with low metal loading was not reducible because of a strong metal-support interaction but that with high metal loading, i. e., 5Ni/HBEA was easier to reduce. The degree of reduction depends on temperature and time exposed to hydrogen.

Toluene desorption study on calcined 5Ni/HBEA showed geometry changes of NiO from octahedral to tetrahedral or square planar form with increasing temperature. No Ni-C interaction was observed from in situ XANES results of toluene desorption at all temperatures indicating that toluene did not adsorb on Ni active sites but only acid sites of the HBEA support. Moreover, toluene might be oxidized by oxygen from NiO because the coordination number of Ni decreased during the in situ XANES measurement. In toluene hydrogenation on calcined 5Ni/HBEA, the NiO was slowly reduced by hydrogen as indicated by an appearance of Ni(0) edge. Although some products were detected, the catalyst performance was not fully studied.

5.5 References

- Bernardi, F., Alves, M. C. M., Scheeren, C. W., Dupont, J., and Morais, J. (2007). In situ studies of nanoparticles under reaction with sulfur by XAS. **J. Electron Spectrosc.** 156-158: 186-190.
- Burattin, P.; Che, M., and Louis, C. (1997). Characterization of the Ni(II) Phase Formed on Silica Upon Deposition–Precipitation. **J. Phys. Chem. B.** 36: 7060-7074.
- Bus, E., Ramaker, D. E., and van Bokhoven, J. A. (2007). Structure of Ethene Adsorption Sites on Supported Metal Catalysts from in Situ XANES Analysis. **J. Am. Chem. Soc.** 129: 8094-8102.
- Bus, E., and van Bokhoven, J. A. (2007). Electronic and Geometric Structures of Supported Platinum, Gold, and Platinum–Gold Catalysts. **J. Phys. Chem. C.** 111: 9761-9768.

- Carriat, J. Y., Che, M., Kermarec, M., Verdaguer, M., and Michalowicz, A. (1998). Control of Dispersion of Ni²⁺ Ions via Chelate Ligands in the Preparation of Ni/SiO₂ Materials. A XAFS Study. **J. Am. Chem. Soc.** 120: 2059-2070.
- Fernando, D. S. R., Simon, L. C., and Maria D. C. M. A. (2003). XAS study of the nickel(α -diimine) catalyst for olefin polymerization. **J. Catal.** 214: 165-168.
- Lin, S. D., and Vannice, M. A. (1993). Hydrogenation of aromatic hydrocarbons over supported Pt catalysts. **J. Catal.** 143: 539-553.
- Odzak J. F., Argo, A. M., Lai, F. S., Gatesa, B. C., Pandya, K., and Feraria, L. (2001). A flow-through x-ray absorption spectroscopy cell for characterization of powder catalysts in the working state. **Rev. Sci. Instrum.** 72: 3943-3945.
- Van der Eerdena A., van Bokhoven, J., Smith, A., and Koningsberger, D. (2000). Apparatus for in-situ Xafs studies on catalytic systems in the energy range 1000 eV < E < 3500 eV. **Rev. Sci. Instrum.** 71: 3260-3266.
- Wang, J., Li, Q., and Yao, J. (1999). The effect of metal-acid balance in Pt-loading dealuminated Y zeolite catalysts on the hydrogenation of benzene. **Appl. Catal. A.: Gen.** 184: 181-188.
- Wu, L., Wu, Y., Wei, H., Shi, Y., and Hu, C. (2004). Synthesis and characteristics of NiO nanowire by a solution method. **Mater. Lett.** 58: 2700-2703.
- Yang, J. C., Shul, Y. G. Louis, C., and Che, M. (1998). In situ EXAFS study of the nucleation and crystal growth of Ni particles on SiO₂ support. **Catal. Today.** 44: 315-325.
- Yoshimoto, R., Hara, K., Okumura, K., Katada, N., and Niwa, M. (2007). Analysis of toluene adsorption on Na-form zeolite with a temperature-programmed desorption method, **J. Phys. Chem. C.** 111: 1474-1479.

CHAPTER VI

CONCLUSIONS

In this thesis, zeolite beta (BEA) was successfully prepared with utilization of amorphous rice husk silica. The prepared BEA products with gel Si/Al ratios from 8 to 20 showed the pure phase of BEA. The highest crystallinity and the largest crystal size were observed in the sample with gel Si/Al ratio of 13. The samples with gel Si/Al ratios from 50 to 200 showed a mixed phase of BEA and MTW. The transformation of BEA phase to MTW became more significant with a higher gel Si/Al ratio and the MTW phase was almost pure at the gel ratio of 200.

BEA was used as a catalyst support for Pt and Pd to catalyze toluene hydrogenation. The catalytic enhancement of Pt/HBEA by addition of Pd for the reaction was studied. Monometallic and bimetallic PtPd/HBEA catalyst was prepared by co-impregnation and the structure of HBEA was maintained. The XRD results showed a presence of metallic Pt particle with monometallic Pt/HBEA and bimetallic PtPd/HBEA but the presence of Pd particles were not observed on both Pd/HBEA and PtPd/HBEA. Moreover, Pt size on bimetallic catalysts were smaller than those on the bimetallic one probably due to the presence of Pd. Results from NH₃ - TPD indicated that the metals occupied strong acidic sites of HBEA. However, the changes of Pd after calcination and reduction could not be observed by XAS. The catalytic performance of bimetallic 3Pt3Pd/HBEA over toluene hydrogenation was studied and the presence of Pd enhanced both toluene conversion and selectivity for

methylcyclohexane. The most suitable temperature for toluene hydrogenation on 3Pt3Pd/HBEA was 150°C in which a complete toluene conversion and 100% selectivity for methylcyclohexane were achieved.

Monometallic Ni/HBEA and bimetallic NiPt/HBEA were prepared by impregnation. The calcined 5Ni/HBEA showed characteristic peaks of HBEA and peaks corresponding to crystalline NiO with the size of 28.63 nm. The crystal size indicated the occupation of Ni atom outside BEA channels. From XANES results, the oxidation state of Ni of all catalysts was 2+. Nickel in the catalysts with low metal loading had lower coordination than that with high loading. The catalysts with low metal loading was not reducible because of a strong metal-support interaction but that with high metal loading, i. e., 5Ni/HBEA was easier to reduce. The degree of reduction depends on temperature and time exposed to hydrogen.

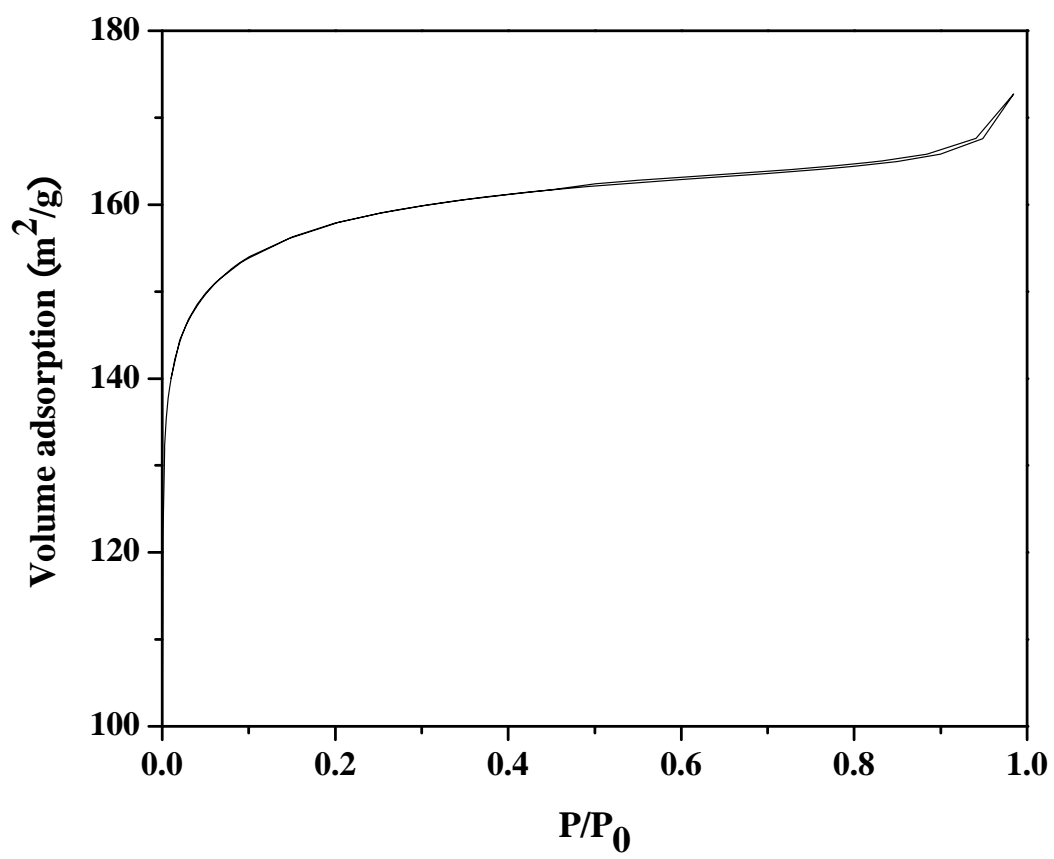
Toluene desorption study on calcined 5Ni/HBEA showed geometry changes of NiO from octahedral to tetrahedral or square planar form with increasing temperature. The Ni-C interactions were not observed from in situ XANES results of toluene desorption at all temperature indicating that toluene did not adsorb on Ni active sites but only acid sites of the HBEA support. Moreover, toluene might be oxidized by oxygen from NiO because the coordination number of Ni decreased during the in situ XANES measurement. In toluene hydrogenation on calcined 5Ni/HBEA, the NiO was slowly reduced by hydrogen as indicated by an appearance of Ni(0) edge. Although some products were detected, the catalyst performance was not fully studied.

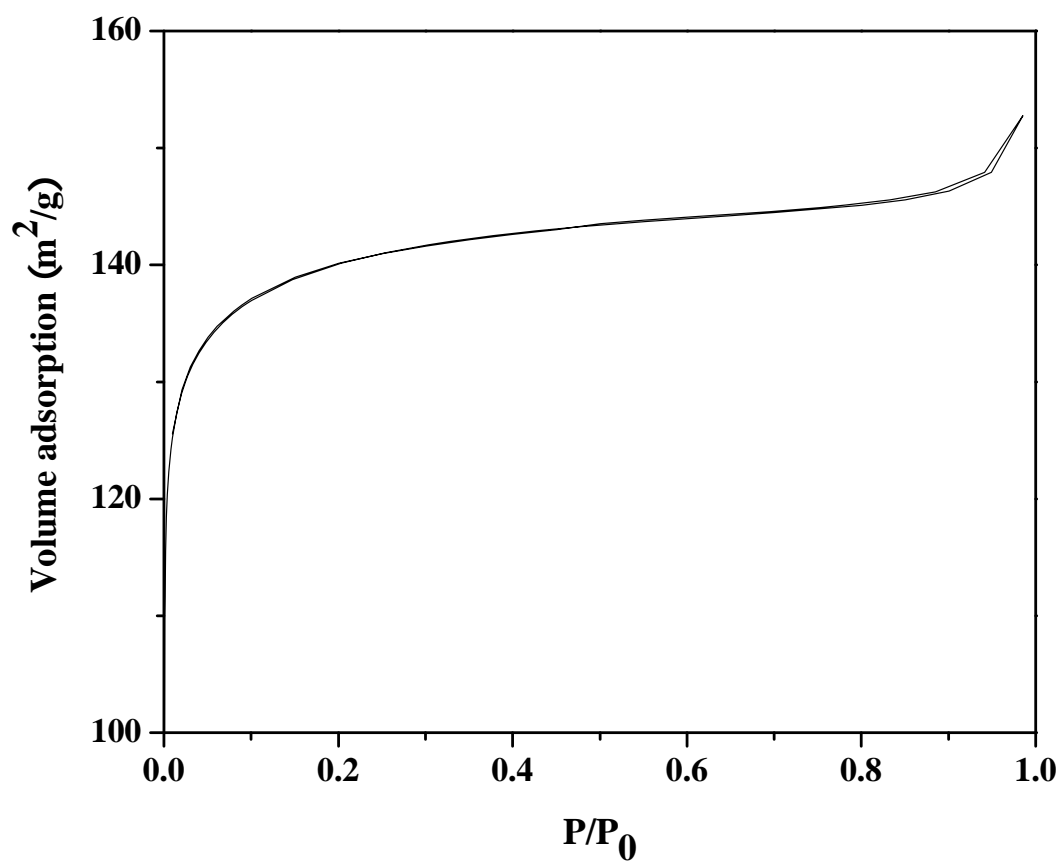
APPENDICES

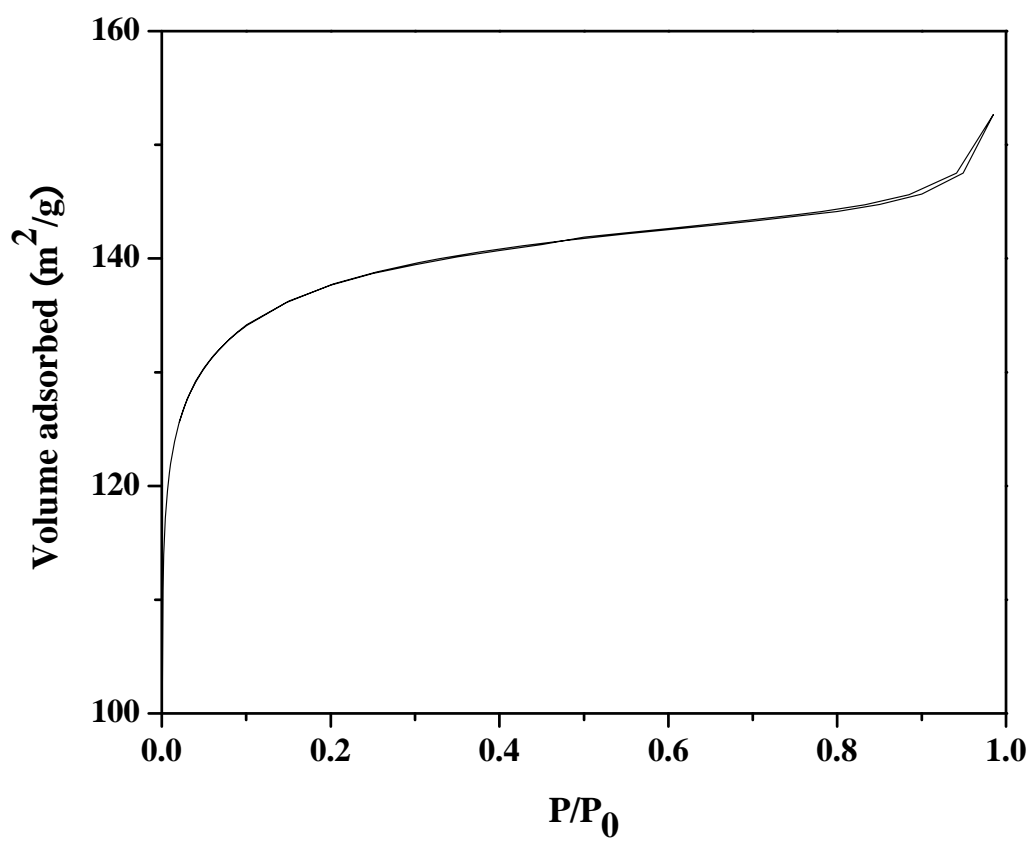
APPENDIX A

NITROGEN ADSORPTION-DESORPTION ISOTHERMS

OF 3Pd/HBEA, 3Pt/HBEA and 3Pt3Pd/HBEA

3Pd/HBEA

3Pt/HBEA

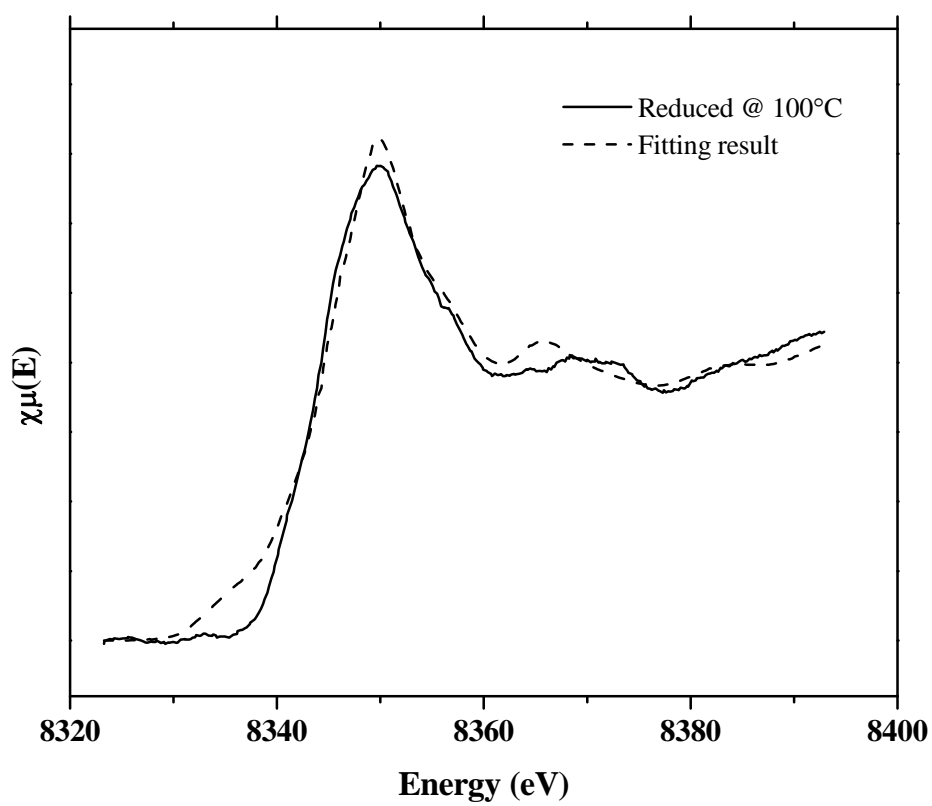
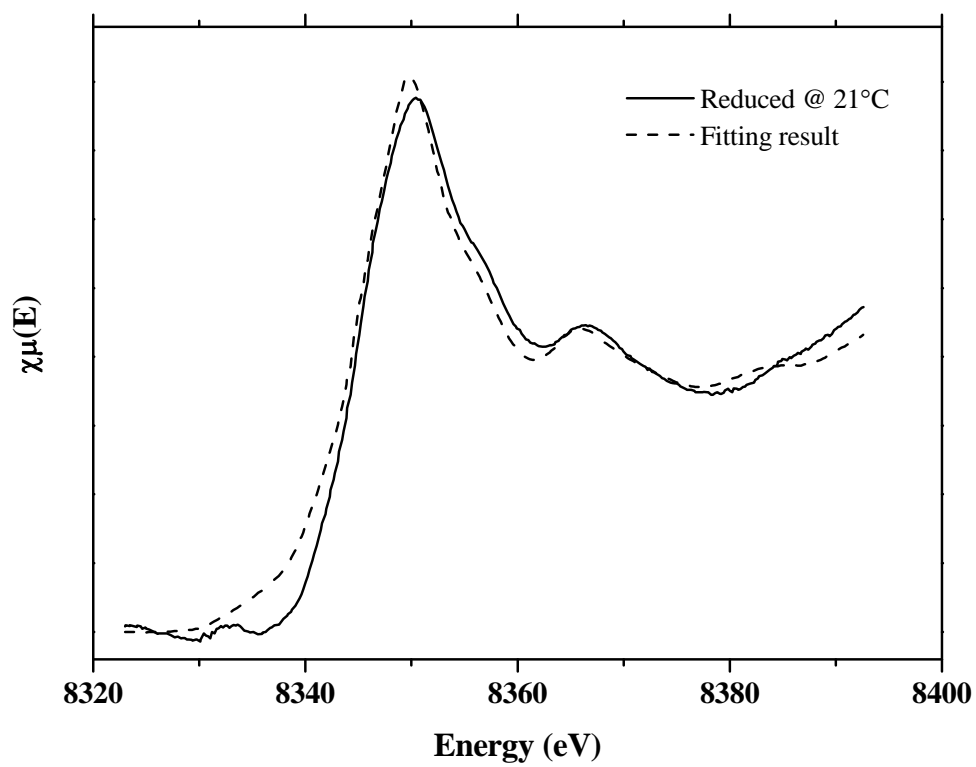
3Pt3Pd/HBEA

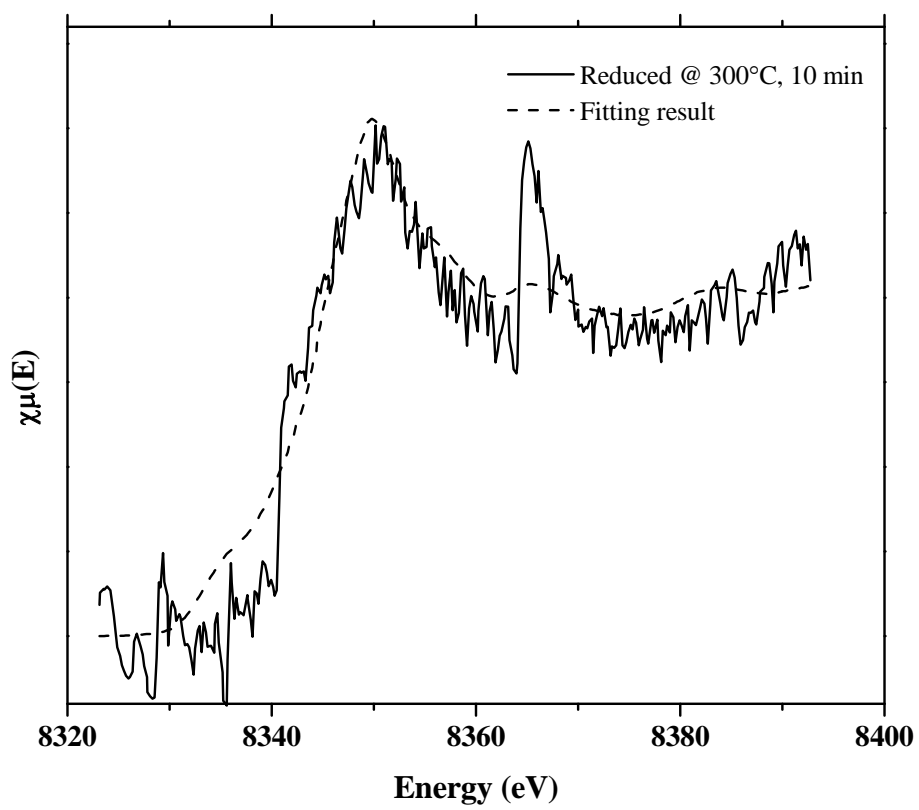
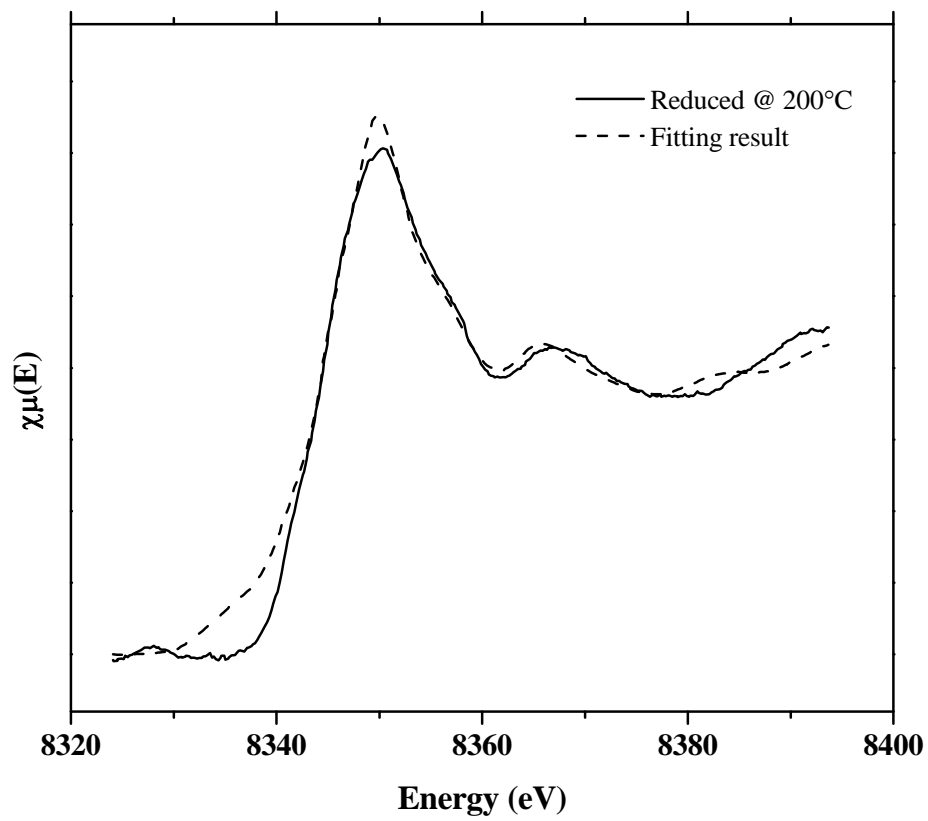
APPENDIX B

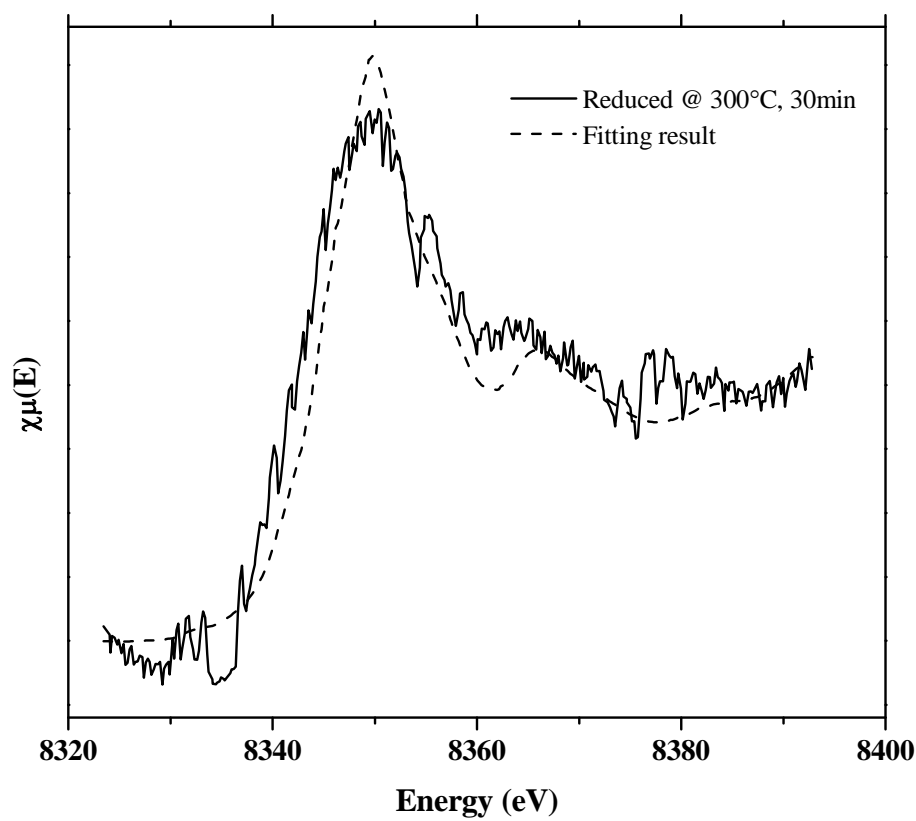
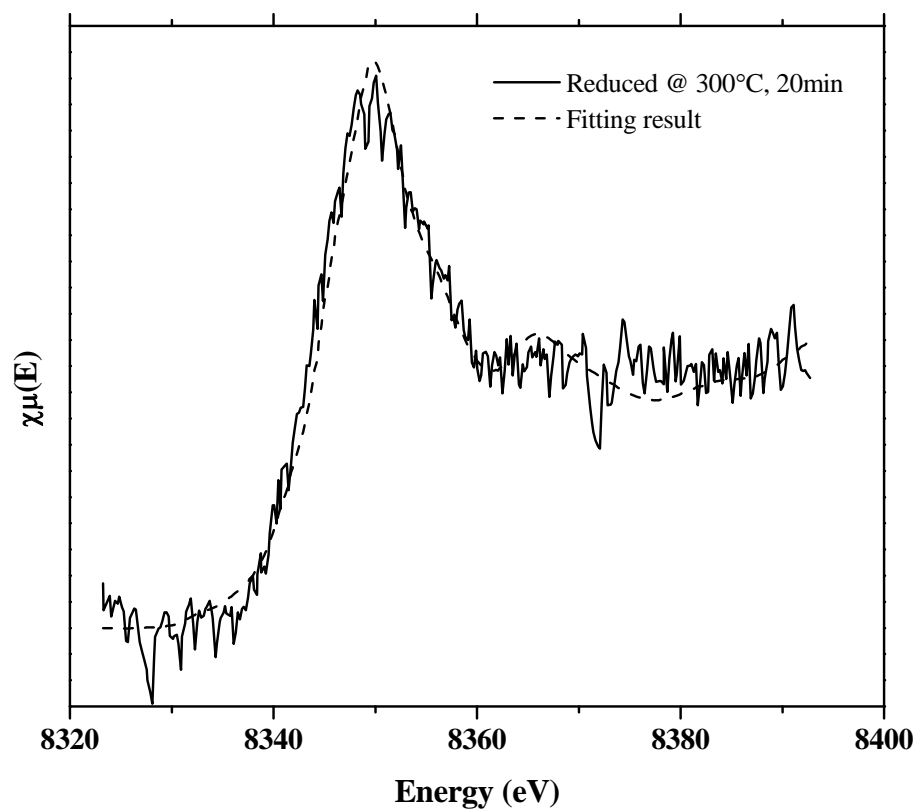
LINEAR COMBINATION FITTING RESULTS OF

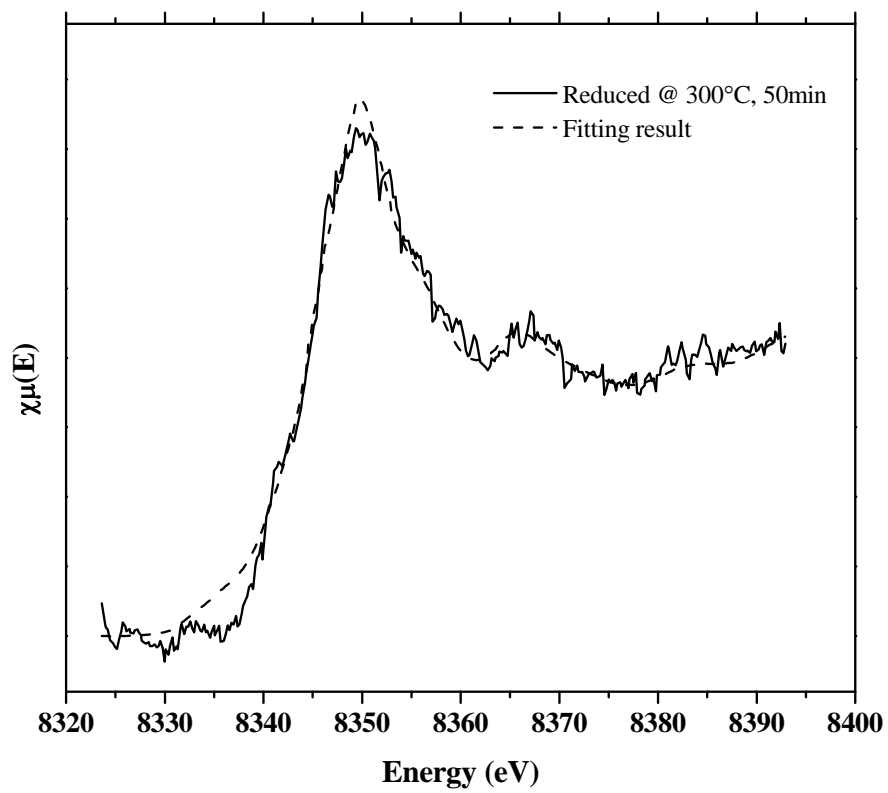
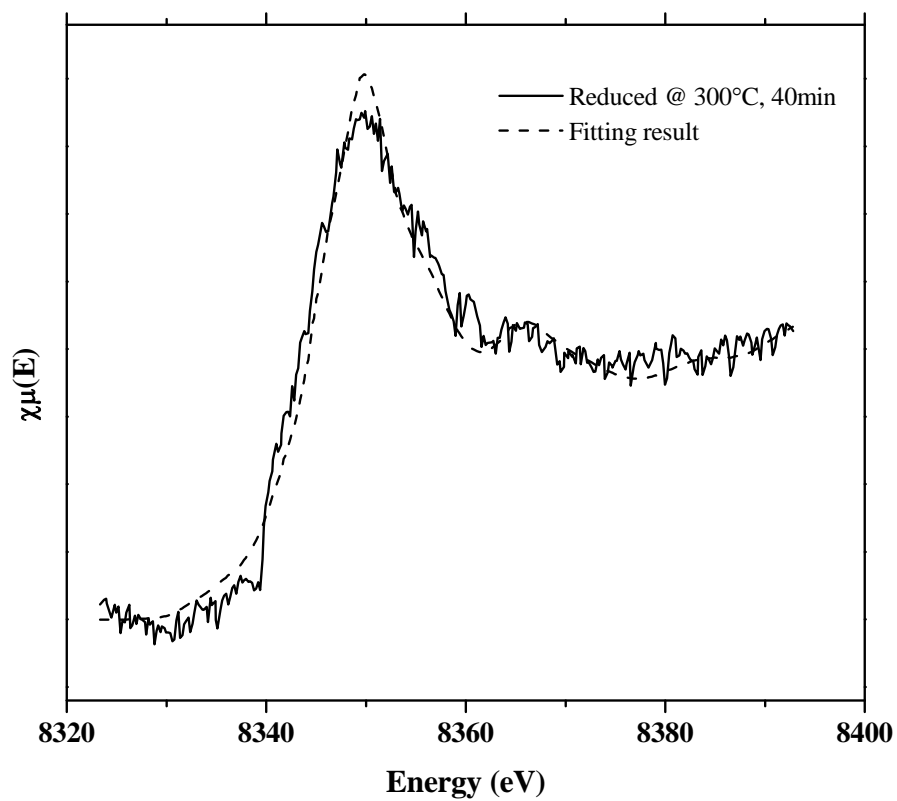
5Ni0.5Pt/HBEA DURING IN SITU REDUCTION FROM

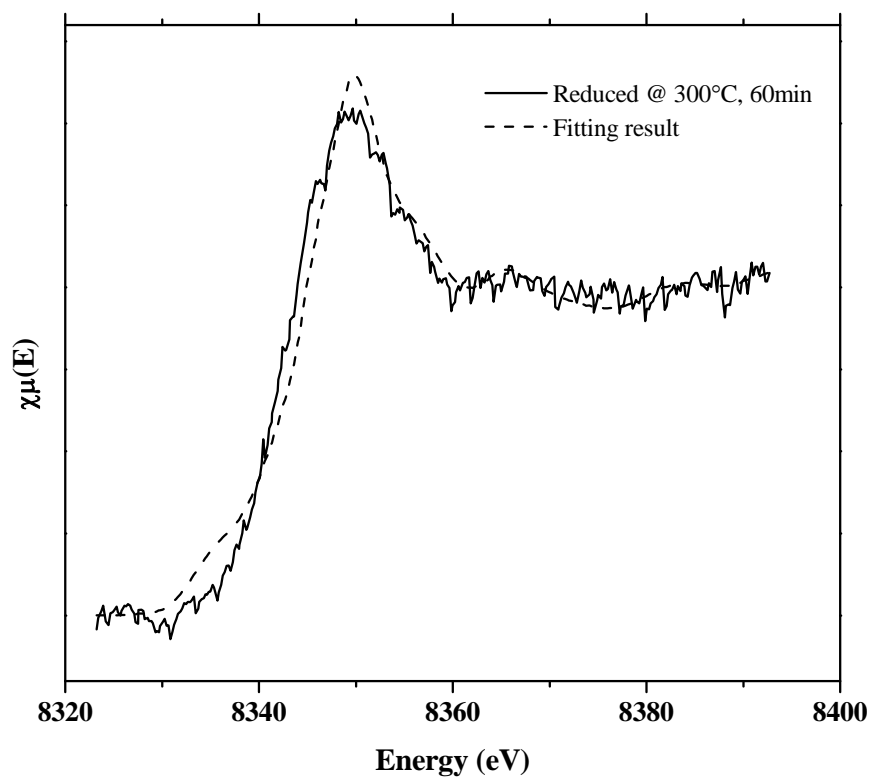
ROOM TEMPERATURE TO 300°C





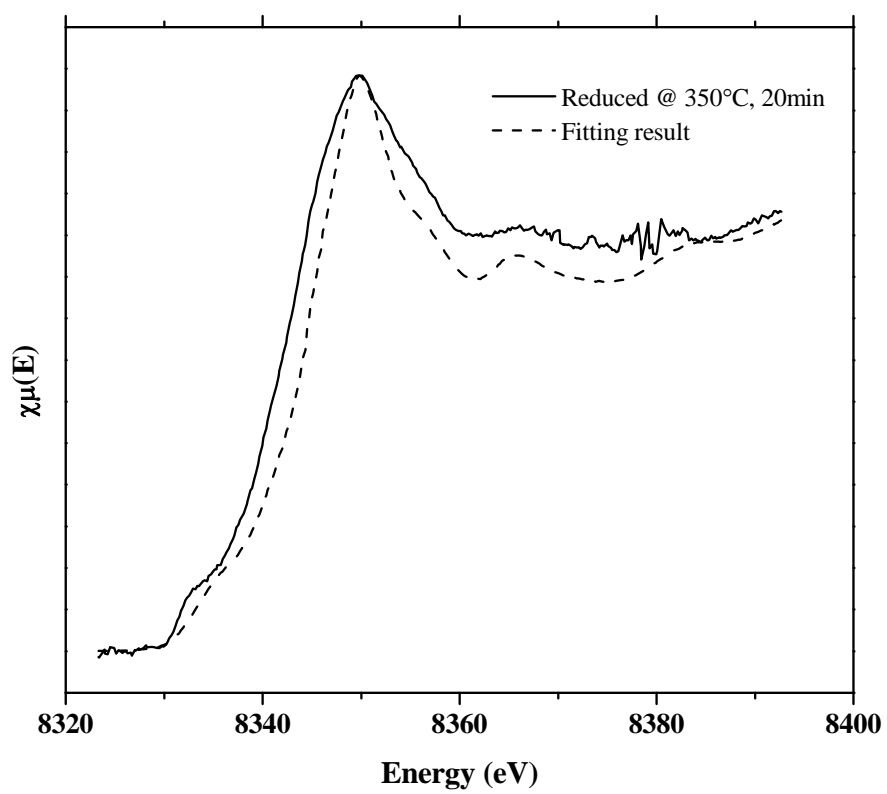
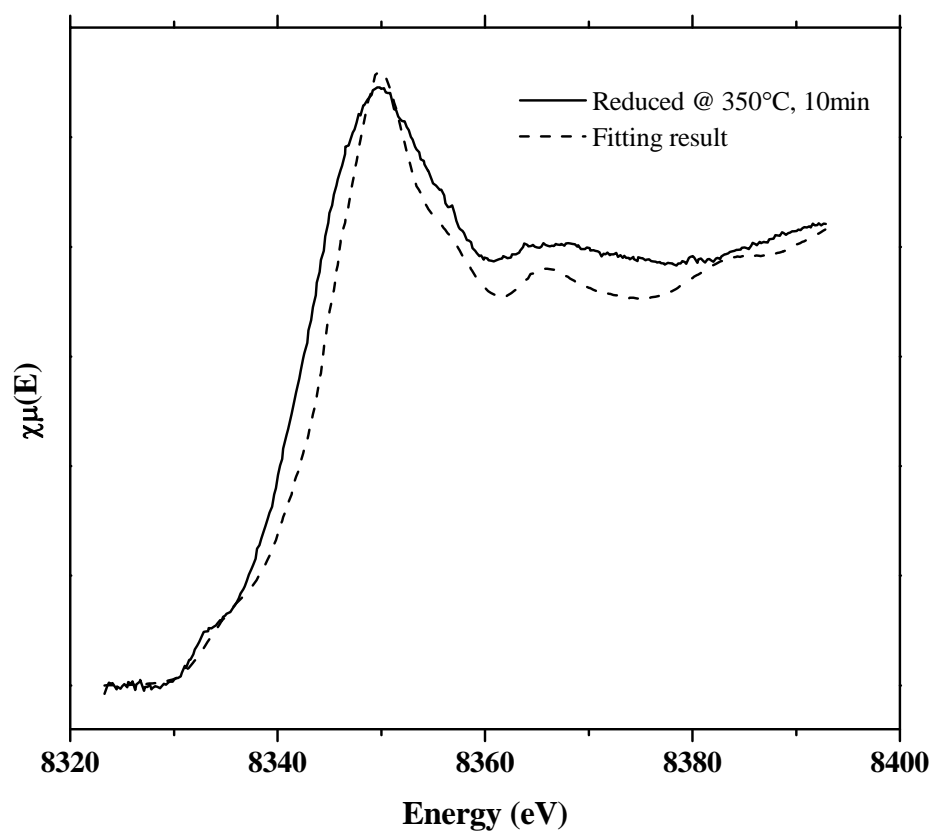


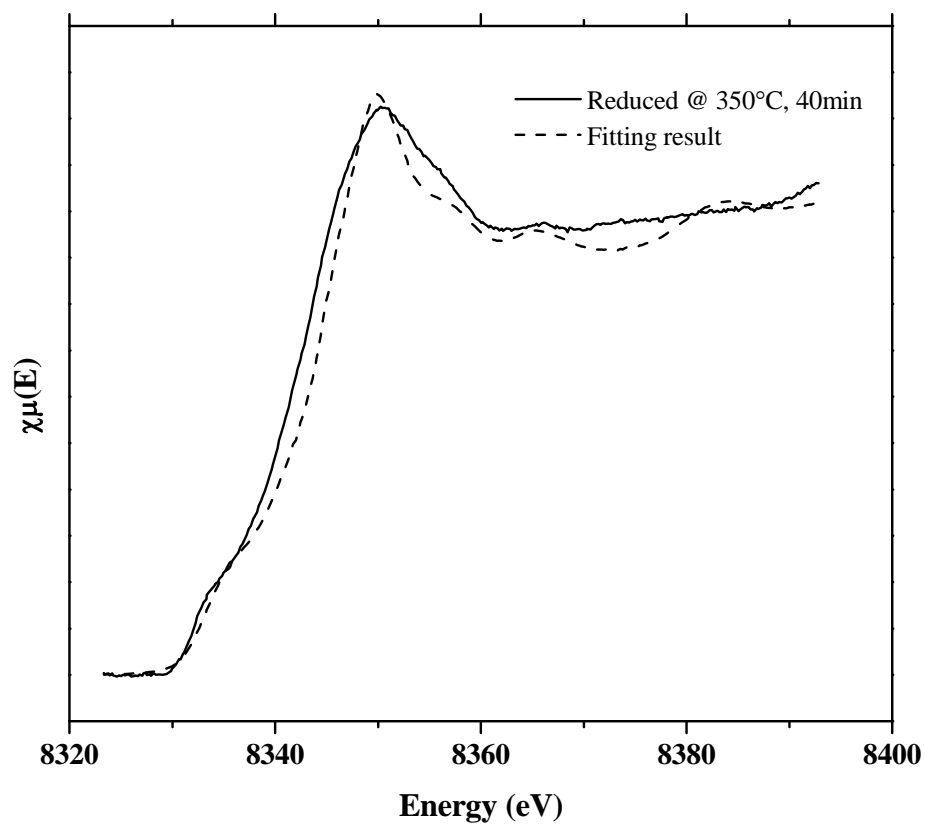
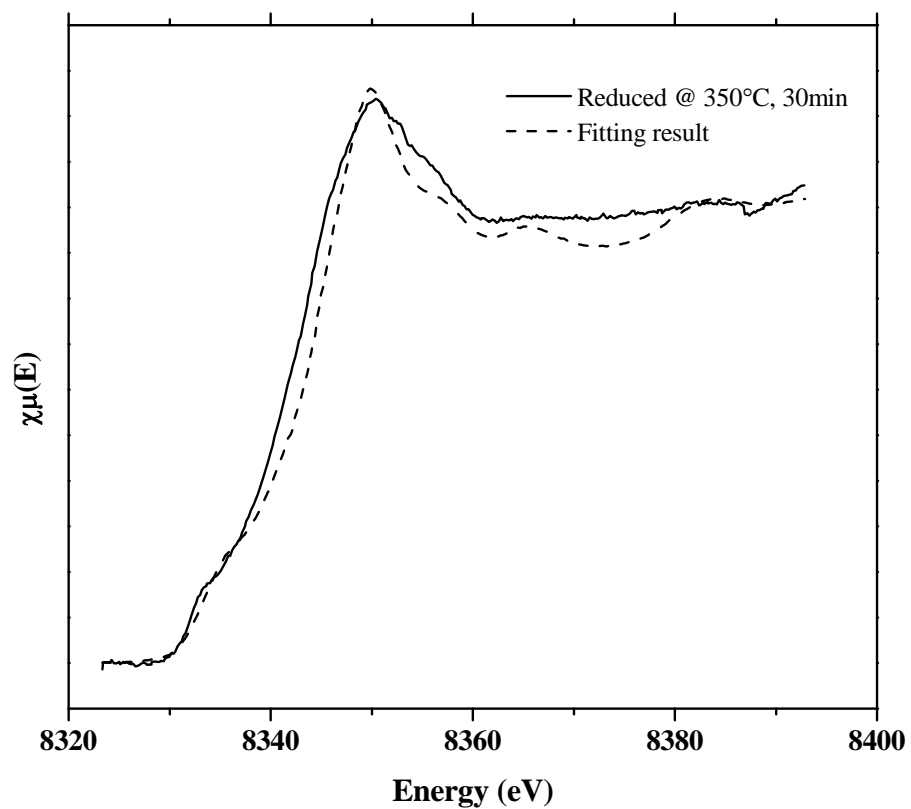


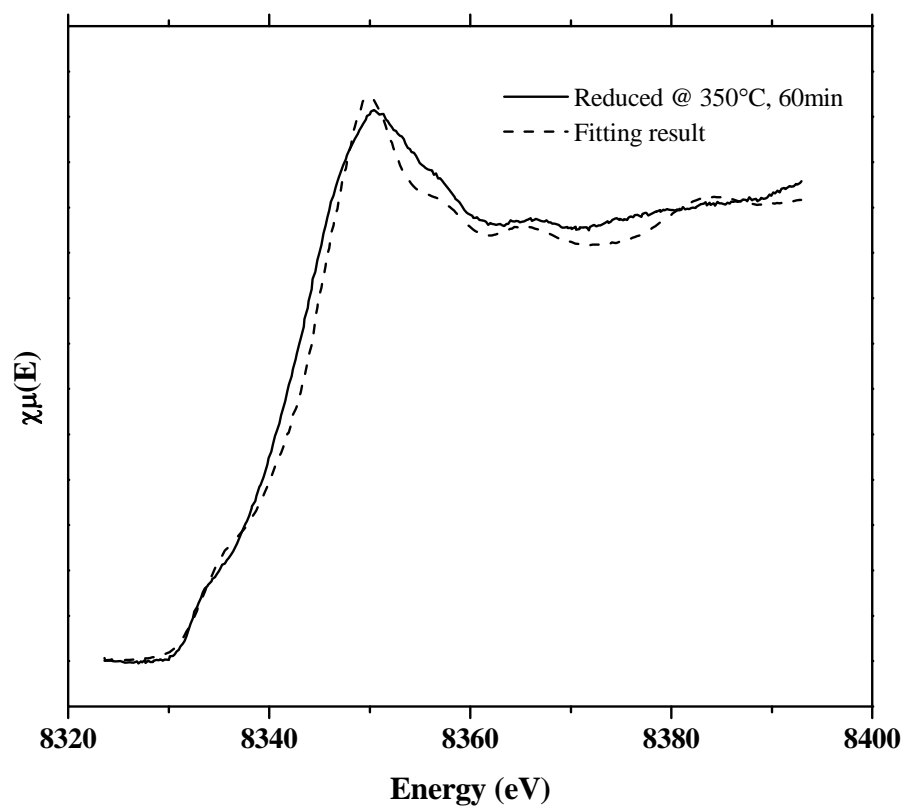
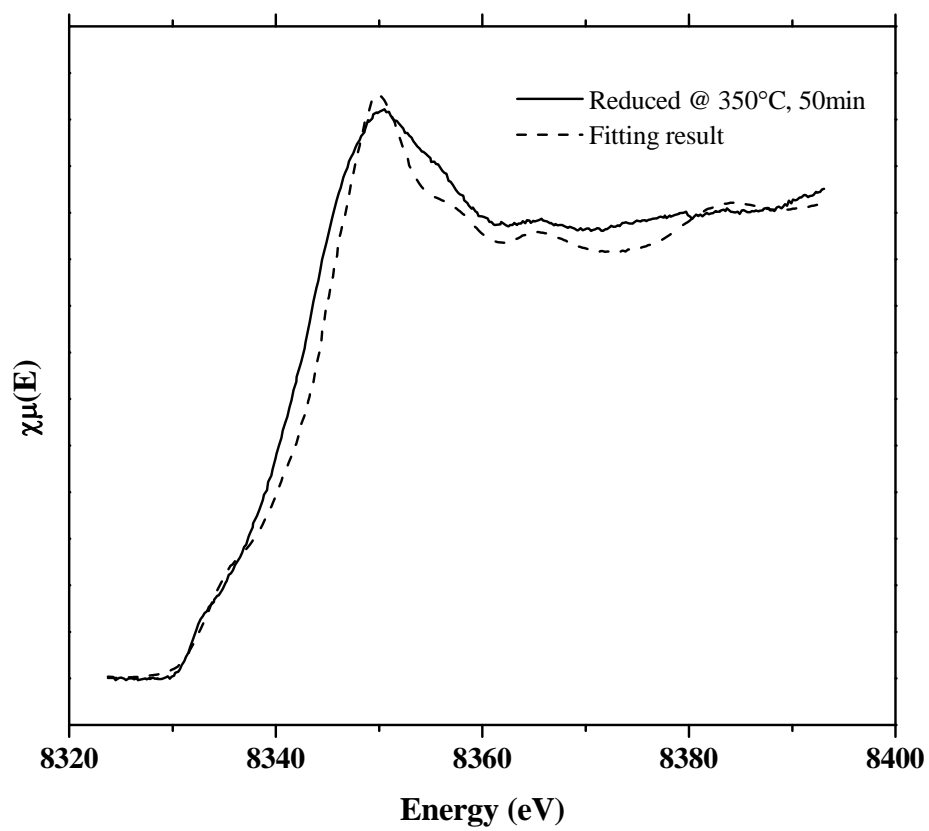


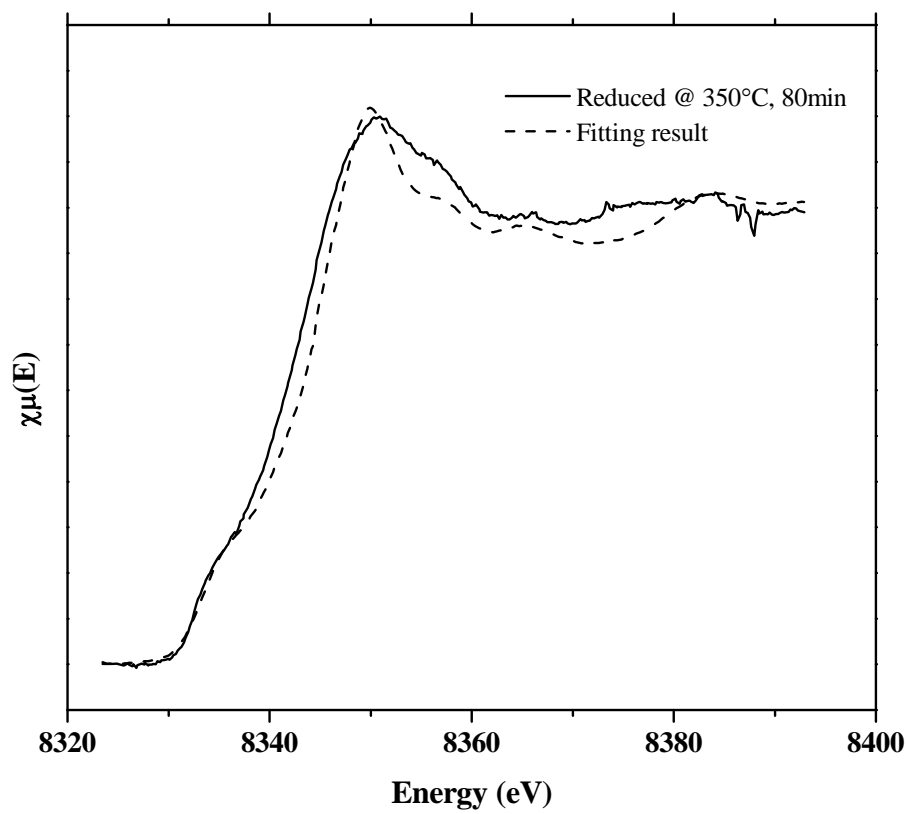
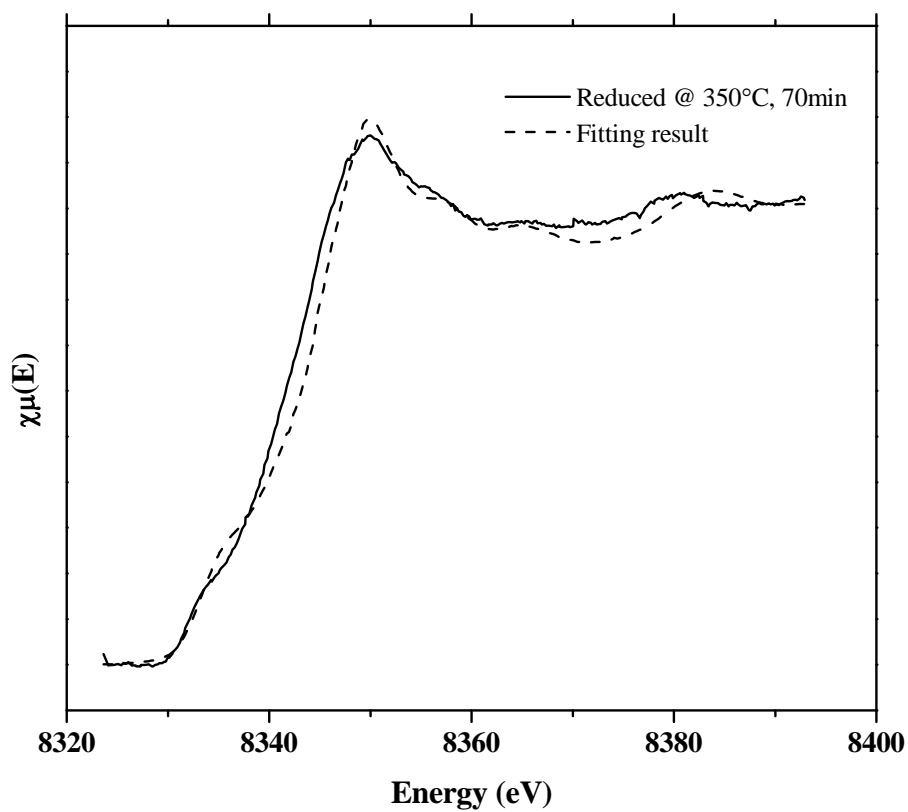
APPENDIX C

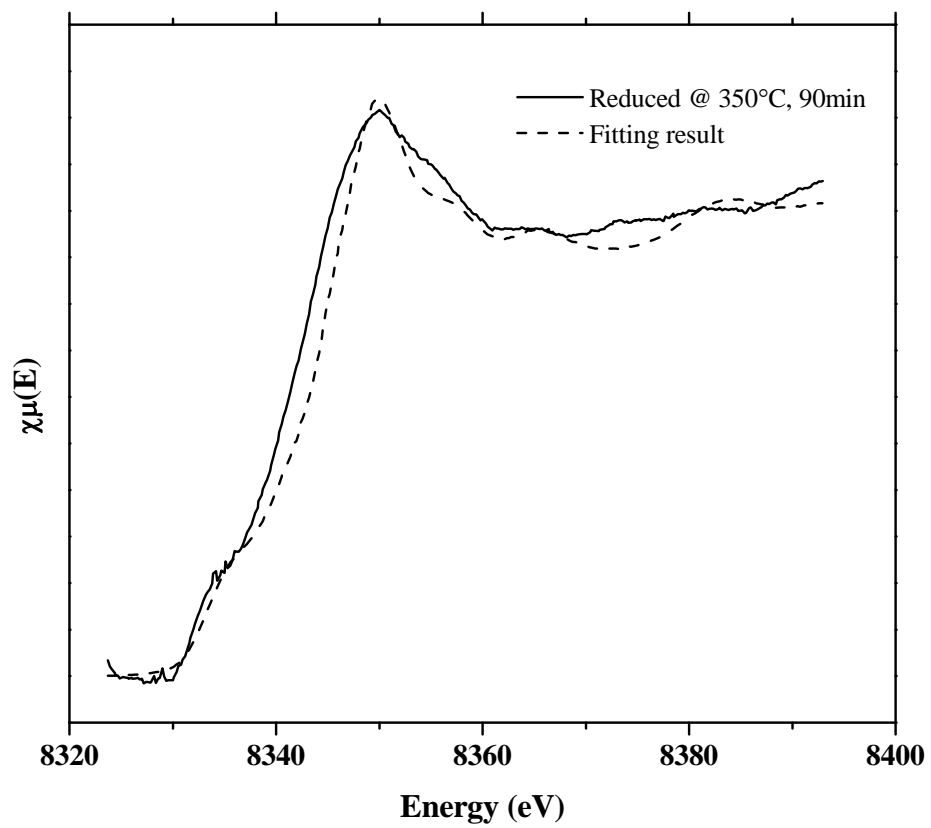
**LINEAR COMBINATION FITTING RESULTS OF
5Ni0.5Pt/HBEA DURING IN SITU REDUCTION AT 350°C
WITH HOLDING TIME OF 90 MINUTE**











CURRICULUM VITAE

Name Miss Sirinuch Loiha

Education

- 2000 – 2004 B.Sc. (Chemistry with honors) Ubon Ratchatane University,
Ubon Ratchatani, Thailand with scholarship from The Institute for the
Promotion of Teaching Science and Technology (IPTST)
- 2004 – 2005 Grad. Dip. (Teaching Profession) Srinakharinwirot University,
Bangkok, Thailand with scholarship from IPTST
- 2005 – 2009 Ph.D. (Chemistry) Suranaree University of Technology with
scholarship from The Synchrotron Light Research Institute (Public
Organization)

Publications

1. **Loiha, S.**, Prayoonpokarach, S., Songsiriritthigun, P., and Wittayakun, J. Synthesis of zeolite beta with pretreated rice husk silica and its transformation to ZSM-12, *Materials Chemistry and Physics*, 115 (2009) 637–640.
2. **Loiha, S.**, Föttinger, K., Zorn, K., Klysubun, W., Rupprechter, G., and Wittayakun, J. Catalytic enhancement of platinum supported on zeolite beta for toluene hydrogenation by addition of palladium, *Journal of Industrial and Engineering Chemistry*, (2009), Accepted.
3. **Loiha, S.**, Klysubun, W., and Wittayakun, J. Geometry change of NiO on zeolite beta during *in situ* reduction using X-ray absorption investigation, manuscript in preparation.